Departament de Física
Universitat de les Illes Balears

Programa Oficial de Postgrau de Ciències Experimentals i Tecnologies (Física).
Doctor per la Universitat de les Illes Balears

Numerical study of intense cyclogenesis events in the Mediterranean basin

Tesis doctoral

Lluís Fita Borrell

Directors:
Dr. Climent Ramis Noguera
Dr. Romualdo Romero March

A la Laura,
als de casa

La ciència és com l'art,
però amb lògica i matemàtiques

Agraïments

Tota la tsasca d'investigació s'ha dut a terme dins del *Grup de Meteorologia* del *departament de física* de la *Universitat de les Illes Balears*. Sense l'ajuda, la paciència i la seva infrestructura, la meva tasca hauria estat impossible. Molt agraït a la confiança que em féu el Dr. Climent Ramis, quan m'oferí la beca FPI i incorporar-me al grup al juny del 2003, sabedor que ha realitzat un doble esforç. Car, altres compromisos que adquirí a posteriori no m'ha permés tenir més temps amb ell per a poder aprendre'n molt més del que he après. Al Dr. Romualdo Romero, el qual sense ell, la seva gran capcacitat de traball i paciència, res no hauria estat possible. Climent i Romu, gràcies per permetre desenvolupar-me en la meva indisciplina i independència.

Al Dr. Víctor Homar per les profundes reflexions i meditacions al voltant de la meva recerca durant llargues i enriquidores converses. Al Dr. Joan Cuxart per l'ajuda en dubtes sobre la capa límit. A totes les persones que formen i havien format part del grup de meteorologia. Tot el temps passat amb vosaltres no ha estat temps perdut, car, tot i que em treieu temps per a fer la meva recerca, els vostres dubtes, comentaris, reptes i problemes han estat un estímul que m'ha dut a adquirir molts altres coneixements. No dubteu que he après molt més jo de vosaltres. A en Toni, Marional, Alberto i Ángel, per tot allò que us he fet compartir, patir i créixer plegats.

A en Krisitian Horvath del *Državni Hidrometeorološki Zavod* per la tasca i enriquiment comú del qual en segueix una bona amistat. Al Dr. Eduardo García de la *Univerdiad de León* per la tasca comuna realitzada. Al Dr. Kerry A. Emanuel del *Massachusetts Institute of Technology* per permetre'm treballar amb ell. A les llargues i iniciàtiques converses amb el Dr. Chuck Doswell III de *The University of Oklahoma*. A en Joan Campins del l'*Agencia Estatal de Meteorología* per l'ajuda donadada. A en Toni Borràs per agunatarme els desvariejos al cubicle. A la comunitat i mentalitat open-source.

A totes aquelles altres persones que m'he trobat pel camí i que sense el seu suport hagués estat impossible tirar endavant una tesi lluny de casa i lluny de tot, vosaltres heu estat el meu sosteniment. La llista és llarga, però especial agraïment (en ordre alfabètic): Arancha, Benet, Cesc, Joan Miquel, Marga, Maria, Maria del Mar, Marta, Noelia, Pau, Sara, Tanja, Toni. A totes les altres persones que han fet de casa meva l'*Hostal Lluís*, que ha estat una de les experiències més intenses i engrescadores de la meva vida. A totes les persones de la travessa i a les seves amistats que m'han permés re-conèixer, redescobrir i gaudir de l'illa de Mallorca, les seves persones i la seva cultura.

A uns companys de camí de Barcelona com l'Isaac en Quim, Makarres i FpD. A tothom que em va ajudar a començar-lo iseguir-lo, Héctor, Carles Albert, la gent de Salt i la de l'A. E. Pare Claret.

Contents

1 Introduction **9**
1.1 Mediterranean characteristics 12

2 Methodology **21**
2.1 Atmospheric numerical model 21
2.1.1 MM5 26
2.1.2 Axisymmetric cloud resolving model 50
2.2 Piecewise PV Inversion 52
2.2.1 Invertibility principle 60
2.2.2 PV-based prognostic equations 62
2.3 Factor Separation 65
2.3.1 Differential application 66

3 Dynamical aspects of the cyclogenesis **69**
3.1 Baroclinicity 70
3.1.1 November 2001 case 70
3.1.2 Quantification of the initial modification 78
3.1.3 Sensitivity to upper level trough 91
3.1.4 Sensitivity to low level thermal disturbances 91
3.1.5 Sensitivity to to the Atlantic high pressure zone 95
3.2 Intercomparison throughout Mediterranean basin 97
3.2.1 Description of cases 99
3.2.2 Results 112
3.2.3 Geographical sensitivity 115
3.2.4 Dynamical sensitivity 115

4 Thermal and topographic lee influences **119**
4.1 Thermal influences 120
4.1.1 Extreme hail event on August 16th 2003 121
4.1.2 Sensitivity to orography and solar radiation 123
4.1.3 Sensitivity to thermal anomaly using PV inversion 134

4.2 Topographic lee influences 140
4.2.1 Extreme Bura case on November 11-14th 2004 140
4.2.2 Sensitivity tests 151

5 Medicanes: Tropical-like Mediterranean storms 163
5.1 Description of studied cases 166
5.2 Air-sea mechanism 178
5.3 Sensitivities of Medicane environments with cloud model 182
5.3.1 Sensitivity on dimension of initial vortex 192
5.3.2 Sensitivity on initial humidty 192
5.3.3 Sensitivity on initial vortex strength 193
5.4 Air-sea mechanism sensitivity study in 3 Medicanes 196
5.4.1 Sensitivity methodology and control simulations 196
5.4.2 Sensitivity results 203
5.4.3 Collection dependence 211
5.4.4 Temporal dependence 216
5.5 Sensitivity study on January 1995 medicane 228
5.5.1 Methodology of 2-d effects 228
5.5.2 Validation of control simulation 229
5.5.3 PBL Air-sea structure correspondence 235
5.5.4 Effects on the vertical radial structure 239

6 Assimilation of observational data in simulations 251
6.1 Effects of assimilating data in medicane simulations 252
6.1.1 Methodology 252
6.1.2 Results 260

7 Conclusions 285
7.1 Strong cyclogenesis: November 2001 286
7.2 Intercomparison of 11 Mediterranean cyclogenesis 287
7.3 Thermal influences 288
7.4 Lee influences 289
7.5 Medicane environments 291
7.6 Medicane sensitivity 293
7.6.1 Sensitivity of January 1995 295
7.7 Assimilation of observational data in numerical simulations 297
7.8 Numerical methodologies 298
7.8.1 MM5 numerical model 298
7.8.2 Piecewise PV inversion 300
7.8.3 Factor Separation 300
7.9 Final remarks by the Author 301

A Statistics of trajectories **303**
A.1 Minimum BIAS 303
A.2 Distance Correlation 304
A.3 Pure coordinate Correlation 304
A.3.1 Bias correction 305
A.3.2 BIAS temporal lack correction 305

Chapter 1

Introduction

The relation between humanity and atmospheric phenomena is still at the beginning of the 21st century, a matter of necessity, hope and fear. The atmosphere provides the suitable environment for life, but at the same time, destruction and death. It is a complex system with several different aspects interacting at the same time, such as: the sun, seas, mountains, coastal-lines, terrestrial rotation, humanity, and much more. It provides a double challenge. One is related to its inherent complexity and the ways to understand it. And the other is about the mechanisms that the humanity can develop to mitigate the negative impacts of hazardous weather (e.g. large hail, heavy precipitation, strong winds, tornadoes, hurricanes, etc). The better the atmosphere is understood, the lower can be the impacts that are suffered from its nature.

Results obtained from the study of some of the negative atmospheric phenomenas will be presented. This document is devoted to the study of strong cyclogenesis (formation of a cyclone) in the scope of the Mediterranean basin. It is focused in the analysis of some episodes where a strong cyclone developed or a strong social impact occurred as a result of the formation of a cyclone. Cyclones can generate a large list of consequences in some cases related with severe weather (weather phenomena with a high potential destructive effect on the environment or the societies) such as: heavy precipitation, strong winds, strong snow falls, tornadoes, large hail. As a result of it, floods or flash floods and high sea-waves can be derived. They can be considered one of the most suffered atmospheric phenomena all around the world. Giving a little more of knowledge about cyclones and their formation, might help to prevent their strong impacts in our societies.

Different aspects, that play a role during the formation of a cyclone, have been analysed. The study of the roles of different features of the environment that contribute, enhance or provoke the formation of a cyclone is done throughout tools and techniques applied on the results obtained from atmospheric numerical simulations. Although, numerical models presented some limitations of accuracy and confidence due to approxi-

mations and simplifications that they contain, they provided a good tool for carry out a complete description of dynamics and thermodynamics of the atmosphere, which is very helpful in the study of the gas layer that surrounds the Earth.

The study of the cyclogenesis has been focused on the characteristics of one specific region. The localisation of the knowledge into a specific region of the planet should not be a penalty for the results. It should be considered as a way to consolidate, confirm and verify the assumptions, theories and concepts developed for other regions. The validation of theories and concepts in different regions might contribute to enhance their accuracy and avoid restrictions such as case dependencies or regional particularities. At the same time, it helps in the recognition of the specific aspects of each region. In this way, studied phenomena become better understood in the region, and their potential negative impact can be mitigated.

The selected laboratory has been the Mediterranean basin due to the interest of the author and the scientific team (Grup de Meteorologia de la Universitat de les Illes Balears[1]) with which the activity has been carried out. The Mediterranean Sea is a blue bridge that connects a wide range of cultures, societies and states. It is a densely populated region and presents a large wide of characteristics and peculiarities that can be found all around the world. This makes the Mediterranean basin a perfect region to develop the studies of the extra tropical cyclogenesis (out of tropical regions and without tropical characteristics), since a large variety of cyclogenesis types can be developed.

Numerical analyses of extreme cyclogenic events have been carried out using the MM5 model. MM5 (version 3.2 to 3.7) primitive equations non-hydrostatic model has been developed by the Pennsylvania State University and the National Center for Atmospheric Research (NCAR)[2] (Grell et al., 1995). Results of numerical simulations have been analysed with numerical tools and methodologies. Selected methodologies help in to the analyses of dynamics, influences and evolution of a wide range of features involved in the episodes. Two methodologies have mainly been used ; Piecewise Potential Vorticity inversion technique in the non linear version developed by Davis and Emanuel (1991) and/or the Factor Separation technique (Stein and Albert, 1993).

Piecewise PV Inversion technique has been used to modify the initial conditions of the simulations. In this way, a sensitive study to changes in the initial conditions of the simulations could be done (Huo et al., 1999; Romero, 2001). This methodology allowed to determine which pieces of a PV anomaly field are relevant for the case, and their role in the evolution of the episode could be derived.

[1] `http://www.uib.es/depart/dfs/meteorologia/`
[2] `http://www.mmm.ucar.edu/mm5/mm5-home.html`

Factor Separation technique allows the study of the role of isolated factors of the environment as well as interactions between two or more factors (Homar et al., 2002a). The results should clarify what dynamic role has been developed by the specific feature or interaction during the evolution of the case.

The techniques have been used to analyse some episodes occurred in the Mediterranean basin. The variety of the analysed cases is wide and should help to provide a main scope of the cyclogenesis in the Mediterranean basin. Baroclinic and barotropic mechanisms (Hoskins et al., 1985) are usually present in the Mediterranean cyclogenesis. At the same time, mountain range lee cyclogenesis (Buzzi and Tibaldi, 1978) and thermal low (Alonso et al., 1994) formation also have an important role. These and other aspects have been analysed in: the November 9-12th 2001 West Mediterranean case (Fita et al., 2007b), an intercomparison between 11 deep cyclogenetic cases occurred all over the basin (Fita et al., 2006), a strong hail event in the Ebro basin over the Iberian Peninsula (García-Ortega et al., 2007) and in the extreme Bura episode in Croatia during the November of 2004 (Horvath et al., 2006).

The cyclogenesis study is concluded by the analyses of a particular kind of Mediterranean systems. These systems have the appearance of a tropical storm and occurred only above maritime regions. They exhibited a well-defined rounded cloud structure in cyclonic rotation and some of them also showed a clear cloud-free zone in the centre. Although they have strong similarities with the tropical cases and are related to heavy rains and strong winds, they did not reach the hurricane intensity. The dynamics of the environment where they are developed have been analysed with a conceptual model of hurricane (Fita et al., 2007a). Factor separation technique has been used to analyse the dynamics and sensitivity of this kind of tropical-like storms (Fita et al., 2008b,c) that is similar to the air-sea mechanism (Emanuel, 1986) developed by the hurricanes, but altered by an upper level trough (Emanuel, 2005). Finally, a satellite-based methodology for the improvement of numerical simulations of these episodes (Fita et al., 2008a) has also been developed.

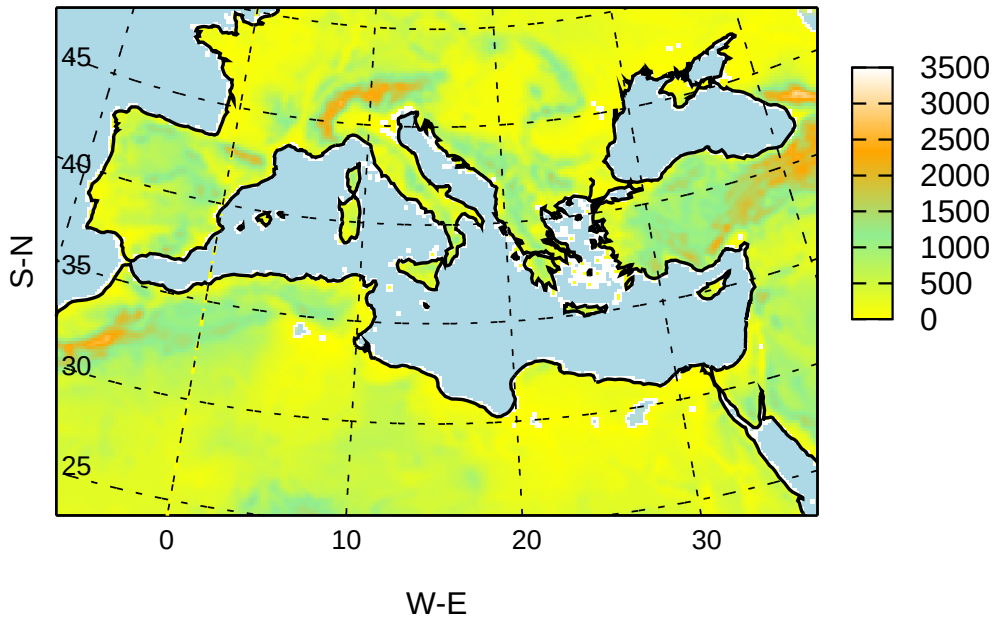

Figure 1.1.1: Mediterranean basin with the orography (colour shaded)

1.1 Mediterranean characteristics

The Mediterranean basin is defined as the land region that is surrounding the Mediterranean Sea (See figure 1.1.1). It reaches approximately the region comprised between 5 degrees West to 35 degrees East and 30 to 45 degrees North. Mediterranean sea is almost a closed sea that has a small connection (narrowest part is about 27 km) to the Atlantic ocean in its west extreme. It is a small sea with two major river tributaries: Nile river in its south-east extreme and the Rhône in its North-West extreme. It is mainly rounded by mountainous systems some of them with peaks above the 3000 m. Southern part of the basin is mainly dominated by extreme hot and dry desert areas. It has an irregular coastal line and relatively wide islands. Due to its morphological characteristics, Mediterranean basin has specificities unique in the world and it has been widely studied. *Plinius Conference on Mediterranean Storms* is a specific European Geosciences Union Topical Conference devoted to the Atmospheric behaviour in the Mediterranean area[3].

[3]web page of the 10th edition: `http://meetings.copernicus.org/plinius10`

Western part of the Mediterranean basin is surrounded by important mountain ranges (see top figure 1.1.2). Alps, Pyrenees and Atlas ranges have mountains that are overpasses 3000 m. Moreover, Iberian peninsula (south-eastern mountains are higher than 3000 m), Corsica, Sardinia and Sicily islands are also mountainous land surfaces. Another aspect of the ranges is their orientation. Western Mediterranean most relevant mountain ranges are latitudinal oriented and they do not have an important blocking effect to the westward general circulation of the air. Eastern part of the basin (see bottom figure 1.1.2) is less mountainously encircled. Highest mountains are on the north and southern and eastern part is almost flat. At the same time, no large islands are located in this part of the sea.

In spite of the non-blocking effect of the mountain ranges on the general circulation in the Mediterranean basin, they have an important role on specific atmospheric flow conditions that become relatively usual in the Mediterranean area. One of this atmospheric patterns, in which orography plays an important role, is in the lee cyclogenesis. In this case, cyclone formation occurs when a strong flow is blocked by a mountain range. Inward zone becomes a high pressure zone, meanwhile in the down wind or leeward zone pressure falls. It is frequent that Alps or Atlas (Buzzi and Tibaldi, 1978; Buzzi and Speranza, 1983; Horvath et al., 2006) ranges recipe southward winds and consequently Alps and Atlas lee zones are cyclogenetic zones. In fact, Alps lee region is one of the most cyclogenetic zones in the world (Reiter, 1975; Alpert et al., 1990; Maheras et al., 2001; Trigo et al., 1999, 2002; Campins et al., 2006).

Another characteristic effect derived from the mountainous Mediterranean coasts are the flash-floods episodes. Due to the proximity of the mountains to the coastal lines, Mediterranean maritime areas are very abrupt. Shallow, short and highly step torrents are distributed allover the Mediterranean basin. Due to its characteristics, relatively strong precipitation can provoke fast and important growing in the rushing streams (one example is found in the Montserrat episode, in North Eastern part of Iberian peninsula on June of 2000, Martín et al. (2007); Amengual et al. (2007)).

Aside of the intensification of the rainfall effects on the runoff, mountain ranges play an important role in the localisation of the precipitation. Low level air-flows over sea surfaces acquires usually high quantities of moisture (see a scheme on figure 1.1.3). When one of these flow patterns reaches the coast and hit a mountain range air-flow is upward promoted. A result of it, due to its high moisture content, strong cloud or even convection can be developed and heavy rainfall can occur (Romero et al., 1997; Doswell et al., 1997; Ramis et al., 1998). Both mountain derived effects on rainfall (fast floods and localisation of precipitation) produce high impact weather in the Mediterranean zone. Large list of cases with large number of fatalities, casualties and economic costs can be found allover the Mediterranean zone that follow a similar pattern of heavy and very localised precipitation.

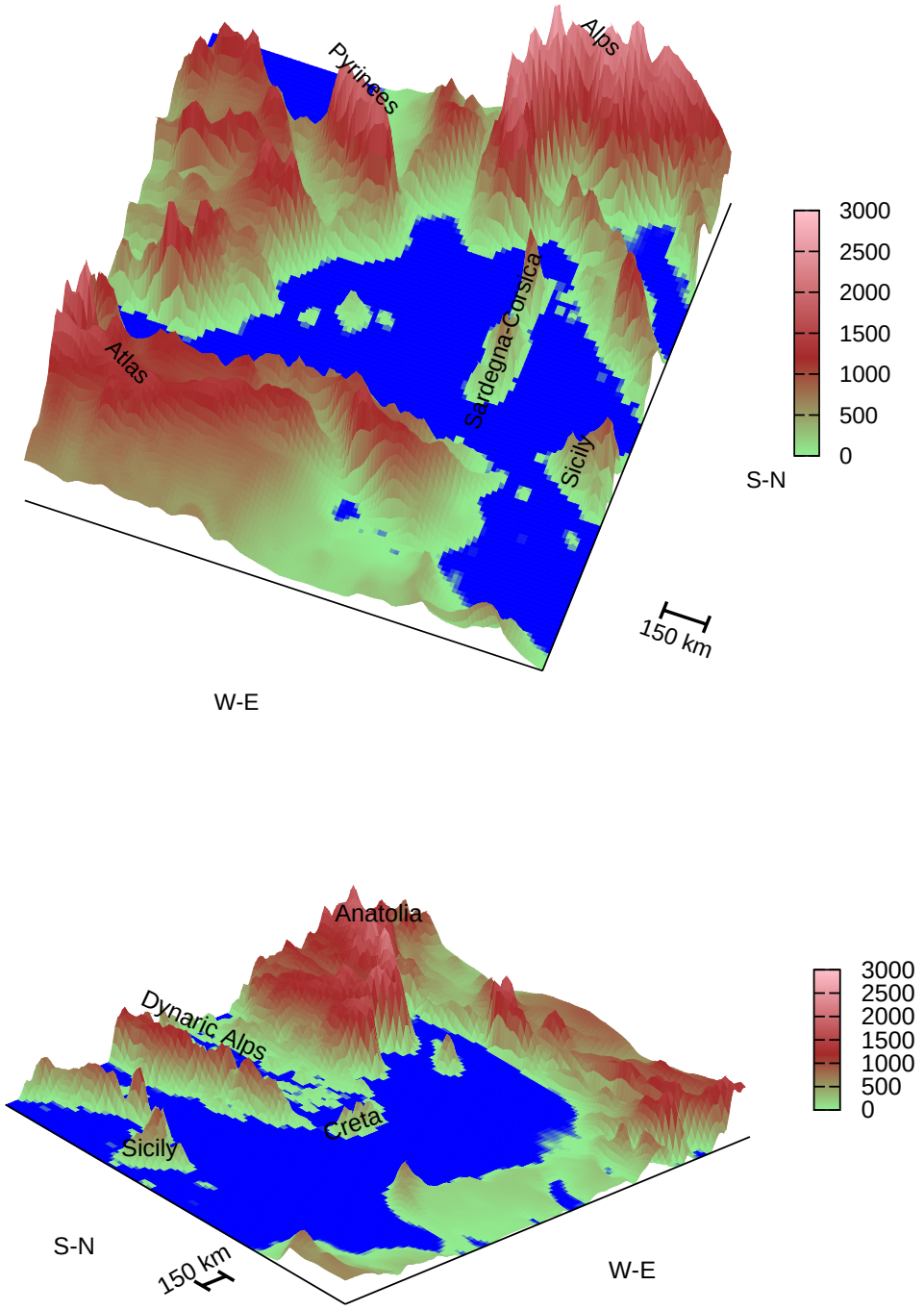

Figure 1.1.2: 3-dimensional representation of the orography of the Mediterranean basin. Western (top), Eastern (bottom)

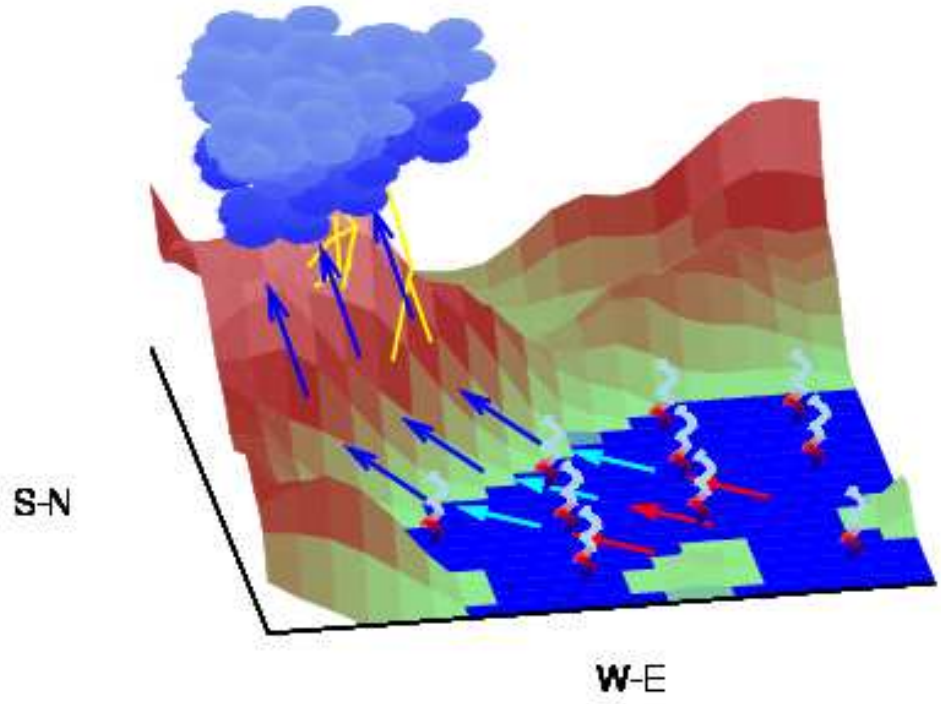

Figure 1.1.3: Schematic representation of the orographic effect on the Eastern coast of the Iberian peninsula. Warm air (red arrows) advects above sea surface gains moisture (spirals as evaporation from sea). Wet and warm air (blue arrows) reaches coastal line. Due to orographic effect, air ascends and cools and moisture might be condensed. Formation of clouds would provoke heavy rainfalls if the situation persists for a long period of time.

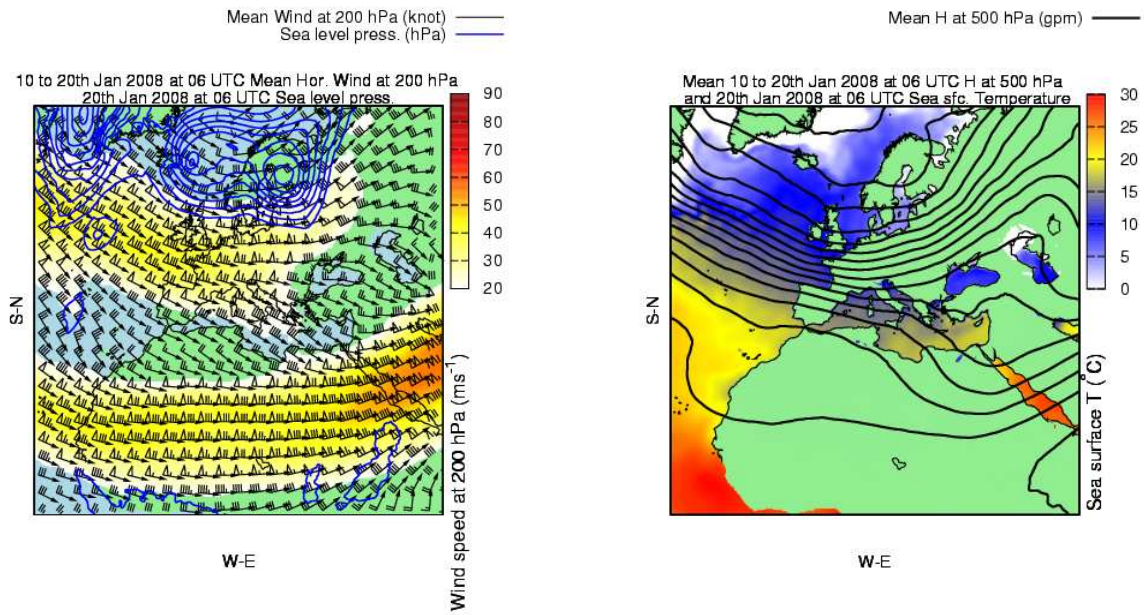

Figure 1.1.4: Atmospheric situation over Central mid-latitudes. Left panel: Mean horizontal wind at 200 hPa (vectors in barbs notation; triangle: 50 knot, pennant: 10 knot, half pennant: 5 knot), sea level pressure at 20 Jan. 2008 at 06 UTC (top), from 950 hPa to 1010 hPa (every 4 hPa, blue line) and mean horizontal wind speed at 200 hPa (ms^{-1}, colour shaded). Right panel: Sea surface temperature ($°C$, colour shaded) at 20th Jan 2008 at 06 UTC (top) and mean geopotential height at 500 hPa (black line, every 50 gpm). Mean values from 10 to 20th January 2008 at 06 UTC

In order to mitigate these effects a large number of studies (Homar et al., 1999; Romero, 2001) and projects have been carried out devoted to this topic. Some of the most recent inter-governmental projects have been: MEDiterranean EXperiment on "Cyclones that produce high impact weather in the Mediterranean" (MEDEX[4], WMO recognised project), or EU – Interreg IIIB projects HYDROPTIMET[5] and AMPHORE[6].

Mediterranean basin is affected by two major features of the global circulation. During the summers (see figure 1.1.5), subtropical jet shifted polarward and flows above the

[4] http://medex.inm.uib.es/
[5] http://hydroptimet.medocc.org/
[6] http://amphore.medocc.org/

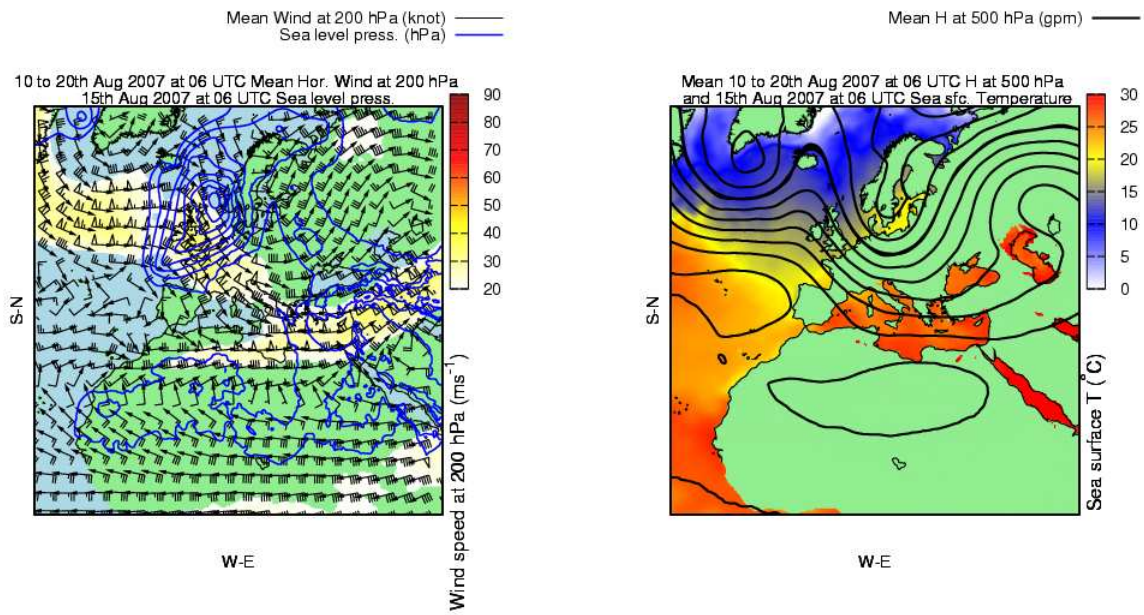

Figure 1.1.5: As in figure 1.1.4, but on 15th Aug. 2007 at 06 UTC and mean values from 10 to 20th August 2007 at 06 UTC

southern part of the basin. At the winter, intrusions of polar air usually reach the region (see figure 1.1.4). The effect of these two major patterns in the basin is reflected as a strong seasonality of the atmosphere in the Mediterranean area. Spring and Autumn are the seasons during which both flow patterns can occasionally be relatively close provoking a strong instabilisation of the air in the area. Moreover, high temperature of the Mediterranean Sea in Autumn, due to high isolation during summer, provides a third major element of instability in the area. By this way, for example Western Mediterranean basin has the largest amounts of precipitation and cyclone activity during Autumn (Campins et al., 2006; Reiser and Kutiel, 2007b). The persistence of the Azores anticyclone generates a North Atlantic blocking of the general flow that has a strong impact on the Western part of the Mediterranean basin. Eastern region is affected by the moist advections from the equatorial tropics of Africa (Krichak et al., 2004).

Geographical and general dynamic circulation patterns define the Mediterranean basin as a warm sea surrounded by mountains. Dry and hot advections of air from the southern deserted regions can interact with cold wet/dry air masses. At the same time, mountain ranges enhance the formation of cyclones as a consequence of the mountain-lee cyclogen-

esis. Strong isolation on the terrestrial areas allow the formation of shallow thermal lows (Alonso et al., 1994). All the aforementioned conditions make the Mediterranean basin as one of the most cyclogenetic regions in the world (Reiter, 1975). At the same time, atmospheric systems present a complex evolution and dynamics due to the high number of features interacting in the basin.

Strong and continuous cyclone formation in the Mediterranean area presents different particularities and dependencies. Alps-lee cyclogenetic zone is the largest one and presents its maximum activity in winter season (Trigo et al., 1999, 2002; Campins et al., 2000, 2006). Western Mediterranean area presents a duality of cyclogenesis. One kind are deep cyclones or Atlas-lee formed. Another kind of shallow but numerous cyclones are summer thermal formation of lows over the Iberian and Sahara land regions (Alonso et al., 1994). Eastern part of the cyclogenetic activity is mainly driven by the sea thermal origin, Turkish mountains or incoming Atlas cyclones (Maheras et al., 2001).

Coastal lines of the Mediterranean sea are mountainous and densely populated. For this reason, coastal lines are very sensitive to any kind of atmospheric phenomena. Fatalities and strong economical and social impacts can occur quite often allover the basin (see compilation in the MedEx database[7]) some times in the presence of weak systems. The potentiality of destruction from atmospheric phenomena in the region claims to an accurate study of the severe weather conditions. With the adequate response of the involved actors, the negative impact of the atmospheric phenomena in the Mediterranean basin can be properly mitigated. See statistical social and economical impact of weather phenomena in the EM-DAT: The OFDA/CRED International Disaster Database[8] and Dartmouth Flood Observatory[9]. Principal natural disasters that occurred in the Mediterranean basin are mainly derived from atmospheric phenomena (see figure 1.1.6).

Complexity and variety of characteristics of the Mediterranean basin become the adequate combination of features, in which a large variety of phenomena can be developed. It has been studied and shown how extreme weather (tornadoes, heavy rainfalls, large hail or extreme winds) highly frequent in the North American great plains also occurred in the European and Mediterranean zones (Tous and Romero, 2006). There is even an European Conference on Severe Storms (ECSS[10]) dedicated to this topic.

Waterspouts and tornadoes have been reported allover the Mediterranean area (Gayà et al., 2001; Homar et al., 2003a). Moreover, storm activity has been characterised also by mesocale convective systems (MCSs) activity with strong and fatal consequences (Romero

[7] `http://medex.inm.uib.es/`
[8] `http://www.emdat.be/`
[9] `http://www.dartmouth.edu/~floods/archiveatlas/index.htm`
[10] http://essl.org/ECSS/

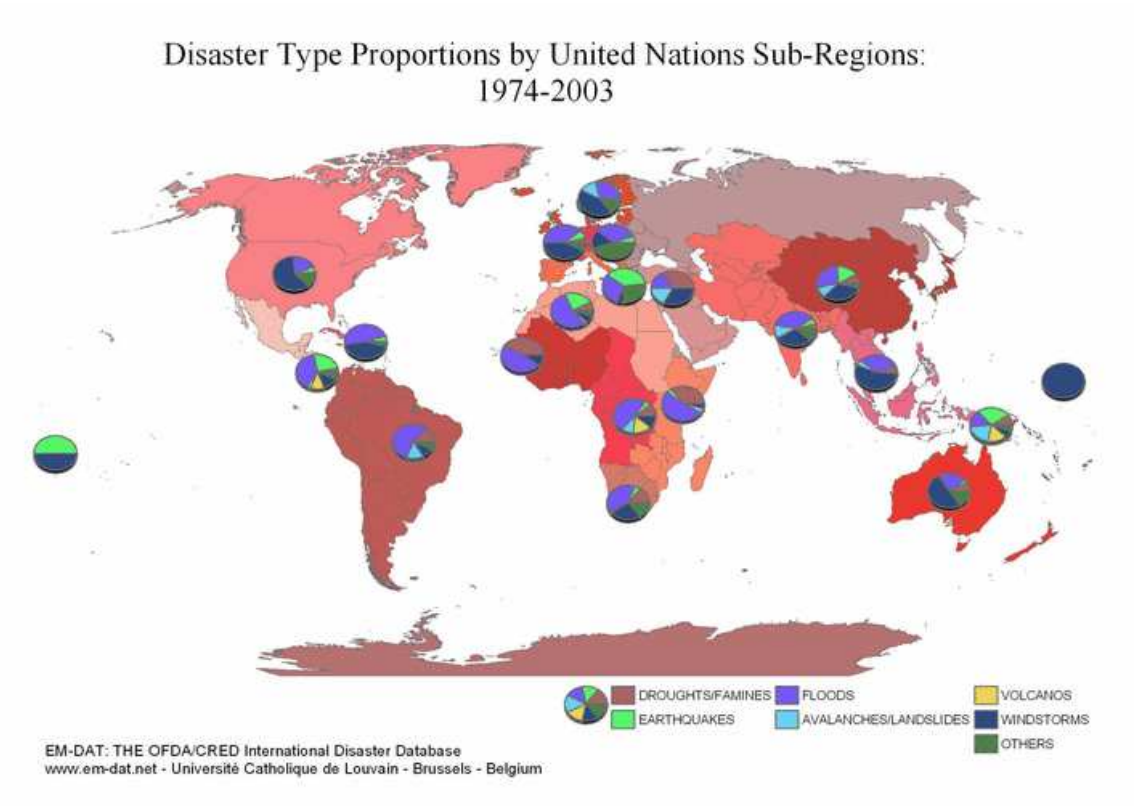

Figure 1.1.6: Disasters type allover the world. Source *EM-DAT: The OFDA/CRED International Disaster Database* `www.emdat.be` *Université Catholique de Louvain Brussels (Belgium)*

et al., 2001, 2000). Moreover extreme hail events (Tudurí et al., 2003; García-Ortega et al., 2007) or even strong snowfalls (Tayanç et al., 1998; Cucurull et al., 2004; Houssos et al., 2007). It has also also found that Mediterranean basin presents a tropical-like storm activity (Rasmussen and Zick, 1987; Businger and Reed, 1989; Homar et al., 2003b; Fita et al., 2007a). Another atmospheric phenomena strongly linked to the sea is found in a atmospheric-induced tsunamis or meteotsunamis like '*rissaga*' in Balearic islands (Ramis and Jansà, 1983), *marubbio* in Sicily or *milghuba* in Malta (Monserrat et al., 2006). In these cases oceanic barotropic waves induced by pressure fluctuations of the atmosphere are enhanced when they reach the coast throughout specific resonance conditions.

A large number and variety of atmospheric phenomena within the Mediterranean basin has been described. Moreover Mediterranean basin presents a complex climatological pattern with large and wide fluctuations of atmospheric characteristics in zones, seasons and year to year. Rainy patterns are not constant and present a wide fluctuation in climatological amounts allover the basin (Reiser and Kutiel, 2007b), and large differences from Western zone to Eastern one (Reiser and Kutiel, 2007a). Different synoptic patterns are related to strong precipitations specifically for each region, according to their relative position with respect to the Mediterranean Sea. In general Eastern Mediterranean Sea heavy precipitation events are related to westerly flows, meanwhile for example in the western region of the Iberian peninsula to easterly flows (Romero et al., 1998, 1999). Event climatological fluctuations of rainy extreme events is also found allover the Mediterranean region (Alpert et al., 2002).

Climate change scenarios project a warmer and dryer Mediterranean climate (IPCC, 2007). Increase of temperatures are projected to be higher than global values, with hotter and longer summer periods. At the same time, rainy days are likely to decrease with an increase of summer drought episodes. Even some studies project the possibility of a tropical cyclones in the late 21st century (Gaertner et al., 2007).

Chapter 2

Methodology

Numerical methodologies are very powerful in the study of the atmosphere. Real observations are sparse and they are taken with low temporal frequencies. This lack of observations does not give an entire view of the real state of the environment. A useful way to correct this lack of knowledge of the atmosphere can be approximately solved with the use of atmospheric numerical models. Numerical models give an approximation to the real evolution of the atmosphere. They are computational simplifications of a big portion of the atmospheric knowledge. However, in comparison to the observations, they give a complete and continuous spatial and temporal description of the environment and of its evolution.

Numerical methodologies applied in the results of numerical models can bring a kind of information that is very difficult to be obtained from the observations. Numerical tools can give a detailed information of a large variety of dynamic or structural details that the observations can not provide. However, one should maintain a contact with the information obtained from the observations. Numerical results should be verified, tested and contrasted with the best approach of the reality obtained from the observations. At the same time, it must bear in mind that numerical results are obtained from the approximated perspective given by a numerical model and the lack of knowledge of some atmospheric processes.

2.1 Atmospheric numerical model

Atmospheric numerical models try to solve the equations that describe the dynamical and thermo-dynamical behaviour of the atmosphere (a brief list of available atmospheric numerical models is provided in table 2.1.a). Numerical models are a useful tool, since atmospheric equations are non linear and they do not have an analytical solution. Thus, the numerical solution of the equations is the unique (for the moment) way to solve them. Atmospheric numerical models solve the equations in different ways. At the same time,

Table 2.1.a: Alphabetically ordered brief list of numerical models giving the name of the model or the centre that has develop it accompanied with a web-source of information

Name	**web access**
Aladin	http://www.cnrm.meteo.fr/aladin/
Arpege	http://www.meteofrance.com/FR/index.jsp
BOLAM-QBOLAM	http://www.isac.cnr.it/dinamica/bolam/index.html
COSMO	http://cosmo-model.cscs.ch/
ECMWF	http://www.ecmwf.int/
GEM	http://collaboration.cmc.ec.gc.ca/science/rpn/gef_html_public
GEM-LAM	http://www.msc-smc.ec.gc.ca/
GFS (new AVN)	http://www.emc.ncep.noaa.gov/modelinfo/
GME	http://www.dwd.de/en/en.htm
HadCM	http://www.metoffice.gov.uk/research/hadleycentre/models/modeltypes.html
Hirlam	http://hirlam.org/
IGCM	http://www.met.rdg.ac.uk/~mike/dyn_models/igcm/
Lokal	http://www.dwd.de/en/en.htm
MASS	http://www.meteosimtruewind.com/
Meso-NH	http://mesonh.aero.obs-mip.fr/mesonh/
MM5	http://www.mmm.ucar.edu/mm5/mm5v3/
RAMS	http://bridge.atmet.org/users/software.php
UKWMO	http://www.metoffice.gov.uk/
WRF	http://www.wrf-model.org/index.php

some models give multiple available configurations. As result of it, the computation is not unique and it is case, model and configuration dependant.

The development of the atmospheric numerical model is strongly related to the history of the computation and the capacity of management of digital information. The degree of complexity and confidence in the models has been increasing in parallel with the growing of the computational capacities and research (g.e.: MM4 was a hydrostatic model of the MMM community until the MM5[1] non-hydrostatic version of the model was released on July 31st 1999). A numerical model is based in different pieces or modules. Each one of these modules has a specific function with its degree of simplification, approximation or complexity.

[1] http://www.mmm.ucar.edu/mm5/mm5-home.html

- **Atmospheric equations:** The atmosphere is a mixture of different gases. However, due to the spatial and temporal scales in which it is studied it is treated as a fluid. Fluids such as oceans, atmosphere or magma are described by the *Navier-Stokes* equations (Bluestein, 1992). The NS-equations (also known as *primitive equations*) give the dynamics of a given state of a continuous system. These equations are nonlinear, and multi-coupled equations of six variables ($\vec{V}, T, q$ and p). Numerical models solve these equations in different degrees, throughout the simplification of some terms of the equations. Initial versions of the models (g.e.: MM4, Hirlam, ...) were hydrostatic, in which equation for third coordinate is substituted by the hydrostatic approximation (pressure, height and density have the relation: $\delta p = -g\rho\delta z$). Actual models try to deal with the complete complexity of the equations including the non-hydrostatic terms. The computation of the equations is solved in different ways such as: finite differences, finite volumes and spectral.

- **Resolution:** Numerical models are used to compute spatially and temporally the variables that describe the atmosphere. In order to carry out this computations space and time need to be discretized (the variable will be computed at specific spatial and temporal values; some assumptions are made within the unresolved temporal and spatial scales). The degree of discretization will give the resolution of the simulation. In finite volumes or finite differences models the space is usually discretized in horizontal regular net of grid points. This regular horizontal nets of points are not homogeneously distributed vertically. The density of horizontal grids are usually higher in the lower than in the upper levels of the atmosphere. In spectral models, the resolution is given by the lowest wave of the spectra of typically a Gaussian spectral distribution. In order to avoid grid troubles in the poles, some models use a triangular net of points (GME).

- **Global and limited area models:** Two big groups of numerical models can be established. The are the global and the limited area models. Global models are used to simulate the dynamics of the atmosphere allover the planet. Limited area models are used to simulate a fraction of the atmosphere. Usually, global models present less complexity than the limited area ones. Limited area models allow a major precision and detail in the simulations. Climate global models such as HadCM3 use a horizontal resolution of 2.5 terrestrial degrees. Meanwhile mesoscale limited area models such as Meso-NH can be used in simulations with a horizontal resolution of 500 m or even less.

- **Terrain characteristics:** Terrestrial information needs to be provided in order to have a realistic simulation. Thus, geographical coordinates are provided, as such as the morphology of the earth surface. Topography and orography information are also inserted in the model. At the same time is included the information of land-

use such us: forest/urban characteristics, kind of vegetation, ice, desert, land/water mask. Assuming at the same time, particular characteristics to each category such as albedo, moisture, emissivity, roughness length, thermal inertia.

- **Initial and boundary conditions:** In order to simulate the 'real' atmosphere the initial state introduced in the models should be as accurate as possible. Initial conditions are used as the first state from which numerical model will start. They are mainly derived from combination of observations and numerical adjustments through atmospheric models. Atmospheric models are used as a way to obtain the entire state of an atmosphere described by the equations in agreement with the observations. The generation of an entire state of the atmosphere with concordance on observations is mainly used in the global models. Global models will compute a forecast of the entire planetary atmosphere initiated with the numerical adjustment of the observations. Numerical adjustment of the observations is carried out with different tools or methodologies such as 3DVAR (Lorenc et al., 2000; Barker et al., 2003), Kalman Filter (Evensen, 2003), or 4DVAR (Rabier et al., 1998). Limited area models also use initial conditions, however, due to their spatial limitations, they need information about the state of the atmosphere at the limits of their domain of integration. With the boundary conditions a limited area model acquires the state of the surrounding atmosphere. These surrounding conditions are mainly derived from other global simulations. By this way, specific local simulations are maintained in concordance with the entire state of the atmosphere. Thus, structures outer of the area that were not present in the initialisation of the simulation are properly introduced in later stages. There are different centres that generate the global simulations used as initial and Boundary conditions. They are carried out every day in a large variety of temporal (usually every 12 or 6h) and horizontal resolutions (from 2.5 to 0.25 degrees). Most of them are generated by state agencies like: NCEP, ECMWF, Deutscher Wetterdienst, Meteo France or UK Met Office. They can be atmospheric analyses or global forecasts. ECMWF (Uppala et al., 2005) and NCEP have been developed a new set of re-analyses in which have been used the best numerical adjustments with all the available sources of observations and measurements.

- **Observations:** Some models allow the insertion of observations in the simulations. With the observations is ensured a better representation of the real state of the atmosphere and the capture of smaller features that are not represented in the global analyses of a low resolution. The global standard network of observations of the WMO [2] are one of the major sources of observations. A source of observations are the 3h or 1 hourly surface observations taken from the land surface or ships and the rawinsonde at every 12 hours. Network of observations are sparse and they are

[2] `http://www.wmo.in`

insufficient to give a detailed description of the state of the atmosphere. Last years techniques have been developed that allow to introduce other kind of observations like satellite or radar data. At the same time complex methodologies of adjustment between observations and model simulations have been developed. Two of these are observation nudging (Stauffer and Seaman, 1990) and 4DVAR variational method (Rabier et al., 2000).

- **Physical processes:** Within dynamics of the atmosphere there is a wide variety of processes that are developed at different scales and strates. Some of these processes such as: evaporation, condensation, rain, convection, take place on different scales of time and space (synoptic, mesoscale and microscale). All them are related with each other and they present different characteristics and behaviours. At the same time, different aspects of the atmosphere occurs in specific regions (g.e.: drop formation, eadies in the boundary layer). Some of these processes have a high complexity or even are not well known. Due to the difficulty and limited computational resources in order to simulate these aspects with the primitive equations, some of them are not simulated directly and are simulated with a scheme. A scheme is a simplified representation of the process with which is attempted to reproduce the phenomena. These schemes are applied on specific zones of the simulation, when according to appropriate conditions of the prognostic variables, the phenomena can be developed. As a result of the application or activation of the scheme, general dynamics of the atmosphere (computed via the *Navier-Stokes* equations) would be altered by the interaction of the general dynamics of the atmosphere with the particular outputs of the schemes at a given grid point (e.g.: increasing of the temperature as a result of a drop formation simulated by the cloud-microphysics scheme). There is a large variety of schemes and they present different degrees of complexity. Even though schemes are secondary aspects of the fluid dynamics, the processes simulated with them can have a strong impact in the simulations. Changes in the selection of one scheme can induce significant differences between simulations of the same episode (Wisse and de Arellano, 2004; Fita et al., 2008a).

- **Nesting:** Limited area models are used to study in detail some atmospherics events. In order to increase the detail, different regions of one area are usually defined. In these subareas or domains, different temporal and spatial resolutions are used. By this way, a major detail is obtained from a region with a minimal increase of the computational cost. Different domains established an order of levels or hierarchy where a 'mother' domain is defined. Smaller domains use the outputs of the bigger domains as their initial and boundary conditions of the atmosphere. *Two-way nesting* is established when the results of smaller domain are allowed to influence simulation in the bigger domain.

- **Coupling:** In some studies have been started to couple atmospheric models to other

numerical models such as ocean in the global clime models such as: HadCAM, runoff (Amengual et al., 2007) or contaminant dispersion (Grell et al., 2000).

In spite of the impossibility to solve all the factors and processes involved in the atmosphere, the results of the models are reasonably good (Buzzi and Tibaldi, 1978; Alpert et al., 1995; Leslie et al., 1998; Lagouvardos et al., 1999; Pytharoulis et al., 2000; Wisse and de Arellano, 2004) and their results are improving in time (WMO, 2002). Dynamics of the phenomena obtained from numerical simulations seem to be quite similar to the phenomena that occurred in the atmosphere. Numerical results of the models are quite well corresponded with the observations and measurements. There are basically two elements that avoid a complete success of the numerical models: lack of knowledge and technical computational limitations. Moreover, it must bear in main the strong non-linear behaviour of the atmosphere (with a fractal dimensionless bigger than 6 Lorenz (1991); Zeng et al. (1992)) makes impossible a perfect numerical simulation of the system (Lorenz, 1963). In some cases, major aspects of the atmosphere are actually significantly well simulated. However, small scale events such as; localisation and value of strong precipitation, tornadoes or fog are sometimes not well captured. Unfortunately most of severe weather episodes are related to small scale aspects of some events. This fact must aim to improve numerical atmospheric models allowing a correct forecast of these phenomenas. During recent years, a statistical use of atmospheric models has been made. It is assumed that forecast statistics of an ensemble of different simulations (using multi model, multi physical, perturbed or other ways of generation of the members) of the same phenomena will provide a better result that an unique simulation (Toth and Kalnay, 1993; Molteni et al., 1996; Toth and Kalnay, 1997; WMO, 2006).

2.1.1 MM5

Equations

MM5 model (last version 3.7, Grell et al., 1995) is a mesoscale nonhydrostatic primitive equation limited area model. Numerical solution of the equations is done by the finite differences method and it allows two-way nested coupling between different domains. MM5 solves the *Primitive equations* in a vertical terrain following coordinates (x,y,σ). Vertical coordinate σ is defined following the orography of the domain (see equation 2.1.1).

$$\sigma = \frac{p - p_{top}}{p_{surf} - p_{top}} \tag{2.1.1}$$

where p, pressure; p_{top}, highest pressure value; p_{surf}, surface pressure. σ takes the interval between 0 (top) and 1 (surface). The dry version of the equations are discussed.

- **pressure**

$$\frac{\partial p'}{\partial t} - \rho_0 g w + \gamma p \nabla \cdot \vec{V} = -\vec{V} \cdot \nabla p' + \frac{\gamma p}{T}\left(\frac{\dot{Q}}{C_p} + \frac{T_0}{\theta_0} D_\theta\right) \tag{2.1.2}$$

where p', nonhydrostatic perturbation of the hydrostatic pressure (p_0, $p = p_0 + p'$)). Hydrostatic pressure presents a lineal relation with the density (ρ), gravity (g) and with differential of height (δz), [according to $\delta p = -\rho_0 g \delta z$]; ρ_0, hydrostatic density; g, gravity; w, vertical velocity; $\gamma = C_p/C_v$; $C_{p(v)}$, thermal capacity of the air preserving pressure(volume); $\vec{V} = (u, v, \dot{\sigma})$, speed vector; $\nabla = (\partial_x, \partial_y, \partial_\sigma)$, differential operator; $\dot{Q}$, heat changes with the environment; T_0, temperature of the buoyancy term ($\rho_0 = p_0/R_d T_0$); θ_0, potential temperature of reference; D_θ, viscosity and turbulent dissipation term of heat. This equation establishes a relation of the temporal variations of pressure (Ist term in the left) with: updrafts/downdrafts of the fluid ($\rho_0 g w$), convergence/divergence ($\gamma p \nabla \cdot \vec{V}$), pressure advections ($-\vec{V} \cdot \nabla p'$) and thermal variations (last term of equation)

- **Momentum** $u = \vec{V} \cdot \hat{e}_x$ (x component of the speed)

$$\begin{aligned}\frac{\partial u}{\partial t} + \frac{m}{\rho}\left(\frac{\partial p'}{\partial x} - \frac{\sigma}{p^*}\frac{\partial p^*}{\partial x}\frac{\partial p'}{\partial \sigma}\right) &= -\vec{V} \cdot \nabla u + v\left(f + u\frac{\partial m}{\partial y} - v\frac{\partial m}{\partial x}\right) \\ &- ew\cos\alpha - \frac{uw}{r_{earth}} + D_u \end{aligned} \tag{2.1.3}$$

where m: map scale factor; $p^* = p_{surf} - p_{top}$, pressure differences (σ coordinates); f, Coriolis term; $u\frac{\partial m}{\partial y}, v\frac{\partial m}{\partial x}, r_{earth}$, terrestrial curvature terms; $e = 2\Omega\cos\lambda$, Coriolis component (λ, latitude); $\alpha = \phi - \phi_c$, ϕ longitude, ϕ_c, central longitude; D_u, dissipative term due to friction and turbulence following $\hat{e}_x$ direction. From the equation is obtained that the variations of the momentum in the $\hat{e}_x$ direction are made by variations on the pressure field (IInd term), advection of the momentum ($\vec{V} \cdot \nabla u$, nonlinear term), variations respect to the curvature (terms with ∂m and r_{earth}) and as a reflect of rotation of the Earth (terms of Coriolis, fu and $ew\cos\alpha$)

- **Momentum** $v = \vec{V} \cdot \hat{e}_y$ (y component of the velocity)

$$\begin{aligned}\frac{\partial v}{\partial t} + \frac{m}{\rho}\left(\frac{\partial p'}{\partial y} - \frac{\sigma}{p^*}\frac{\partial p^*}{\partial y}\frac{\partial p'}{\partial \sigma}\right) &= -\vec{V} \cdot \nabla v - u\left(f + u\frac{\partial m}{\partial y} - v\frac{\partial m}{\partial x}\right) \\ &+ ew\sin\alpha - \frac{vw}{r_{earth}} + D_v \end{aligned} \tag{2.1.4}$$

- **Momentum** $w = \vec{V} \cdot \hat{e}_\sigma$ (z(σ) component of the velocity)

$$\begin{aligned}\frac{\partial w}{\partial t} - \frac{\rho_0}{\rho}\frac{g}{p^*}\frac{\partial p'}{\partial \sigma} + \frac{g}{\gamma}\frac{p'}{p} &= -\vec{V} \cdot \nabla w + g\frac{p_0}{p}\frac{T'}{T_0} - \frac{gR_d}{C_p}\frac{p'}{p} + e(u\cos\alpha - v\sin\alpha) \\ &+ \frac{u^2 + v^2}{r_{earth}} + D_w \end{aligned} \tag{2.1.5}$$

where R_d, universal constant for dry air.

- **Thermodynamics**

$$\frac{\partial T}{\partial t} = -\vec{V} \cdot \nabla T + \frac{1}{\rho C_p}\left(\frac{\partial p'}{\partial t} + \vec{V} \cdot \nabla p' - \rho_0 g w\right) + \frac{\dot{Q}}{C_p} + \frac{T_0}{\theta_0} D_\theta \tag{2.1.6}$$

Thermal variations are derived from thermal advections ($\vec{V} \cdot \nabla T$), dynamics of the fluid (IInd term), heat fluxes ($\dot{Q}/C_p$) and frictional and turbulence dissipative effects (last term)

- Expansion of the advective terms

$$\begin{aligned} \vec{V} \cdot \nabla \chi &\equiv mu\frac{\partial \chi}{\partial x} + mv\frac{\partial \chi}{\partial y} + \dot{\sigma}\frac{\partial \chi}{\partial \sigma} \\ \dot{\sigma} &= -\frac{\rho_0 g}{p^*}w - \frac{m\sigma}{p^*}\frac{\partial p^*}{\partial x}u - \frac{m\sigma}{p^*}\frac{\partial p^*}{\partial y}v \end{aligned} \tag{2.1.7}$$

Advective terms 2.1.7 add a coupled and nonlinear term in the equations. It is expanded and solved at the second order.

- Divergence term expansion is shown in equation 2.1.8

$$\begin{aligned} \nabla \cdot \vec{V} &= m^2\frac{\partial}{\partial x}\left(\frac{u}{m}\right) - \frac{m\sigma}{p^*}\frac{\partial p^*}{\partial x}\frac{\partial u}{\partial \sigma} + m^2\frac{\partial}{\partial y}\left(\frac{v}{m}\right) - \frac{m\sigma}{p^*}\frac{\partial p^*}{\partial y}\frac{\partial v}{\partial \sigma} \\ &- \frac{\rho_0}{p^*}g\frac{\partial w}{\partial \sigma} \end{aligned} \tag{2.1.8}$$

- Difussion terms
In order to control growing of nonlinear instabilities and remove small scale computational noise, an experimental diffusion scheme is used (Grell et al., 1995; Xu et al., 2001; Zängl, 2002) in all the tendencies of the prognostic variables ($\nabla_t \chi$). In MM5 horizontal second order diffusion is applied in the boundaries of the coarse domain and fourth-order diffusion at the inner points. Another second-order vertical diffusion term is also applied on the physical sub-grid transport following mixing-length theory. The second order form of the horizontal diffusion term is

$$F_{H2\alpha} = p^* K_H \vec{\nabla}^2_\sigma \chi \tag{2.1.9}$$

where χ, any prognostic variable at level σ, $p^* = p_{sfc} - p_{top}$, pressure different between surface and top level; K_H, diffusion coefficient. The fourth-order form is

$$F_{H4\alpha} = p^* K'_H \vec{\nabla}^4_\sigma \chi \tag{2.1.10}$$

Fourth-order diffusion term is applied on any prognostic variable (χ) at all sigma levels that there is not any intersection with the lower-most half-sigma surface at any grid point. $\vec{\nabla}^2, \vec{\nabla}^4$ are applied on sigma constant surfaces. It is established the relation between diffusion coefficients of different order,

$$K_H^{'} = \Delta s^2 K_H \tag{2.1.11}$$

Second order diffusion coefficient K_H (see equation 2.1.12) is obtained according to a background value K_{HO} accompanied with a term proportional to the deformation of the flow.

$$K_H = K_{HO} + 0.5k^2(\Delta s)^2 \left[\left(\frac{\partial u}{\partial x} - \frac{\partial v}{\partial y} \right)^2 + \left(\frac{\partial v}{\partial x} + \frac{\partial u}{\partial y} \right)^2 \right]^{1/2} \tag{2.1.12}$$

where $K_{HO} = 3.0 \times 10^{-3}(\Delta x)^2/\Delta t$ and to ensure computational stability a upper limit has been imposed $K_H \leq (\Delta x)^2/(64\Delta T)$ in MM5v3.7 version; Δx, horizontal grid distance; k, von Kármán constant, Δt, temporal increment. Has been shown how the background term is dominant at all levels and locations in contrast to the deformation term (Xu et al., 2001).

Land Use data type

MM5 numerical model simulates with three different classifications of terrain: old 13 (PSU/NCAR), USGS (see table 2.1.b for the 24 categories of vegetation data from U.S. Geological Survey - USGS[3] specifications used in MM5 model) and SiB (North-American 17-category data used by Simple Biosphere model, from USGS). At the same time, MM5 model works with different classifications of soil data. Both tables are provided at different resolutions from 1 terrestrial degree (about 111.0 km) to 30 sec. (about 0.925 km)

Cumulus Schemes

These schemes determine the subgrid processes that occur within a cumulus cloud, like vertical fluxes, transportation between cloud species and convective rainfall. Convection is activated for a given trigger and need a closure in order to determine the strength. MM5 has 7 different cumulus schemes with different uses, purposes and approximations (see stable 2.1.c. This scheme can not be activated for grid lengths smaller than 5 km. In this case, cumulus processes are simulated directly by the primitive equations.

[3] `http://www.usgs.gov/`

Table 2.1.b: Characteristics of the 24 USGGS vegetation categories used in MM5. albedo (%, third column), moisture available (%, 4th col.), surface emissivity (% at 9 μm, 5th col.), roughness length (cm, 6th col.) and thermal inertia ($cal\ cm^{-2}k^{-1}s^{-1/2}$, 7th col.) For the Summer (15th April - 15th October, first sub-col) and winter (15 October - 15 April, second sub-col). Source MM5 model notes

Number	**Vegetation Description**	**Albedo** (%)		**Moisture Avail.** (%)		**Sfc. Emissivity** (% at 9 μm)		**Roughness Length** (cm)		**Thermal Inertia** ($cal\ cm^{-2}k^{-1}s^{-1/2}$)	
		Sum	Win	Sum	Win	Sum	Win	Sum	Win	Sum	Win
1	Urban and Built-Up Land	15	15	10	10	88	88	80	80	0.03	0.03
2	Dryland Cropland and Pasture	17	23	30	60	98.5	92	15	5	0.04	0.04
3	Irrigated Cropland and Pasture	18	23	50	50	98.5	92	15	5	0.04	0.04
4	Mixed Dryland/Irrigated Cropland and Pasture	18	23	25	50	98.5	92	15	5	0.04	0.04
5	Cropland/Grassland Mosaic	18	23	25	40	99	92	14	5	0.04	0.04
6	Cropland/Woodland Mosaic	16	20	35	60	98.5	93	20	20	0.04	0.04
7	Grassland	19	23	15	30	98.5	92	12	10	0.03	0.04
8	Shrubland	22	25	10	20	88	88	10	10	0.03	0.04
9	Mixed Shrubland/Grassland	20	24	15	25	90	90	11	10	0.03	0.04
10	Savanna	20	20	15	15	92	92	15	15	0.03	0.03
11	Deciduous Broadleaf Forest	16	17	30	60	93	93	50	50	0.04	0.05
12	Deciduous Needleleaf Forest	14	15	30	60	94	93	50	50	0.04	0.05
13	Evergreen Broadleaf Forest	12	12	50	50	95	95	50	50	0.05	0.05
14	Evergreen Needleleaf Forest	12	12	30	60	95	95	50	50	0.04	0.05
15	Mixed Forest	13	14	30	60	94	94	50	50	0.04	0.06
16	Water Bodies	8	8	100	100	98	98	.01	.01	0.06	0.06
17	Herbaceous Wetland	14	14	60	75	95	95	20	20	0.06	0.06
18	Wooded wetland	14	14	35	70	95	95	40	40	0.05	0.06
19	Barren or Sparsely Vegetated	25	25	2	5	85	85	10	10	0.02	0.02
20	Herbaceous Tundra	15	60	50	90	92	92	10	10	0.05	0.05
21	Wooden Tundra	15	50	50	90	93	93	30	30	0.05	0.05
22	Mixed Tundra	15	55	50	90	92	92	15	15	0.05	0.05
23	Bare Ground Tundra	25	70	2	95	85	95	10	5	0.02	0.05
24	Snow or Ice	55	70	95	95	95	95	5	5	0.05	0.05

Table 2.1.c: Main characteristics of the MM5v3 cumulus schemes

Scheme name	**Main characteristics**	**Recomm. resol. (km)**
Anthes-Kuo	driven by moisture convergence (M_t) parametrised heating and moistening profiles moistening depends on RH critical threshold $M_t \geq 3. \times 10^{-6} kgm^{-2}s^{-1}$ cloud-depth $\Delta\sigma \geq 0.3$	> 30
Grell	simple scheme driven by compensation of mass flux clouds as stability agents steady-state updraft and downdraft circulations mixing with environment at top and bottom	10-30
Arakawa-Schubert	Three parts: static, dynamic, feedback Multi-cloud scheme with updrafts and downdrafts cloud population	> 30
Fritsch-Chappel	driven by temporal releasing of instability (CAPE) representation of up/downdrafts Mass-flux type compensation scheme	20-30
Kain-Fritsch	sofisticated scheme up/downdraft given by cloud-mixing temporal releasing of CAPE mass-flux considerations	
Betts-Miller	relaxation following a post-convective sounding no explicit downdrafts	> 30
Kain-Fritsch 2	Improvement of Kain-Fritsch Add Shallow convection	

The Kain-Fritsch scheme (Kain and Fritsch, 1990, 1993) and its improved version (Kain, 2004) is one of the most used cumulus parameterisation in the *Grup de Meteorologia del departament de física de les Illes Balears* (UIB-Meteo. group). It is structured (following brief description of Kain (2004)) in three parts: the convective triggering func-

tion, the mass flux formulation and the closure assumptions.

- *The trigger function:* A parcel of air is obtained from a vertical mixing following adjacent layers from surface until 60 hPa. Lifted condensation level for this parcel (T_{LCL}) is compared to the environmental one (T_{ENV}) (usually $T_{LCL} \leq T_{ENV}$). According to the observational suggestion that environment makes easier convection, a relation between thermal perturbation (δT_{vv}) of the parcel and the grid resolving vertical motion is established (with a vertical threshold value). A potential convective parcel of air will be given by this parcel of air, that its mixed temperature and the grid-resolved derived anomaly becomes higher (positive buoyancy) than the environmental temperature ($T_{LCL} + \delta T_{vv} > T_{ENV}$). Vertical velocity of the upper part of the LCL is computed at each layer following a Lagrangian methodology that includes environmental effects. Deep convection will be activated when the Lagrangian computed vertical velocity keeps positive until a cloud height of about 3-4 km. In case of fail values, this methodology is repeated following an iterative process in which iterative parcels are recomputed according to the elevation of its lowest layer until a threshold of 300 hPa.

- *Mass flux computation:* A steady-state entraining-detraining plume model for the equivalent potential temperature (θ_e) and water vapour q_v will determine the convective updrafts in the scheme. Plume model establishes that high(low) parcel buoyancy and moist(dry) environment promotes entrainment(detainment). Convective downdrafts are lived on a fraction of evaporation of the total condensate generated within the updraft. This fraction of evaporation is given by precipitation efficiency and established the mass relative magnitudes between up/downdrafts according to other downdrafts parameters such as: starting/ending levels, relative humidity profile and characteristics and amounts of entrained air. Downdraft is finished when it reaches the surface or it becomes warmer than its environment. Finally the net convective mass flux (defined as the compensation between environment and transports within up/downdrafts) at any level of the column is established to be zero.

- *Closure:* Closure assumptions are reached when 90% of CAPE of the column is removed according to balance of environmental mass fluxes and up/downdrafts. CAPE is computed within the convective parcel and is vanished by a combination of lowering θ_e in the convective parcel and warming the environment aloft. The convective time scale (within the limits of 1/2 and 1 hour) is determined according to the advective time scale in the cloud layer. Scheme has a feedback effect on the tendency of temperature, water vapour and cloud water mixing ratios.

Planetary Boundary Layer schemes

Planetary boundary layer (commonly referred as PBL) describes the first levels of the atmosphere in contact with the surface (Stull, 1988). It presents a variable range of

dimensions and usually the air in this layer presents turbulent characteristics. Under turbulent dynamics, from which the flow presents unpredictable fluctuations in the three directions of the flow, has powerful mixing properties. PBL is a clear example of the utility of the schemes in the numerical weather models, since it has not been completely resolved. In contrast to the general fluid mechanic equations, a complete set of equations that could explain the turbulence have not been already proposed. Some assumptions and approximations are done in order to provide a properly way to complete the set of equations that try to describe the turbulence. These approximations and assumptions can vary significantly and are derived from the observations. Therefore, PBL schemes can present significant differences. MM5 model has 7 PBL schemes (see table 2.1.d).

In the UIB-Meteo. group, Eta (Janjić, 1990, 1994) and MRF (Troen and Mahrt, 1986; Hong and Pan, 1996) schemes are the most used PBL schemes. A short description of each scheme is given:

- **MRF:** Regime conditions of the PBL are given by $|z_h/L|$, z_h, height of the mixed layer (determined by the bulk Richardson number, equation 2.1.14, $\mathcal{B}_r$); L, Monin-Obukhov length (see equation 2.1.15), in terms of the momentum diffusivity $\mathcal{K}_m$ (equation 2.1.13).

$$\mathcal{K}_m = u_* k z \Phi_m^{-1} \left(1 - \frac{z}{h}\right)^P \tag{2.1.13}$$

$$h = \mathcal{R}_i \frac{T_0 |\vec{v}(h)|^2}{g(\theta_v(h) - \theta_0)}, \quad \begin{cases} \mathcal{R}_i = \dfrac{\dfrac{g}{\overline{\theta}_v}\dfrac{\partial \overline{\theta}_v}{\partial z}}{\left[\left(\dfrac{\partial \overline{U}}{\partial z}\right)^2 + \left(\dfrac{\partial \overline{V}}{\partial z}\right)^2\right]} \\ \mathcal{B}_r = \dfrac{g \Delta \overline{\theta}_v \Delta z}{\overline{\theta}_v [(\Delta \overline{U})^2 + (\Delta \overline{V})^2} \end{cases} \tag{2.1.14}$$

$$L = \frac{-\overline{\theta_V} u_*^3}{k g (\overline{w' \theta_V'})_s} \tag{2.1.15}$$

where u_*, surface friction velocity, k von Kármán constant, Φ_m, nondimensional shear, z, height above ground and h boundary layer height; $\overline{\theta}_v$, averaged value of virtual temperature; $\overline{U}, \overline{V}$, averaged values of wind speed, $(\overline{w' \theta_V'})_s$, vertical turbulent flux of temperature fluctuations at the surface

  - Stability: $\Phi_m = 1 + \dfrac{4.7z}{L}$

Table 2.1.d: Brief description of MM5v3 PBL schemes

Name	**Characteristics**	**Vertical resolution**
Bulk	two regimes: stable, unstable bulk coefficients	coarse ($\delta z > 250\ m$)
High-Resolution Blackdadar	four stability regimes nonlocal mixing implicit vertical diffusion scheme driven by Monin-Obukhov similarity	high
Burk-Thompson	prediction of TKE local vertical mixing not call SLAB Louis scheme for surface exchange coefficients	coarse/high
Eta	prediction of TKE local vertical mixing driven by Monin-Obukhov similarity allow use of Noah-LSM surface scheme 2.5 order scheme	high
MRF	countergradient transport theorem nonlocal mixing driven by bulk Richardson number allow use of Noah-LSM surface scheme implicit vertical diffusion scheme	high
Gayno-Seaman	prediction of TKE conservation of liquid-water potential temperature allow coupling between cloud-topped PBL better for saturated situations	high
Pleim-Chang	based on Blackadar scheme can only be used with Pleim-Xiu LSM surface scheme asymmetric convective model	high

- Instability: $\Phi_m = (1 + \frac{7z}{L})^{-1/3}$

1. $\mathcal{B}_r \geq 0.2$ Nighttime stable conditions
2. $0.0 < \mathcal{B}_r < 0.2$ Damped mechanical turbulent conditions
3. $\mathcal{B}_r = 0.2$ Forced convection conditions
4. $\mathcal{B}_r < 0.0$ Free convection conditions

Surface temperature is computed according to a *scaled virtual temperature excess* as follows:

$$\theta_T = C\frac{(\overline{w'\theta'_v})_0}{w_s h} \tag{2.1.16}$$

Eady diffusivities of moist (q), momentum (m; u and v) and temperature (t) are computed following the Prandtl number ($\mathcal{P}r$, equation 2.1.17) imposing that heat and momentum fluxes match at the top of the surface layer

$$\mathcal{P}r = \frac{\mathcal{K}_t}{\mathcal{K}_m} = \left[\frac{\Phi_t}{\Phi_m}\left(\frac{z}{L}\right) + k\frac{z}{h}C\right]^{-1} \tag{2.1.17}$$

where Φ_m, Φ_t, momentum (m) and humidity/temperature (t) adimensional gradients with a nonlinear term in the formulation of the fluxes. k approach (Louis, 1979) is applied for the diffusion in the free atmosphere, keeping the diffusion in the free atmosphere:

- $\mathcal{R}ig > 0$, stably stratified free atmosphere; $f_{m,t}(\mathcal{R}ig) = e^{-8.5\mathcal{R}ig} + \frac{0.15}{\mathcal{R}ig + 3.0}$, and $\mathcal{P}r = 1.5 + 3.08\mathcal{R}ig$
- $\mathcal{R}ig \leq 0$, neutral and unstably stratified free atmosphere; same as in previous regime but replacing in $\Phi_m, \Phi_t(z/L) \rightarrow \Phi_m, \Phi t(\mathcal{R}ig)$.

where $\mathcal{R}ig = (g/T)(\partial\theta_v/\partial z)(|\partial U/\partial z|)^{-2}$, local gradient Richardson number. MRF becomes very sensible to the surface fluxes (heat and evaporation) and water content of the surface.

- **Eta:** The 2.5 dimensional local mixing model governed by turbulent kinetic energy (TKE) is described by the system of equations as follows as in (Mellor and Yamada,

1982):

$$\begin{cases} \frac{d}{dt}\frac{q^2}{2} - \frac{\partial}{\partial z}\left[\ell_q S_q \left(\frac{\partial}{\partial z}\frac{q^2}{2}\right)\right] = \mathcal{P}_s - \mathcal{P}_b - \epsilon \\ \mathcal{P}_s = -\overline{wu}\left(\frac{\partial U}{\partial z}\right) - \overline{wv}\left(\frac{\partial V}{\partial z}\right) \\ \mathcal{P}_b = \beta g \overline{w\theta_v},\ \epsilon = \frac{q^3}{B_1 \ell} \\ -\overline{wu} = \mathcal{K}_M \frac{\partial U}{\partial z},\ -\overline{wv} = \mathcal{K}_M \frac{\partial V}{\partial z} \\ -\overline{w\theta_v} = \mathcal{K}_H \frac{\partial \Theta_v}{\partial z},\ -\overline{ws} = \mathcal{K}_H \frac{\partial S}{\partial z} \\ \mathcal{K}_M = \ell_q S_M,\ \mathcal{K}_H = \ell_q S_H \\ S_M(6A_1A_2G_M) + S_H(1 - 3A_2B_2G_H - 12A_1A_2G_H) = A_2 \\ S_M(1 + 6A_1^2G_M - 9A_1A_2G_H) - S_H(12A_1^2G_H + 9A_1A_2G_H) = A_1(1 - 3C_1) \\ G_M = \frac{\ell^2}{q^2}\left[\left(\frac{\partial U}{\partial z}\right)^2 + \left(\frac{\partial V}{\partial z}\right)^2\right],\ G_H = -\frac{\ell^2}{q^2}\beta g \frac{\partial \Theta_v}{\partial z} \end{cases} \tag{2.1.18}$$

where $S_q, \beta, A_1, A_2, B_1, B_2, C_1$, empirical constants; $q^2/2$, ℓ, master length. Capital letters is for motions resolved by the dynamical part of the model, and lower case are for the turbulent fluctuations. v, denotes virtual potential temperature; S passive quantity. $\mathcal{K}_M, \mathcal{K}_H$, vertical turbulent exchange coefficients for momentum (M) and heat (H). $\mathcal{P}_S, \mathcal{P}_b$, production of the TKE by shear (S) and buoyancy (b); ϵ, dissipation; in order to avoid zero determinant the following thresholds are imposed: $G_H \leq 0.0024$ and $G_M \leq 0.36 - 16G_H$. Master length scale ℓ is computed as follows:

$$\begin{cases} \ell = \frac{\ell_0 kz}{\ell_0 + kz} \\ \ell_0 = \alpha \frac{\int_{P_{sfc}}^{P_{top}} dq\ |z| q}{\int_{P_{sfc}}^{P_{top}} dq\ q} \\ \lim_{z\to 0} \ell = kz \\ \lim_{z\to\infty} \ell = k \\ \ell \leq \ell_{max} = 0.53q\left(\beta g \frac{\partial \Theta}{\partial z}\right)^{-1/2} + H \end{cases} \tag{2.1.19}$$

where α, empirical constant; $P_{top/sfc}$, top and surface pressures; k, von Kármán constant. An improvement of the model has been applied (Janjić, 1994), in which a marine viscous sublayer has been defined and an upper level limit has been imposed in to the master length scale ℓ_{max}; H, constant. Boundary layer height is fixed

according to the drop of TKE for a specific threshold:

$$\begin{cases} 0.5min(0.6, TKE_{max}) & TKE_{max} > 1.2 \\ kL & TKE_{max} < 0.4 \end{cases} \tag{2.1.20}$$

Owing to the vertical differences of mixing between Eta and MRF schemes, significant differences between characteristics of the simulated PBL are obtained. It has been shown how the nonlocal or local vertical mixing properties can affect processes such as strong convective rain over land (Hong and Pan, 1996; Wisse and de Arellano, 2004) or even tropical-like systems such as medicanes (Fita et al., 2008a).

One of the most relevant difference between simulated PBL is the strength of the mixing developed within the layer. MRF scheme (similar characteristics presents Blackadar scheme, Fita et al. (2008a)), show stronger rates of mixing than Eta scheme. At the same time, diurnal cycle of the boundary layer (PBL characteristics during day and night in one day) is much more marked in the nonlocal mixing scheme than in Eta scheme. Wisse and de Arellano (2004) found that Eta capping inversion at the top of the boundary layer is stronger than in the MRF scheme.

Table 2.1.e: Brief description of MM5v3 moist microphysics schemes

Name	**Characteristics**
Dry	no vapour or clouds
Stable Precipitation	grid saturation immediately as rain nonconvective precipitation no rain evaporation no cloud prediction
Warm Rain (Hsie)	cloud and rain are separated 3D fields no ice phase
Simple Ice (Dudhia)	adaptation with ice of Hsie scheme different arrays for ice, rain and snow no supercooled water snow melt at melting layer
Mixed-Phase (Reisner 1)	cloud ice and snow arrays same processes as Simple Ice supercooled water gradual melting of the snow
Goddard microphysics	prediction of graupel suitable for cloud-resolving models
Reisner 2 (graupel)	concentrations for graupel and ice suitable for cloud-resolving models strong improvements along MM5 versions
Schultz	ice and graupel simple and efficient

Explicit Moisture schemes

These schemes provide the information about the processes that occur between the water species that form the cloud. It also provides part of the resultant tendencies in the trends of the prognostic fields, as well as radiation information due to cloud formation. In MM5 model there are 8 schemes (see table 2.1.e).

Most used moisture scheme in the UIB-Meteo. group is the Reisner 2 (graupel) scheme (Reisner et al., 1998). Reisner2 model is specially designed to avoid the lack of accuracy in the determination of the supercooled liquid water (hereafter, SLW) in the winter storms over North America. It was started as a bulk rain model with mixing ratios of cloud water (q_c), rain (q_r), snow (q_s). Low predictions of SLW suggest the addition of a mixing ratio of cloud ice (q_i) and graupel (q_g) with the addition of a prediction of the

number concentration of cloud ice (N_i) with a prescribed prediction of the N_s and N_g as function of their precipitation rates $N_{o,s}$, $N_{o,g}$. Last improvement of the moist microphysics included explicit predictions of the N_s and N_g species with remarkable improvement in the simulations.

A brief description of the dynamics between species follows similar structure as in (Ikawa and Saito, 1991):

- **Prognostic mixing ratios**

$$\left\{\begin{array}{lll}
\dfrac{\partial q^* q_v}{\partial t} & = & -\mathcal{ADV}(p^* q_v) + \mathcal{DIV}(p^* q_v) + \mathcal{D}(q_v) + p^* \displaystyle\sum_{\ell}^{\Gamma(q_v)} \varsigma_\ell \mathcal{P}_\ell \\
\dfrac{\partial q^* q_c}{\partial t} & = & -\mathcal{ADV}(p^* q_c) + \mathcal{DIV}(p^* q_c) + \mathcal{D}(q_c) + p^* \displaystyle\sum_{\ell}^{\Gamma(q_c)} \varsigma_\ell \mathcal{P}_\ell \\
\dfrac{\partial q^* q_r}{\partial t} & = & -\mathcal{ADV}(p^* q_r) + \mathcal{DIV}(p^* q_r) + p^* \displaystyle\sum_{\ell}^{\Gamma(q_r)} \varsigma_\ell \mathcal{P}_\ell - \mathcal{P}_{rprc} \\
\dfrac{\partial q^* q_i}{\partial t} & = & -\mathcal{ADV}(p^* q_i) + \mathcal{DIV}(p^* q_i) + \mathcal{D}(q_i) + p^* \displaystyle\sum_{\ell}^{\Gamma(q_i)} \varsigma_\ell \mathcal{P}_\ell \\
\frac{\partial q^* q_s}{\partial t} & = & -\mathcal{ADV}(p^* q_s) + \mathcal{DIV}(p^* q_s) + p^* \displaystyle\sum_{\ell}^{\Gamma(q_s)} \varsigma_\ell \mathcal{P}_\ell - \mathcal{P}_{sprc} \\
\dfrac{\partial q^* q_g}{\partial t} & = & -\mathcal{ADV}(p^* q_g) + \mathcal{DIV}(p^* q_g) + p^* \displaystyle\sum_{\ell}^{\Gamma(q_g)} \varsigma_\ell \mathcal{P}_\ell - \mathcal{P}_{gprc}
\end{array}\right. \tag{2.1.21}$$

- **Prognostic number concentrations**

$$\left\{\begin{array}{lll}
\dfrac{\partial p^* N_i}{\partial t} & = & -\mathcal{ADV}(p^* N_i) + \mathcal{DIV}(p^* N_i) + \mathcal{D}(N_i) + p^* \left\{ \displaystyle\sum_{\ell}^{\Xi(N_i)} N_\ell + \dfrac{\rho}{m_{io}} \displaystyle\sum_{\ell}^{\Phi(N_i)} \mathcal{P}_\ell \right. \\
 & & \left. - \dfrac{N_i}{q_i} \displaystyle\sum_{\ell}^{\Psi(N_i)} \mathcal{P}_\ell \right\} \\
\dfrac{\partial p^* N_s}{\partial t} & = & -\mathcal{ADV}(p^* N_s) + \mathcal{DIV}(p^* N_s) + p^* \left\{ \displaystyle\sum_{\ell}^{\Xi(N_s)} N_\ell + \dfrac{\rho}{m_{so}} \displaystyle\sum_{\ell}^{\Phi(N_s)} \mathcal{P}_\ell \right. \\
 & & \left. - \dfrac{N_s}{q_s} \displaystyle\sum_{\ell}^{\Psi(N_s)} \mathcal{P}_\ell \right\} - N_{sprc} \\
\dfrac{\partial p^* N_g}{\partial t} & = & -\mathcal{ADV}(p^* N_g) + \mathcal{DIV}(p^* N_g) + p^* \left\{ \displaystyle\sum_{\ell}^{\Xi(N_g)} N_\ell + \dfrac{\rho}{m_{go}} \displaystyle\sum_{\ell}^{\Phi(N_g)} \mathcal{P}_\ell \right. \\
 & & \left. - \frac{N_g}{q_g} \displaystyle\sum_{\ell}^{\Psi(N_g)} \mathcal{P}_\ell \right\} - N_{gprc}
\end{array}\right. \tag{2.1.22}$$

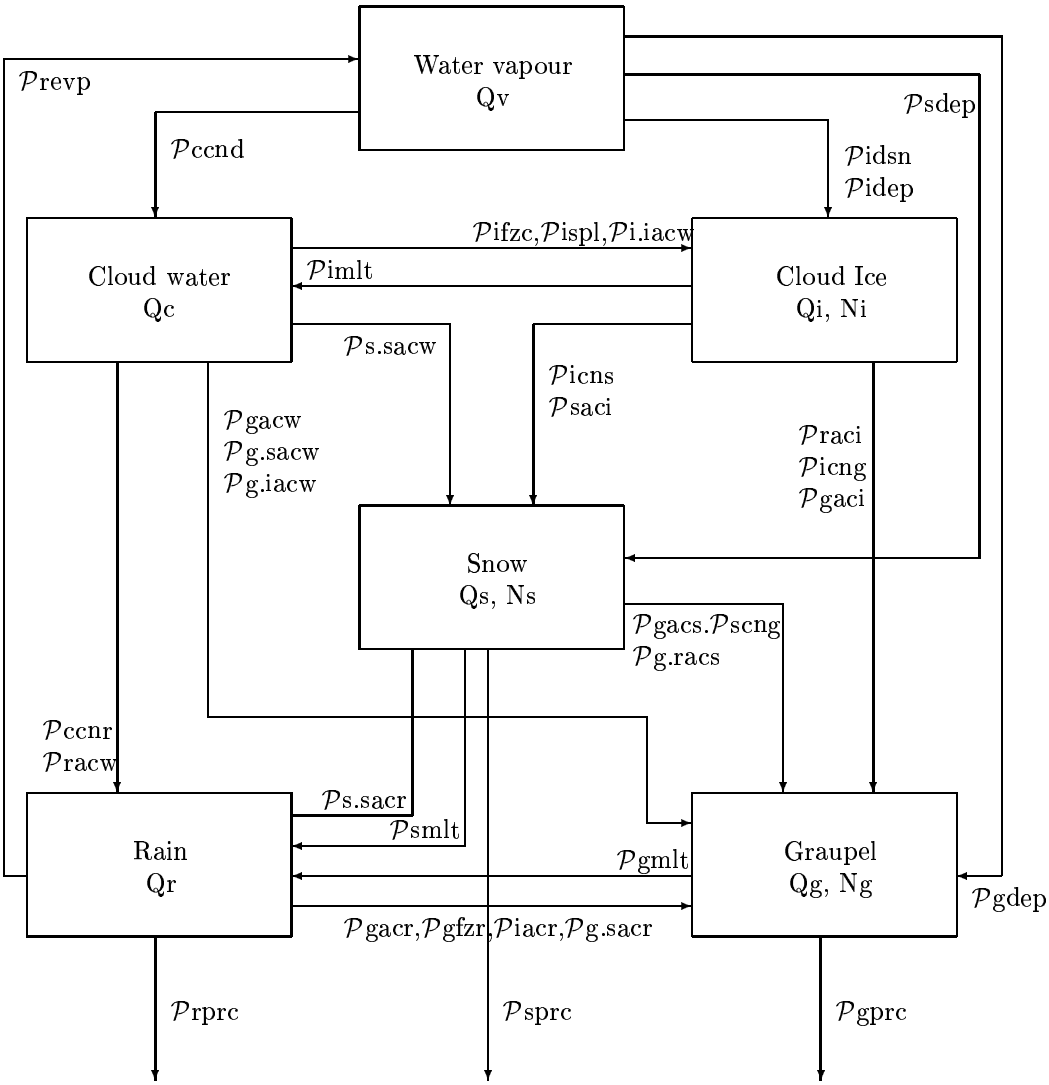

Figure 2.1.1: Schematic representation of the processes between species contained in the Reisner2(graupel) explicit moisture scheme of the MM5 model according to Ikawa and Saito (1991) formulation. Abbreviations for the species χ are: χdep, depositional growth; χmlt, melting; χprc, precipitation; χag, aggregation; χcn$\aleph$, conversion of χ to $\aleph$; χfz$\aleph$, freezing of $\aleph$ to χ; χac$\aleph$, collection of $\aleph$ by χ; χ.$\aleph$acγ, generation of χ as result of collection of γ by $\aleph$; idsn, initiation of q_i; ispl, ice multiplication processes

where, $p^* = p_{sfc} - p_{top}$, pressure differences between surface and top; $\mathcal{D}$, diffusion on subgrid-scale turbulence; $\mathcal{ADV}, \mathcal{DIV}$ 3-dimensional advection and divergence terms (equation 2.1.23, m, map scale factor, $\sigma = (p - p_{top})/p^*$, terrain-following vertical coordinate). $\mathcal{P}_\ell$, source/sink mass terms; $\mathcal{N}_\ell$, source/sink number terms than can be: depositional growth, melting, precipitation, aggregation, conversion, freezing, collection, generation as result of a collection and ice initiation and multiplication processes. As example: $\mathcal{P}_{rprc}$, precipitation of cloud water. Γ, Ξ, Φ, Ψ, processes related to source/sink of each species.

$$\begin{cases} \mathcal{ADV}(p^*\chi) = m^2 \left(\dfrac{\partial p^* u\chi/m}{\partial x} + \dfrac{\partial p^* v\chi/m}{\partial y} \right) + \dfrac{\partial p^* \chi \dot{\sigma}}{\partial \sigma} \\ \mathcal{DIV} = m^2 \left(\dfrac{\partial p^* u/m}{\partial x} + \dfrac{\partial p^* v/m}{\partial y} \right) + \dfrac{\partial p^* \dot{\sigma}}{\partial \sigma} \end{cases} \tag{2.1.23}$$

- **Size distribution**

$$\begin{aligned} N_\chi = \frac{N_{o,\chi}}{\lambda_\chi},\ \rho Q\chi &= \int_0^\infty dD\chi\ \rho_\chi \frac{\pi}{6} D\chi^3 N_{o,\chi} exp\left(-\lambda\chi D\chi\right) \\ &= \frac{\pi \rho_\chi N_{o,\chi}}{\lambda\chi^4} \begin{cases} N_{o,\chi} = N_\chi \left(\dfrac{\pi \rho_\chi N_\chi}{\rho q_\chi} \right)^{1/3} \\ \lambda_\chi = \left(\dfrac{\pi \rho_\chi N_\chi}{\rho q_\chi} \right)^{1/3} \end{cases} \end{aligned} \tag{2.1.24}$$

where, ρ_χ, density of an hydrometer ($\chi = (v, c, r, i, s, g)$); ρ, density of dry air. The changes in the number of concentration (N_χ) or mixing ratio ($\mathcal{P}_\chi$) of meteor χ due to precipitation is given by:

$$\begin{cases} N_{\chi prc} = -\dfrac{\partial \overline{U}_{n\chi} \rho g N_\chi}{\partial \sigma}, & \overline{U}_{n\chi} = \dfrac{a_\chi \Gamma(1 + b_\chi)}{\lambda_\chi^{b\chi}} \\ \mathcal{P}_{\chi prc} = -\dfrac{\partial \overline{U}_\chi \rho g q_\chi}{\partial \sigma}, & \overline{U}_\chi = \dfrac{a_\chi \Gamma(4 + b_\chi)}{6\lambda_\chi^{b\chi}} \end{cases} \tag{2.1.25}$$

where $\overline{U}_{n\chi}$, number-weighted terminal velocity; $\overline{U}_\chi$, mass-weighted terminal velocity; $g = 9.81\ ms^{-2}$, gravitational acceleration; a_χ, b_χ, constants. Precipitation terms are computed at each split time steps $\Delta t'$, ensuring numerical stability $\overline{U}_\chi \Delta t'/\Delta x < 1$, with the size of $\Delta t'$ based on the maximum value of $U_\chi \Delta t/\Delta z$ in the column where Δt, model time step.
Finally, each process of formation of species has its own expression. These processes are listed below for each species:

- ice: *nucleation, freezing of cloud droplets, multiplication process, depositional growth of cloud, riming growth of cloud*

- snow: *conversion from cloud ice, aggregation among, depositional growth and melting, collection of cloud ice*
- graupel: *conversion from cloud ice, generation by collisions between rain water and cloud ice, snow conversion, collisions between rain water and snow, generation via freezing of rain water, depositional growth and melting, production by collection of cloud water*
- rain: *conversion from cloud water, collection of cloud water, sublimation/evaporation*
- cloud water: *conversion from water vapour, melting of cloud ice*

In order to prevent zero values of some species, the total sum of source/sink terms are adjusted by the sum total of the rates. Negative values are considered as null values. Finally some constrains are imposed in some species:

$$\begin{cases} \textit{cloud ice} & \dfrac{0.5 \times \rho q_i}{0.8 m_{s,o}} < N_i < \dfrac{100 \rho q_i}{m_{i,o}} \\ \textit{snow} & \left(\dfrac{N_{o,s}}{1000}\right)^{3/4} \left(\dfrac{\rho q_s}{\rho_s \pi}\right)^{1/4} < N_s < (1000 N_{o,s})^{3/4} \left(\dfrac{\rho q_s}{\rho_s \pi}\right)^{1/4} \\ \textit{graupel} & 10^{-7} \times \left(\dfrac{\rho q_g}{m_{g,o}}\right) < N_g < 100 \times \left(\frac{\rho q_g}{m_{g,o}}\right) \end{cases} \tag{2.1.26}$$

Radiation schemes

These schemes provide the radiative effects in atmosphere (cloud interaction, clear sky and/or absorvation) radiative effects at surface (longwave absorbation/emission, albedo, surface fluxes) and thermal column tendencies due to vertical radiative flux divergence. MM5 has 4 radiation schemes and also it can be switched off. Main characteristics of these schemes are summarised in table 2.1.f.

Most used radiation scheme in the UIB-Meteo. group is the Cloud scheme (Dudhia, 1989).

This scheme computes the radiative effects in the vertical resolution of the model in vertical layers 50 hPa thick. The net absorption at each level results in radiative heating. It computes down/upward fluxes of longwave radiation (usually of terrestrial origin) and the downward flux of shortwave radiation (of solar origin), taking into account the solar angle. Resultant net flux at the ground is used for the land surface scheme. Each radiative flux is compute separately with the following characteristics:

- **Longwave scheme:** Temperature-dependent emissivity in clear-air follow an accurate fitting for the water vapour absorption bands in a clear-air conditions from

Table 2.1.f: Brief description of MM5v3 radiation schemes

Name	**Characteristics**	
None	no effects in the atmosphere surface still active	Surface radiation active in these two options
Simple cooling	cooling as function of temperature no cloud interaction no diurnal cycle climatological mean cooling profile surface still active	surface short/longwave flux for ground temperature uses total content of water vapour of the column uses RH to determine low/mid/high cloud fractions coarse grids or no microphysics
Cloud	atmospheric effects according to model cloud provides long/shortwave fluxes	
CCM2	multiple spectral short/longwave bands cloud treated on resolved ones or RH fraction suitable for coarse grid scales suitable for long time integrations provides surface radiative fluxes	
RRTM longwave	uses correlated-k model for the effects of absorption spectrum considering water vapour, CO_2 and O_3 can be combined with cloud-radiation shortwave scheme accurate and efficient	

polar to tropical ($\epsilon(u)$).

$$\begin{cases} \epsilon(u) = \sum_{i=0}^{i=4}(a_i + \overline{T}b_i)x^i \quad u \geq 10gm^{-2}, \quad x = ln(u) \\ \\ \epsilon(u) = \sum_{i=0}^{i=4}(c_i + \overline{T}d_i)y^i \quad u < 10gm^{-2}, \quad y = u^{1/2} \end{cases} \tag{2.1.27}$$

where u, water vapour path; $\overline{T}$, u-weighted $T - 250\ K$; a_i, b_i, c_i, d_i constants. At the tropics e-type absorption is included in the computation. It is missed cloud ceiling conditions from which an error of up to $20Wm^{-2}$ is made. Therefore Up/Downward fluxes at any layer are computed as:

$$F_{u/d} = \int_0^1 d\epsilon_{u/d}B(T) \tag{2.1.28}$$

where $B = \sigma T^4$, frequency-integrated Planck function; σ Stefan's constant. Clouds are assumed as horizontally uniform grey bodies (without wavelength preferences). Downward longwave flux on the top is assumed to be only from CO_2 stratospheric emission. Cloud liquid water (c), ice (i) and water vapour paths are derived from model data with absorption lengths of 60 m for 0.1 gm^{-3} cloud water to 3000 m for 0.1 gm^{-3} of rain water. CO_2 effects are on the infrared spectrum. Thus the band is divided (with a thermal dependency) in carbon/noncarbon spectrum. Each species has its own assumptions and characteristics. They are all together computed in order to obtain the total net emissivity (ϵ_{tot}).

$$\epsilon_{tot} = 1 - T_v T_c T_p \begin{cases} T_v = 1 - \epsilon_v & vapour \\ T_c = exp(-\alpha_c u_c) & cloud\ water \\ T_p = exp(-\alpha_p u_p) & rain\ \&\ snow \end{cases} \tag{2.1.29}$$

With the flux profiles, heating rate is defined as:

$$\mathcal{R}_T = \frac{\partial T}{\partial t} = \frac{1}{\rho C_p}\frac{\partial}{\partial z}(F_d - F_u) = -\frac{g}{C_p}\frac{\partial}{\partial p}(F_d - F_u) \tag{2.1.30}$$

- **Shortwave scheme:** Reflected or backscattered components of the solar radiation are treated as secondary effects. Clear-air scattering and absorption (mainly from water vapour) and cloud scattering are included. At the same time is taking into account the solar zenithal angle, giving the downward flux as:

$$S_d(z) = \mu S_0 - \int_z^{top} dS_{cs} + dS_{ca} + dS_s + dS_a \tag{2.1.31}$$

where μ, solar zenithal cosine; S_0, solar constant. Albedo and absorption of all cloud, precipitation and water vapour are treated as one type of cloud with theoretical

values (as function of $ln(w/\mu)$, w vertically integrated liquid water path) taking into account solar zenith angle. Heating rate is given by:

$$\mathcal{R}_T = \mathcal{R}_T^{longwave} + \frac{1}{\rho C_p}\frac{\partial}{\partial z}S_{abs} \tag{2.1.32}$$

where S_{abs}, absorption term of $S_d(z)$ (equation 2.1.31)

Surface schemes

These schemes simulate effects of land and water in the atmosphere. Ground temperature is computed from radiative net fluxes and boundary layer characteristics. It provide surface sensible and latent heat flux, sub-soil temperature and moisture profiles and can provide tendencies of snow-cover or surface moisture availability. MM5 model has 4 surface schemes (see table 2.1.g).

Most used soil scheme in the UIB-Meteo. group is the Five-Layer soil model (Dudhia, 1996). Two important assumptions are removed from the force-restore scheme: constant tunning for 24 h cycle periods and immediately uniforming distribution of the heating through the slab. The Five-layer soil model works at higher vertical resolution (5 layers, see table 2.1.g), that will allow a faster response of the surface and more addequated propagation depth in the ground of the changes (with a nominal downward propagation at 3cm/hour). Substrate temperature at 31 cm is kept constant. Transfer of heat ($\mathcal{F}$ in Wm^{-2}) follows one-dimensional diffusion equation as the heat flux:

$$\mathcal{F} = -K\rho_s c_s \frac{\partial T_s}{\partial z} \tag{2.1.33}$$

where K is the soil thermal diffusivity (m^2s^{-1}); ρ_s, soil density; c_s, specific heat capacity ($Jkg^{-1}K^{-1}$). Heating is proportional to flux convergence:

$$\frac{\partial T_s}{\partial t} = -\frac{1}{\rho_s c_s}\frac{\partial \mathcal{F}}{\partial z} \tag{2.1.34}$$

After the computation of the diffusion at a given depth $\mathcal{F}(z)$ (equation 2.1.33), heating can be computed assuming that $\mathcal{F}(z=0)$ at the surface is known as the net sensible, latent and radiative flux. In MM5 soil's thermal diffusivity (K), is taken from the thermal inertia χ ($Jm^{-2}K^{-1}s^{-1/2}$) following the relation $\chi = \rho_s c_s K^{1/2}$. By this way, temperature only depends in χ for a given $\rho_s c_s$ and K. MM5 takes a fixed an intermediate K took between sand and clay soils of $K' = 5 \times 10^{-7} m^2 s^{-1}$. This value fixes a numerical stability criterion for the thermal variation of

$$1 > 2\frac{K\Delta t_{soil}}{\Delta z^2} \tag{2.1.35}$$

Table 2.1.g: Brief description of the MM5v3 soil schemes

Name	**Characteristics**
Force-restore (Blackadar)	prediction of ground temperature 2-layer model fixed thermal substrate as diurnal average surface temperature
Five-layer Soil Temperature	soil temperature prediction in 5 layers layers thickness: 1, 2, 4, 8, 16 cm better response to high frequency changes than force-restore substrate fixed by diffusion
Noah LSM	four layers at: 10, 30,60 and 100 cm soil predictions of: temperature, water/ice, canopy water and snow cover demands of additional inputs of: soil texture, $< T_{sfc} >_{anual}$ seasonal vegetation and initial soil temperature and moisture can use albedo datasets use of percentage land-use and soil data prediction of surface and under-ground run-off and snow depth
Pleim-Xiu LSM	two layer model:; 1cm, 1m prediction of soil temperature and moisture prediction of canopy and evapotranspiration allow data assimilation for the initialisation of soil moisture use of percentage land-use and soil data optional plant-growth and leaf-out algorithms

Table 2.1.h: A brief description of a short list of MM5v3 additional schemes

Name	**Characteristics**
LEVSLP	solar slope
OROSHAW	Topography shadowing
IPOLAR	polar physics sea-ice fraction sea-ice snow/ice fluxes ice nuclei conc from Meyers
Shallow convection	prediction of shallow convection non-precipiting clouds strong entrainment, small radius uniform clouds without downdrafts
IFSNOW	snow cover effects

A very simple initialisation of the temperature profile is carried out for this scheme. It is assumed a linear dependant in depth vertical profile (considered as the steady solution of the diffusivity equation). However, is well known, that initial soil temperature is dependent on previous days temperature, but considerations of these order make mandatory the use of a much more complex soil scheme (as Noah LSM).

Other schemes

A large variety of phenomena has also taken into account in the MM5 model. They attain to a large different processes with different order of importance (see table 2.1.h)

FDDA

A Four-Dimensional data assimilation (FDDA) is a way to introduce observational information into numerical simulation. FDDA technique can also be seen as a way to continuously link and dynamical couple successive observations using a numerical model. This technique is actually applied in the global models in two different ways: *dynamic initialisation*, a complete set of observations are introduced into a atmospheric model in order to obtain a complete 3-dimensional dynamically integrated representation of the initial state of the atmosphere; *nudging*, during the period of simulation of a model, diagnostic fields are driven 'towards' the observations according to a dynamical forcing.

FDDA technique has been applied in its *nudging* procedure. It is know also as *Newtonian relaxation*. The gradual forcing of the numerical simulation is assumed to be soft

enough that the fields remain in appropriated balance conditions. Assimilated observations can be of any type: statistical grid derived from different origins, or even, they can be individual measurements (weighted assimilated as simple Cressman-type functions (distance-weighted) or more sophisticated methodologies).

The modification of numerical simulations using observations from different sources has been shown as a successful way to improve the results (Stauffer and Seaman, 1990; Leslie et al., 1998; Zou and Xiao, 1999; Fan and Tilley, 2002; Ducrocq et al., 2002; Davolio and Buzzi, 2004; Orlandi et al., 2004; Lagouvardos and Kotroni, 2005). MM5 model (Grell et al., 1995) uses a four-dimensional data assimilation (FDDA) tool based on a Newtonian-relaxation or nudging (Stauffer and Seaman, 1990) applied on the prognostic equations. Artificial tendency terms are added in the prognostic equations derived from the difference between the simulated and observed value at the given grid point. This artificial tendency term is added in the prognostic equations according to a given spatial and temporal window of influence of the observations or gridded analyses.

- **Analysis nudging:** Nudging term will be proportional to the 'difference' between simulated and analysed fields at every grid point. Prediction of variable $\chi(\vec{x},t)$ is given as:

$$\begin{aligned} \frac{\partial p^*\chi}{\partial t} &= \mathcal{F}(\chi,\vec{x},t) + \mathcal{G}_\chi \cdot W_\chi(\vec{x},t) \cdot \epsilon_\chi(\vec{x}) \cdot p^*(\overline{\chi}_0 - \chi) \\ &+ \mathcal{G}_{p^*} \cdot W_{p^*}(\vec{x},t) \cdot \epsilon_{p^*}(\vec{x}) \cdot \chi(\overline{p}_0^* - p^*) \end{aligned} \tag{2.1.36}$$

where, $\mathcal{F}$, physical forcing terms of the model (advection, Coriolis, etc.); χ, model dependent variables; $\vec{x}$, independent spatial variables; t time. $p^* = p_{sfc} - p_{top}$, pressure difference between surface and top. Terms of the equation with $\mathcal{G}_\chi$ and $\mathcal{G}_{p^*}$ are respectively the nudging terms for χ and p^*. Nudging of surface pressure (included in p^*) must be accompanied by an 'appropriated' change of the vertical structure of the column above. Since there is not an unique possible adequate vertical structure it is not frequent to nudge surface pressure and is fixed a $\mathcal{G}_{p^*} \equiv 0$. Four-dimensional weight function W, determines the spatial and temporal variation of $\mathcal{G}_\chi$. ϵ is the analysis quality factor (from 0 to 1); $\overline{\chi}_0$, estimation of the observation by χ analysed to the grid. $\mathcal{G}_\chi$ must satisfy the stability criterion $\mathcal{G}_\chi \leq 1/\Delta t$. $\mathcal{G}_\chi$ must be small enough to ensure: model ability to adequately solve mass-momentum imbalances imposed by the observations and the generation of model atmospheric features not included in the analysis. Avoiding very small values that will derive to any influence of the observations and a growing of the amplitude of errors of the simulations. Typical values are $10^{-4}\ s^{-1} \leq \mathcal{G}_\chi \leq 10^{-3}\ s^{-1}$. For a simple situation in which is assumed that $W(\vec{x},t) \equiv 1$, $\partial p^*/\partial t = 0$ and observational analysis is

perfect and time invariant, is obtained that:

$$\frac{\partial \chi}{\partial t} = \mathcal{G}_\chi(\overline{\chi}_0 - \chi) \tag{2.1.37}$$

with solution:

$$\chi = \overline{\chi}_0 + (\chi_i - \overline{\chi}_0)e^{-\mathcal{G}\chi t} \tag{2.1.38}$$

where χ_i, initial value of χ at starting nudging time. According to this exponential tendency towards the nudging observation, one obtain a threshold of influence of the nudging observation associated to a e-folding time $\tau_\mathcal{G}$, according to $\tau_\mathcal{G} = 1/\mathcal{G}_\chi$. This implies that high frequency observations will not be retained (for a giving $\mathcal{G}_\chi = 10^{-3}\ s^{-1}$, $\tau_\mathcal{G} \approx 0.93\ h$)

- **Observational nudging:** In this implementation, nudging equation 2.1.36 will be carried out for that observations that are included within a radius of influence (R) and temporal window (δt) at every grid point at each model time step. Tendency for $\chi(\vec{x}, t)$ with $\mathcal{G}_{p^*} \equiv 0$ is:

$$\frac{\partial p^* \chi}{\partial t} = \mathcal{F}(\chi, \vec{x}, t) + \mathcal{G}_\chi \cdot p^* \frac{\left[\sum_{i=1}^{N} W_i^2(\vec{x}, t) \cdot \gamma_i \cdot (\chi_0 - \overline{\chi})_i\right]}{\sum_{i=1}^{N} W_i(\vec{x}, t)} \tag{2.1.39}$$

where $\mathcal{F}, \mathcal{G}_\chi$, have same meaning as before; i, ith observation; within a radius R and δt time at a given grid point; χ_0, observed value of χ; $\overline{\chi}$, model's prognostic variable interpolated to the observation; γ, observational quality factor (0 to 1, instrument errors and representativity). Assuming a perfect observation control quality $\gamma \equiv 1$, therefore the four-dimensional weighting function for the ith observation:

$$W(\vec{x}, t) \equiv w_{xy} w_\sigma w_t \begin{cases} w_{xy} = \begin{cases} \dfrac{R^2 - D^2}{R^2 + D^2} & 0 \le D \le R \\ 0 & D > R \end{cases} \\ w_\sigma = \begin{cases} 1 - \dfrac{|\sigma_{obs} - \sigma|}{\mathcal{R}_\sigma} & |\sigma_{obs} - \sigma| \le \mathcal{R}_\sigma \\ 0 & |\sigma_{obs} - \sigma| > \mathcal{R}_\sigma \end{cases} \\ w_t = \begin{cases} 1 & |t - t_0| < \tau/2 \\ \dfrac{(\tau - |t - t_0|)}{\tau/2} & \tau/2 \le |t - t_0| \le \tau \\ 0 |t - t_0| > \tau \end{cases} \end{cases} \tag{2.1.40}$$

where, w_{xy}, horizontal weight; w_σ, vertical weight; w_t, temporal weight; R, radius of influence; D, distance from the grid point to the ith observation; $\mathcal{R}_\sigma$, vertical radius of influence (usually small, 0.01 or even less); σ_{obs}, vertical position of ith observation; σ, vertical coordinate of the grid point; t, model-relative time; t_0, model-relative time of the ith observation; $\tau = \delta t/2$, half period of the time window δt.

2.1.2 Axisymmetric cloud resolving model

A modified version of the axisymmetric, nonhydrostatic, cloud-resolving model of Rotunno and Emanuel (1987) is used. The model has been modified to ensure global energy conservation, including dissipative heating. Any development in such a model must occur owing to Wind-Induced Surface Heat Exchange (WISHE), since baroclinic instability is absent in axisymmetric geometry. It assume the air-sea description and characteristics of a tropical storm (Emanuel, 1986).

The model is run with a radial grid size of 3.75 km and vertical level separation of 300 m. The model is initiated with a weak vortex (described by an overall radial size and a radius of maximum azimuthal wind, see equation 2.1.43) and a vertical sounding. A vertical sounding is used to determine the initial condition of the atmosphere. It is applied to all the radial grid points of the model. Consequently, an initial horizontally homogeneous environment is established. From gradient balance, the pressure distribution is established. Some other assumptions and simplifications are (with the constant values given in table 2.1.i):

- Hydrostatic and gradient wind balance

$$\frac{dp}{dz} = -\rho g \qquad \frac{V_{gr}}{R} + fV_{gr} = -g\frac{\partial z}{\partial n} \tag{2.1.41}$$

- Neutrality to Slantwise moist convection

$$M \equiv v + fx \quad \frac{du}{dt} = f(M - M_g) \quad \frac{dw}{dt} = B = \gamma_m(s' - s'^*) \tag{2.1.42}$$
$$M = s^* \ (SlantwiseNeutrality)$$

- Initial vortex

$$\begin{aligned} v(r,z,0) &= \frac{z_{sponge} - z}{z_{sponge}} \left\langle \left\{ v_m^2 \left(\frac{r}{r_m}\right)^2 \left[\left(\frac{2r_m}{r + r_m}\right)^3 - \left(\frac{2r_m}{r_0 + r_m}\right)^3 \right] \right.\right. \\ &+ \left.\left. \frac{f^2 r^2}{4} \right\}^{1/2} - \frac{fr}{2} \right\rangle \end{aligned} \tag{2.1.43}$$

Table 2.1.i: Values of some constants in the axisymmetric cloud resolving model

Coriolis Parameter ($10^{-5}s^{-1}$)	9.0	Surf. Drag Coefficient (10^{-3})	1.1
Ratio of Exch. Coeffs. (C_T/C_D)	1.0	Wind-Dep. Surf. Flux ($10^{-5}\ sm^{-1}$)	4.0
Horizontal Mixing Length (m)	200.0	Radiative Time Scale (h)	12.0
Cap. on rad. cooling (C/day)	2.0	Precipitation Fall Speed (ms^{-1})	7.0
Lowest perm. T in sounding (K)	133.0	SST Anomaly Amplitude (K)	0.0
SST Anomaly Decay L (km)	100.0	Large Time Step (s)	10.0
Nbr. small time steps/Delt	5	Asselin Filter constant	0.1
Sponge layer damping coeff.	0.01	Radius of Outer Wall (km)	1500.0
Altitude of Upper Boundary (km)	25.0	Number of sponge layer levels	5
End Time (days)	10.0	Threshold water content (gKg^{-1})	0.2

- "Sponge" layer limit convection in height near tropopause
- Eye in solid body rotation
- Constant sea surface temperature
- Compressible, axisymmetric flow
- Explicit cumulus convection imposing conservation of potential equivalent temperature
- Two dimension turbulence model, on azimuthal average following (Smagorinsky, 1963) and (Lilly, 1962)
- Newtonian cooling

$$R \equiv -\frac{\theta - \overline{\theta}}{\tau_R} \tag{2.1.44}$$

- Rigid lid at upper boundary condition
- $w = 0\ cms^{-1}$ on surface
- Open lateral boundary conditions

2.2 Piecewise PV Inversion

General state of the atmosphere is given by natural variables or state-variables: Temperature (T), Wind speed (u, v, w), Humidity (given by mixing ratio q, or relative humidity RH) and pressure (p). There are another set of variables that are combinations of the state-variables that contribute to a better analysis, understanding or forecasting of the atmosphere. One of these variables is the *Potential Temperature* (θ, equation 2.2.1).

$$\theta = T\left(\frac{p_0}{p}\right)^{\frac{R}{C_p}} \tag{2.2.1}$$

where T, temperature at a giving height; p_0, reference pressure; p, pressure at a giving height; R, ideal gas constant for dry air (287 $Jkg^{-1}K^{-1}$); C_p, specific heat at constant pressure for dry air ($1005.7 \pm 2.5 Jkg^{-1}K^{-1}$).

Potential temperature is an adiabatically conservative variable. This implies that an air parcel which does not exchange heat with the environment (adiabatic process) preserves the potential temperature. The most useful way with which an air parcel exchanges heat with the environment is done throughout the transitions between water phases. By this way, when an air parcel moves without changes in its water phases, the movement is done following a potential isothermal surface. Potential temperature is the temperature that might have an air parcel that adiabatically moves from a reference pressure value (usually 1000 hPa) to another one. The definition of this temperature allows to study the thermal vertical structure of the atmosphere without the effects on vertical pressure changes. In some way it represents the temperature that might have an air parcel at a given height in an ideal dry atmosphere. Thus, one can obtain an idea of the state of the atmosphere. From this point of view, potential temperature is very useful as a way to determine the stability of a forced vertical movement of an air parcel (Bluestein, 1992). The stability of vertical movements of air parcels determine the chance of development of large variety of atmospheric phenomenas such as clouds.

There are a large variety of combined variables (CAPE, divergence, thickness, etc.). Each one helps in the study of a specific aspect of the atmosphere. One of these variables is the *Vorticity*.

- **Vorticity:** It is obtained when the curl operator ($\vec{\nabla}\times$) is applied on the conservation of motion equation (in terms of the Reynolds decomposition $\chi = \overline{\chi} + \chi''$) according to Bluestein (1992):

$$\frac{\partial}{\partial t}\left[\varepsilon_{pqi}\frac{\partial}{\partial x_q}\rho_0\overline{u}_i\right] = - \frac{\partial}{\partial x_j}\left[\overline{u}_j\varepsilon_{pqi}\frac{\partial \overline{u}_i\rho_0}{\partial x_q}\right] - \frac{\partial}{\partial x_j}\left[\rho_0\overline{u}_i\varepsilon_{pqi}\frac{\partial \overline{u}_j}{\partial x_q}\right]$$

$$
\begin{aligned}
&- \varepsilon_{pqi}\frac{\partial}{\partial x_q}\frac{\partial}{\partial x_j}\rho_0\overline{u_j''u_i''} - \varepsilon_{pqi}\frac{\partial}{\partial x_q}\frac{\partial p'}{\partial x_i} \\
&- \varepsilon_{pqi}\frac{\partial}{\partial x_q}\left[\frac{\partial p_0}{\partial x}\delta_{i1} + \frac{\partial p_0}{\partial y}\delta_{i2}\right] + \varepsilon_{pqi}\frac{\partial}{\partial x_q}\frac{\alpha'}{\alpha_0^2}g\delta_{i3} \\
&- 2\varepsilon_{pqi}\varepsilon_{ijk}\Omega_j\frac{\partial \rho_0\overline{u}_k}{\partial x_q}
\end{aligned}
\tag{2.2.2}
$$

where ρ, density; u, velocity components; α, specific volume; p, pressure; g, gravity; Ω, Coriolis term; i, j, p, q, coordinates; ε, permutation symbol; δ, Kronecker delta in Einstein summation. It is known that the curl of a gradient is always null ($\nabla\chi = 0$), thus $\varepsilon_{pqi}(\partial/\partial x_q)(\partial p'/\partial x_i) = 0$. One can define a density-weighted mesoscale vorticity ω_p (equivalent to $\omega_p = \nabla \times \rho_0\vec{V'}$), and the equation is rewritten as:

$$
\begin{aligned}
\frac{\partial \omega_p}{\partial t} = &- \frac{\partial}{\partial x_j}(\overline{u}_j\omega_p) - \varepsilon_{pqi}\frac{\partial}{\partial x_j}\left(\rho_0\overline{u}_i\frac{\partial \overline{u}_j}{\partial x_q}\right) - \varepsilon_{pqi}\frac{\partial}{\partial x_q}\frac{\partial}{\partial x_j}(\rho_0\overline{u_j''u_i''}) \\
&- \varepsilon_{pqi}\frac{\partial}{\partial x_q}\left[\frac{\partial p_0}{\partial x}\delta_{i1} + \frac{\partial p_0}{\partial y}\delta_{i2}\right] + \delta_{i3}g\varepsilon_{pqi}\frac{\partial}{\partial x_q}\frac{\alpha'}{\alpha_0^2} \\
&- 2\varepsilon_{pqi}\varepsilon_{ijk}\Omega_j\frac{\partial \rho_0\overline{u}_k}{\partial x_q}
\end{aligned}
\tag{2.2.3}
$$

each individual term of the equation is related to:

- $\frac{\partial \omega_p}{\partial t}$: local tendency of vorticity
- $\frac{\partial}{\partial x_j}(\overline{u}_j\omega_p)$: gradient of the flux
- $\varepsilon_{pqi}\frac{\partial}{\partial x_j}\left(\rho_0\overline{u}_i\frac{\partial \overline{u}_j}{\partial x_q}\right)$: *tilting term*, vorticity transferation between 3-dimensional spatial components as a result of velocity shear
- $\varepsilon_{pqi}\frac{\partial}{\partial x_q}\frac{\partial}{\partial x_j}(\rho_0\overline{u_j''u_i''})$: source/sink subgrid term
- $\varepsilon_{pqi}\frac{\partial}{\partial x_q}\left[\frac{\partial p_0}{\partial x}\delta_{i1} + \frac{\partial p_0}{\partial y}\delta_{i2}\right]$: larger-scale source/sink term due to curvature of the synoptic-scale horizontal pressure gradients
- $\delta_{i3}g\varepsilon_{pqi}\frac{\partial}{\partial x_q}\frac{\alpha'}{\alpha_0^2}$: *selenoidal term*, source/sink due to gradients in density. In shallow flows ($\alpha'/\alpha_0^2 \sim \rho_0\theta'/\theta_0$) differential heating produces changes in the vorticity field
- $2\varepsilon_{pqi}\varepsilon_{ijk}\Omega_j\frac{\partial \rho_0\overline{u}_k}{\partial x_q}$: *solid-body rotation*, source/sink term due to rotation of earth

In atmospheric sciences, vertical component of the vorticity is a large source of information. Then is defined the Vorticity (ζ, equation 2.2.4) that gives the capacity of a fluid to locally rotate (Holton, 1979). It comes as a result of apply the curl operator ($\vec{\nabla}\times$) to the conservation of motion equation. That means, the capacity of a given flow to present rotation of radial distribution of its kinematic properties. It could be clockwise rotation ($\zeta < 0$), other to the other sense ($\zeta > 0$).

$$\zeta = \hat{k} \cdot \nabla \times \vec{V} = \frac{\partial v}{\partial x} - \frac{\partial u}{\partial y} \tag{2.2.4}$$

A vectorial expression for the vertical component of the vorticity ζ (Holton, 1979):

$$\begin{aligned} \frac{D\zeta}{Dt} = & - (\zeta + f)\left(\frac{\partial u}{\partial x} + \frac{\partial v}{\partial y}\right) - \frac{s\omega\cos\phi}{a}v + \left(\frac{\partial w}{\partial y}\frac{\partial u}{\partial z} - \frac{\partial w}{\partial x}\frac{\partial v}{\partial z}\right) \\ & + \left(\frac{\partial p}{\partial x}\frac{\partial \alpha}{\partial y} - \frac{\partial p}{\partial y}\frac{\partial \alpha}{\partial x}\right) \end{aligned} \tag{2.2.5}$$

The 'natural' coordinates form (equation 2.2.6) express the *vorticity* in an useful intuitive form from which the sources and sinks of vorticity can be clearly obtained. Then it is obtained that the *Vorticity* might change to the shear in the perpendicular direction to the velocity field (first term), and to the curvature of the flow (second term, see figure 2.2.1).

$$\zeta = V\frac{\partial \theta_b}{\partial s} - \frac{\partial V}{\partial n} \tag{2.2.6}$$

Absolute vorticity (η) is obtained, when the Coriolis term is included in the vorticity ($\eta = \zeta + f$) equation.

- **Potential Vorticity:** It is a generalisation of the *vorticity*. One dry formulation was given by (Ertel, 1942, equation 2.2.7). The potential term of the equation takes in to account the capacity of the particle of air developing vorticity. It is a conservative variable under adiabatic and frictionless conditions. An expression of the *potential vorticity* (hereafter, PV):

$$\begin{aligned} q &= \frac{1}{\rho}\vec{\eta} \cdot \vec{\nabla}\theta \\ q &\simeq \frac{g\kappa\pi}{p}\left[\left(f + m^2\Delta\psi\right)\frac{\partial^2\phi}{\partial\pi^2} - m^2\left(\frac{\partial^2\psi}{\partial x\partial\pi}\frac{\partial^2\phi}{\partial x\partial\pi} + \frac{\partial^2\psi}{\partial y\partial\pi}\frac{\partial^2\phi}{\partial y\partial\pi}\right)\right] \end{aligned} \tag{2.2.7}$$

where ρ, density; $\vec{\eta}$, absolute vorticity; θ, potential temperature; ψ, stream function lines; $\phi = gz$, geopotential height; p, pressure; g, gravity; $\kappa = R_d/C_p$; $\pi =$

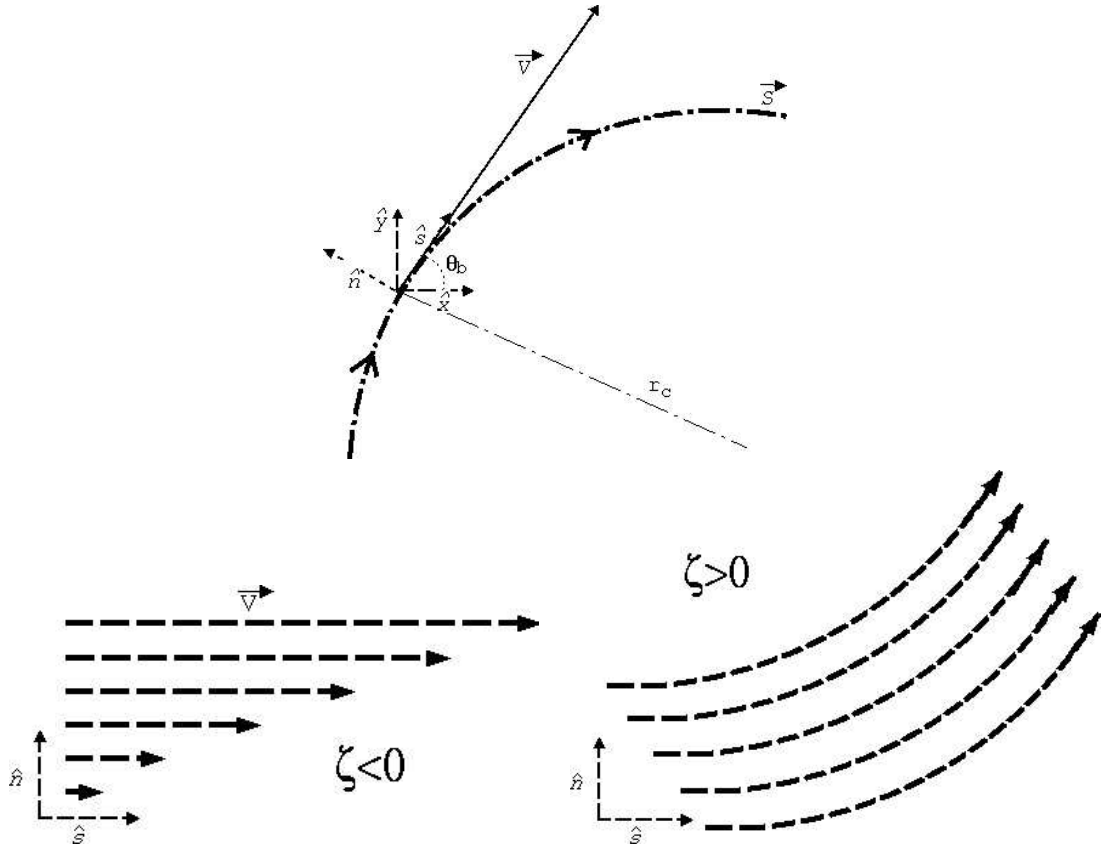

Figure 2.2.1: Top panel: Decomposition of the wind vector to its natural coordinates $(\hat{n}, \hat{s})$. Bottom left panel: A perpendicular wind shear to the direction of movement generates negative vorticity ($\frac{\partial V}{\partial n} > 0$). Bottom right panel: A curvature ($\frac{\partial \theta_b}{\partial s} \neq 0$) of a permanent flow ($\frac{\partial V}{\partial n} = 0$) is depicted as positive vorticity

$C_p(p/p_0)^\kappa$, Exner function (as vertical coordinate). PV field has been shown (Hoskins et al., 1985) as a powerful diagnostic variable with which dynamically unstable regions of the flow (such us high rotational regions and strong gradients of wind) can be identified. PV presents significant values in zones of the flow that can be precursors of significant changes. Therefore, a specific case can present a strong sensitivity in the distribution of the PV field. As a result of PV properties, a large variety of atmospheric phenomena can be explained with the PV. *PV-thinking* is the way in which a set of processes is explained using the PV.

PV-thinking

As a result of the frictionless and adiabatic preservative characteristics of the PV, a large variety of atmospheric processes can be more clearly explained. PV point of view of some processes might help to better understand some phenomena. At the same time, some powerful tools (such as piecewise PV inversion and analysis of PV tendencies) can be derived from the variable.

Potential vorticity combines flow properties and thermal characteristics of the atmosphere. Some of the discussion of atmospheric phenomena using PV thinking are based in the *Stokes'* theorem (combination of the vorticity $\vec{\nabla} \times \vec{U}$ and the circulation $\vec{U} \cdot d\vec{l}$ equation 2.2.8) and the stability of the atmosphere (depicted by the Brunt-Väisälä frequency or buoyancy frequency N, equation 2.2.9). Explanations that will follow will be based on the conservation of the PV under adiabatically and frictionless conditions.

$$\oint \vec{U} \cdot d\vec{l} = \int_A \int dA(\vec{\nabla} \times \vec{U}) \cdot \hat{n} \tag{2.2.8}$$

$$N^2 = \frac{g}{\overline{\theta_v}} \frac{d\overline{\theta_v}}{dz} \tag{2.2.9}$$

where $\oint$, integration following a closed line; $\int_A \int dA$ surface integration; $\vec{U}$, vector field; g, gravity, $\overline{\theta_v}$, averaged virtual temperature between two layers; $d\overline{\theta_v}/dz$, vertical variation of potential potential temperature between two layers.

- **PV, adiabatic process and change of thickness:** Under adiabatic ($\theta = ct$) and frictionless ($\nu = 0$) assumptions potential vorticity is preserved ($q = ct$, equation 2.2.10; Holton (1979)). Applying Stokes' theorem, if an air parcel changes its thickness, this will change vorticity (ζ, see figure left 2.2.2).

$$q = (\zeta + f) \frac{\partial \theta}{\partial p}\bigg|_{(\theta = ct, \nu = 0)} = ct \tag{2.2.10}$$

- **PV and orography:** Taking the expression of vorticity 2.2.11 under preservative conditions ($q = ct$), on changes in the height (δz) will produce changes of vorticity (ζ). As a given example, in right figure 2.2.3 are shown the changes that suffers a parallel and constant ($\zeta = 0$) West flow when it interacts with a S-N mountainous range.

$$q = \frac{\zeta + f}{\delta z} = ct \tag{2.2.11}$$

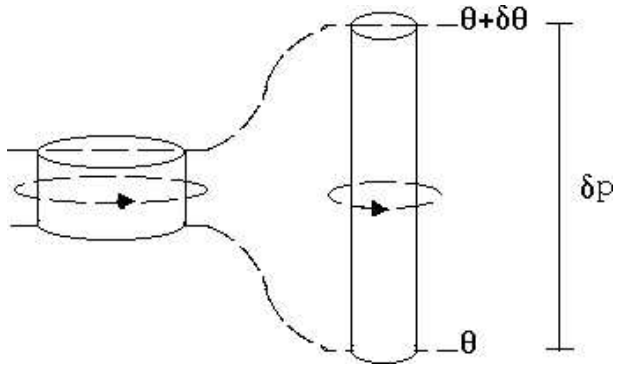

Figure 2.2.2: Expression 2.2.10 gives a relation between thickness or vertical dimension (δp) of a vortex and its absolute vorticity ($\zeta + f$). On frictionless and adiabatic conditions, changes of the thickness of the vortex will derive on changes in its vorticity (assuming not meridional movement $f = ct$), since potential vorticity (q) should not change

- **η & divergence:** Following the conservation of the vorticity, a dynamical property of the vorticity (see figure 2.2.4) could be obtained from the equation of the evolution of the absolute vorticity η (equation 2.2.12). First term of the equation is the divergence; second term relates the generation of vertical velocity due changes on the orientation of the flow; the last term is the selenoidal term from which, η is generated due to changes in pressure/density

$$\begin{aligned} \delta_t \eta = \frac{d}{dt}(\zeta + f) &= -(\zeta + f)\left(\frac{\partial u}{\partial x} + \frac{\partial v}{\partial y}\right) - \left(\frac{\partial w}{\partial x}\frac{\partial v}{\partial z} - \frac{\partial w}{\partial y}\frac{\partial u}{\partial z}\right) \\ &+ \frac{1}{p^2}\left(\frac{\partial \rho}{\partial x}\frac{\partial p}{\partial y} - \frac{\partial \rho}{\partial y}\frac{\partial p}{\partial x}\right) \end{aligned} \tag{2.2.12}$$

- **PV and cloud formation:** Another way to express the potential vorticity q is given by equation 2.2.13. A source of q is obtained from the study of the third term of the equation. During the formation of the clouds, due the condensation of huge amounts of water vapour a lot of heat is released. Latent Heat release from the condensation is developed in low-middle levels of the troposphere. As a result of it, this levels are warmed. Just below the zone of maximum heating, the level increases its stability. Due to the third term of the equation 2.2.13 positive potential vorticity is induced. The presence of positive potential vorticity at middle-low levels has been shown as a mechanism that enhance the cyclogenetic processes (Hoskins et al., 1985; Romero, 2001; Homar et al., 2002a). Middle-low levels positive PV emphasises, reinforces and catalyses coupling situations between upper and low levels disturbances, low level vorticity or instability (Davis and Emanuel, 1991).

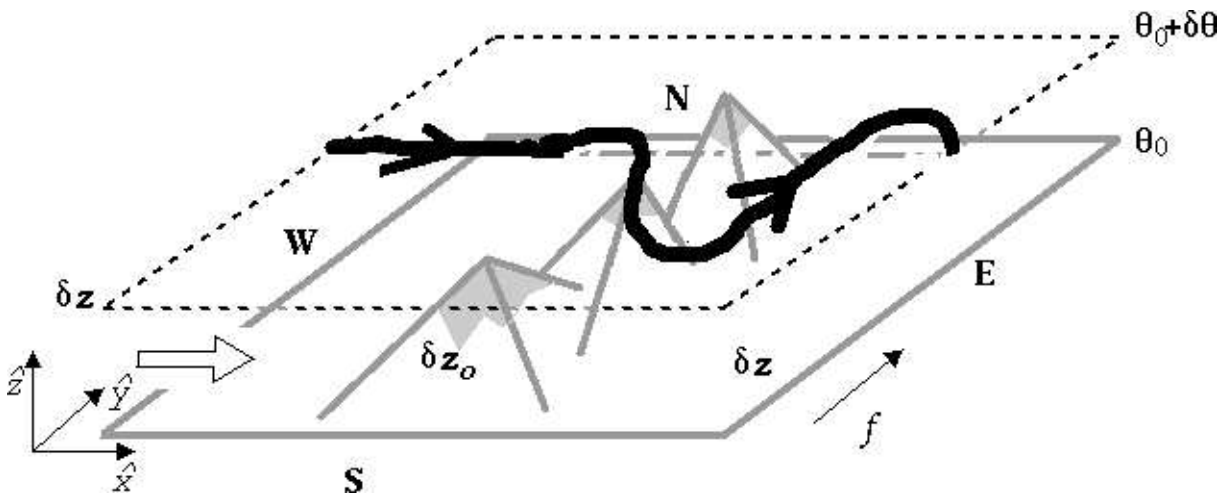

Figure 2.2.3: A constant West flow ($\zeta = 0$) reaches a S-N mountain range. In an adiabatic processes potential isothermal surfaces follow orography of the surface. Meanwhile, upper-level isothermal surfaces keep almost constant. As a result of it, flow decreases significantly its thickness ($\delta z_0 < \delta_z$). Due to the conservation of the Potential Vorticity q, relative vorticity ζ should change. In northern hemisphere where Coriolis term (f) increases towards the North pole, relative vorticity might decrease. Once the air-parcel overpasses the mountain range it is in a region with less Coriolis term with no height variation. In order to preserve the potential vorticity, flow should increase its rotation and it turns back to the north. When the air parcel reaches the original latitude that it was before the mountain range it has a northward component. This northward component should be compensated with negative vorticity (anticyclonic rotation). This process will be periodically reproduced until the flow reaches the initial arrotiational movement

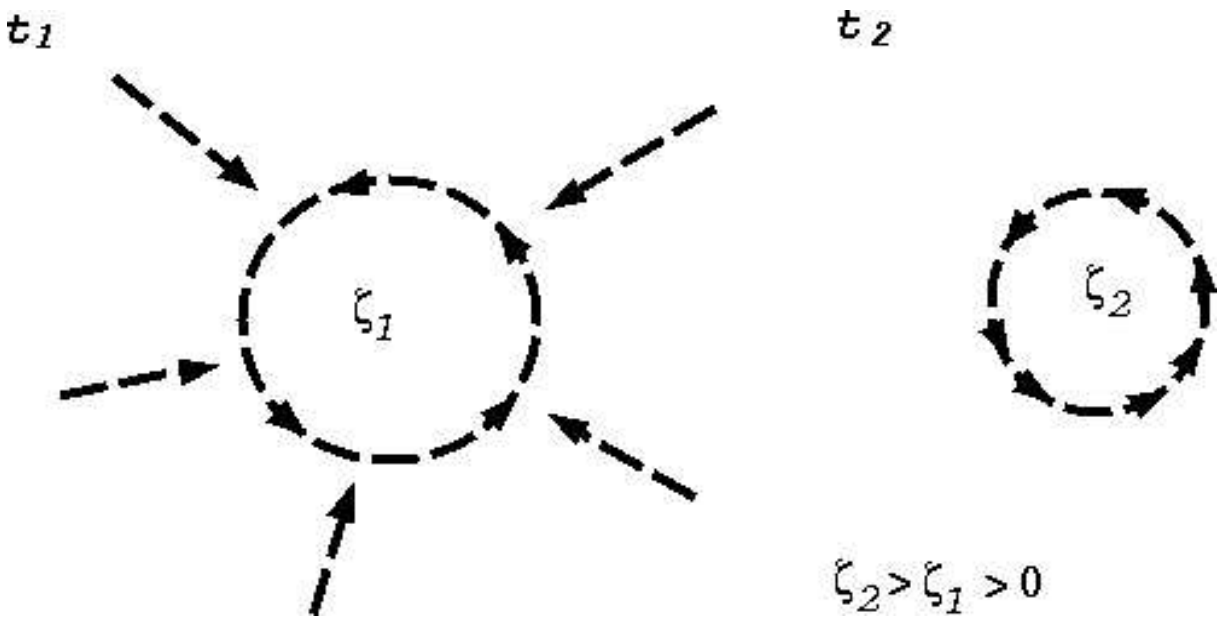

Figure 2.2.4: In a region of positive vorticity there is a convergence of the flow. Some time later air parcels should change the area that enclosed their streamlines. In order to keep constant the circulation, mean vorticity will increase. This process from which the vorticity is enhanced by convergences of the flow is common in cyclogenic processes. The search of convergence zones has been related to unstable zones and useful for the weather forecasters

$$q = \frac{1}{\rho}\Big[\frac{\partial\theta}{\partial x}\Big(\frac{\partial w}{\partial y} - \frac{\partial v}{\partial z}\Big) + \frac{\partial\theta}{\partial y}\Big(\frac{\partial u}{\partial z} - \frac{\partial w}{\partial x}\Big) + \frac{\partial\theta}{\partial z}\Big(\frac{\partial v}{\partial x} - \frac{\partial u}{\partial y} + f\Big)\Big] \tag{2.2.13}$$

2.2.1 Invertibility principle

The invertibility principle of the Potential Vorticity establishes that for a given distribution of PV, assuming a balance equation between the wind and the temperature field and for a given boundary, top and bottom conditions; one can obtain its state-variables (without humidity) at all the space (Hoskins et al., 1985). According to this procedure the PV-related balanced state of the atmosphere will be obtained. The balance condition commonly used is a flow in wind and thermal balance with the expression:

$$\Delta\phi = \vec{\nabla}\cdot f\vec{\nabla}\psi + 2m^2\left[\frac{\partial^2\psi}{\partial x^2}\frac{\partial^2\psi}{\partial y^2} - \left(\frac{\partial^2\psi}{\partial x\partial y}\right)^2\right] \tag{2.2.14}$$

where ϕ, geopotential height; ψ, streamfucntions; m, map factor; f, Coriolis factor.

The PV Inversion used in the UIB-Meteo. group follows the scheme proposed by Davis and Emanuel (1991). Nonlinear *Charney balance equation* (Charney, 1955, equation 2.2.14) has been taken as the appropriate form to give the balance condition. *Dirichlet* boundary conditions are imposed and *Neumann* top and bottom conditions (equation 2.2.15; f, Coriolis term) following Hakim et al. (1996).

$$\frac{\partial\phi}{\partial\pi} = f\frac{\partial\psi}{\partial\pi} = -\theta \tag{2.2.15}$$

The solution of the PV Inversion does not have an unique solution. Obtained inverted fields will obey the chosen balance condition. Thus, the election of an appropriate balance equation will dominate the results of the inversion. It can be proved that nondivergent winds (winds with a smaller irrotational part than the nondivergent) are reasonably close to the balance flows (Davis and Emanuel, 1991). Therefore, it can be assumed that the inverted fields are a good approximation of the flow. If the chosen invertible relation is linear, the solution will be also linear. Therefore, a combination of PV distributions can be also inverted obtaining a combination of solutions. By this way, initial PV field can be disgregated in various pieces allowing a particular study of each piece. In the same way, any linear combination of operation of the PV distribution can be inverted. By this way, choosing a linear methodology to do the inversion different PV regions or individual pieces related to different features of the event can be indepently analysed. Allowing the study of different features of the environment to which they are related. These individual components of the PV field will be identified with relevant anomalies from a reference state of

the atmosphere, and then inverted to produce the initial perturbations in the simulations.

The *piecewise PV Inversion technique* in the meteorologic group of the UIB has mainly been used to perform sensitivity studies to changes in the initial conditions of the simulations of the cases of study. PV features in the PV field are obtained as PV anomalies at the initial conditions. These PV anomalies (hereafter, PVp) are derived according to a 7 to 10-day temporal averaged PV field for all the period of the case (and centred at the maximal strength of the event). It is assumed that the background flow is partially captured by the averaged composite of fields. Computing the PVp at the beginning of the simulation, might allow to capture the specific features that were present in the initial conditions and contributed to generate the episode. The inverted fields obtained for each anomaly are used to linearly modify the initial conditions of the simulations and perform, by this way, a sensitivity test to the changes introduced. Since inverted fields are driven by a balance condition, one can be sure that the modifications will not introduce any inconsistency between the state variables (if huge modifications have not been introduced). Since a linear inversion has been used, linear modifications carried out with the PV anomalies (or their resultant inverted fields) have also a solution. Inverted fields ($I_\Xi = \{I_H, I_T, I_U, I_V\}$) obtained from an anomaly p_i are used to modify linearly (usually change of strength or shifts of the anomalies, see equation 2.2.16) the initial fields ($\Xi_{initial}$).

$$\Xi' = \Xi_{inicial} \pm \begin{cases} \%I_\Xi p_i \\ I_\Xi p_i(x+\chi, y+\gamma, z+\kappa) \end{cases} \tag{2.2.16}$$

PV Inversion is numerically solved throughout an iterative resolution of two-dimensional elliptical equations (commonly Green functions). This technique is known as a successive overrelaxation method (SOR)[4] (Barrett et al., 1994) and will be applied at each vertical level.

According to the methodology previously described it is necessary to illustrate some conditions that might comply the domain. Selected PV anomaly can not be close to the boundaries of the domain. PV Inversion presents a sensitivity to low latitudes due to low Coriolis values. At the same time, PV Inversion has problems to invert high resolution gradients or extreme values in the PV field. Selected domain should be big enough to capture all the PV anomalies that interact during the episode. At the same time, one should not introduce huge modifications and should be sure that the resultant environment is similar enough to the original initial conditions. Some not initially present incoming PV features during the event can derive erroneous conclusions. In order to prevent this in small domains, one could apply the modification of the boundary conditions at each time step that they are assimilated into the domain. This continuously application of the technique used to modify the fields, should be only applied to weak modifications in order to

[4] `http://mathworld.wolfram.com/SuccessiveOverrelaxationMethod.html`

prevent strong discontinuities between simulated and boundary fields.

Theoretically, a positive(negative) surface thermal anomaly can be related to a formal positive(negative) PV anomaly located below the bottom boundary (Bretherton, 1966; Thorpe, 1986; Horvath et al., 2006). Thus, the surface thermal anomaly studied in this work (a bottom boundary in the PV inversion method) is going to be treated as an underground PVp. By this way, the inverted balanced fields will be equivalent to the inverted fields that one can obtain from a PV anomaly under the ground that would produce the same surface thermal anomaly.

2.2.2 PV-based prognostic equations

One can also apply the PV Inversion technique to the prognostic equation of the PV. The closed system of PV-based prognostic equations (Davis and Emanuel, 1991) is used to solve the geopotential height tendency equation. Geopotential height (ϕ) and stream function (ψ) are first obtained from a given PV distribution (q) via the non-linear **PV inversion technique** (explained also in Davis and Emanuel (1991)). The geopotential height, stream function and PV tendencies (ϕ^t, ψ^t, q^t, respectively) can be calculated after applying the tendency operator to the **Charney nonlinear balance equation** (equation 2.2.17), **Ertel's PV definition** (eq. 2.2.18) and the **Ertel's PV conservation equation**, under the frictionless and diabatic form (eq. 2.2.19).

$$\begin{aligned}\nabla^2\phi^t &= \vec{\nabla}\cdot f\vec{\nabla}\psi^t + 2m^2\left[\frac{\partial^2\psi^t}{\partial x^2}\frac{\partial^2\psi}{\partial y^2} + \frac{\partial^2\psi}{\partial x^2}\frac{\partial^2\psi^t}{\partial y^2}\right.\\ &- \left. 2\,\frac{\partial^2\psi}{\partial x\partial y}\frac{\partial^2\psi^t}{\partial x\partial y}\right]\end{aligned} \tag{2.2.17}$$

$$\begin{aligned}q^t &= \frac{g\kappa\pi}{p}\left[\left(f + m^2\nabla^2\psi\right)\frac{\partial^2\phi^t}{\partial\pi^2} + m^2\frac{\partial^2\phi}{\partial\pi^2}\nabla^2\psi^t\right.\\ &- m^2\left(\frac{\partial^2\psi^t}{\partial x\partial\pi}\frac{\partial^2\phi}{\partial x\partial\pi} + \frac{\partial^2\psi}{\partial x\partial\pi}\frac{\partial^2\phi^t}{\partial x\partial\pi}\right.\\ &+ \left.\left.\frac{\partial^2\psi^t}{\partial y\partial\pi}\frac{\partial^2\phi}{\partial y\partial\pi} + \frac{\partial^2\psi}{\partial y\partial\pi}\frac{\partial^2\phi^t}{\partial y\partial\pi}\right)\right]\end{aligned} \tag{2.2.18}$$

$$\begin{aligned}q^t &= -m(\vec{v}_\psi + \vec{v}_\chi)\cdot\vec{\nabla}q - \omega^*\frac{\partial q}{\partial\pi}\\ &+ \overbrace{\frac{g\kappa\pi}{p}\left[\eta\cdot\vec{\nabla}\left(\frac{d\theta}{dt}\right) + \vec{\nabla}\theta\cdot\vec{\nabla}\times\vec{F}\right]}^{\mathcal{DIABI}}\end{aligned} \tag{2.2.19}$$

where $\mathcal{DIABI}$ indicates the diabatic term of the equation. The formulation of the horizontal wind is partitioned in non-divergent and irrotational parts according to equations 2.2.20:

$$\begin{cases} \vec{v}_\psi = m\hat{k} \times \vec{\nabla}\psi \\ \vec{v}_\chi = m\vec{\nabla}\chi \end{cases} \tag{2.2.20}$$

In the above equations m is the map factor, $\kappa = \frac{R_d}{C_p}$, and $\pi = C_p \left(\frac{p}{p_0}\right)^\kappa$ is the Exer function used as vertical coordinates in the formulation. From the **omega equation** (eq. 2.2.21) the vertical velocity ($\omega^* = \frac{d\pi}{dt} = \frac{\kappa\pi}{p}\omega$) can be solved:

$$\begin{aligned}
f\eta\frac{\partial}{\partial\pi} & \left[\pi^{1-\frac{1}{\kappa}}\frac{\partial}{\partial\pi}\left(\pi^{\frac{1}{\kappa}-1}\omega^*\right)\right] + m^2\nabla^2\left(\frac{\partial^2\phi}{\partial\pi^2}\omega^*\right) \\
- & \quad m^2 f\frac{\partial}{\partial\pi}\left(\frac{\partial\omega^*}{\partial x}\frac{\partial\psi}{\partial x\partial\pi} + \frac{\partial\omega^*}{\partial y}\frac{\partial\psi}{\partial y\partial\pi}\right) \\
+ & \quad \left(f\frac{\partial\eta}{\partial\pi}\frac{\frac{1}{\kappa}-1}{\pi} - f\frac{\partial^2\eta}{\partial\pi^2}\right)\omega^* \\
= & \quad m^3\nabla^2[(\vec{v}_\psi + \vec{v}_\chi)\cdot\vec{\nabla}\theta] \\
+ & \quad mf\frac{\partial}{\partial\pi}[(\vec{v}_\psi + \vec{v}_\chi)\cdot\vec{\nabla}\eta] - m^2\vec{\nabla}f\cdot\vec{\nabla}\left(\frac{\partial\psi^t}{\partial\pi}\right) \\
- & \quad 2m^4\frac{\partial}{\partial\pi}\left[\frac{\partial^2\psi^t}{\partial x^2}\frac{\partial^2\psi}{\partial y^2} + \frac{\partial^2\psi}{\partial x^2}\frac{\partial^2\psi^t}{\partial y^2}\right. \\
- & \quad \left. 2\frac{\partial^2\psi}{\partial 10\partial y}\frac{\partial^2\psi^t}{\partial x\partial y}\right] \\
+ & \quad \overbrace{\nabla^2\left(\frac{d\theta}{dt}\right)}^{\mathcal{DIABII}}
\end{aligned} \tag{2.2.21}$$

where $\mathcal{DIABII}$ indicates the diabatic term of the equation. Finally with the **continuity equation** the system is closed (eq. 2.2.22):

$$m^2\nabla^2\chi + \pi^{1-\frac{1}{\kappa}}\frac{\partial}{\partial\pi}(\pi^{\frac{1}{\kappa}-1}\omega^*) = 0 \tag{2.2.22}$$

Lateral homogeneous ($\phi^t = \psi^t = q^t = \omega^* = \chi = 0$) and *Neumman top and bottom* (eq., 2.2.23) boundary conditions are used for the tendencies:

$$\frac{\partial\phi^t}{\partial\pi} = f\frac{\partial\psi^t}{\partial\pi} = -\theta^t$$

$$= \quad -m(\vec{v}_\psi + \vec{v}_\chi) \cdot \vec{\nabla}\theta - \omega^* \frac{\partial \theta}{\partial \pi} \tag{2.2.23}$$

Zero vertical velocity on the top of the domain and topographic vertical velocity on the surface are imposed.

The role of different PV anomalies can be studied by solving the previous system of equations for the geopotential height tendency (an indicator of cyclogenetic/cyclolitic processes) Romero (2008).

2.3 Factor Separation

Factor separation technique (Stein and Albert, 1993) allows to determine individual and mutual sensitivities of a forecasted field to a set of factors. It is a way to study the role of each factor or synergy during the evolution of the selected forecasted field of a numerical simulation. The collection of factors must be made of independent factors. That means that can not be any direct relation between them (g.e.: a specific mountain and its range could not be two different factors).

It is taken a forecasted field f. If for a factor ξ that affected the variable f is made a continuous modification $\xi = c\xi \; with \; 0 \leq c \leq 1$, the forecasted variable will suffer also a continuous modification $f = f(\xi) = f[\xi(c)]$. This characteristics will be also reproduced by a set of various parameters c_i. It is considered as first approximation that the function can be decomposed in two main parts, a dependant term $\hat{f}(c)$ (where $\hat{f}\,|_{c=0} = 0$, $c = c_1, ..., c_n$ as function of a continues modification) and another one that it is non-dependant of all factors called $\hat{f}(0) \equiv f_0$ (see equation 2.3.1).

$$f(c) = \hat{f}_0 + \hat{f}(c) \tag{2.3.1}$$

The free term is redefined as $f(0) \equiv f_0$, and $f(c_i) \equiv f_i$. For an unique factor the decomposition of the forecasted field is shown in equation 2.3.2.

$$\begin{aligned} \hat{f}_0 &= f(0) \\ \hat{f}(1) &= f(1) - f(0) \end{aligned} \tag{2.3.2}$$

For a given set of n parameters the decomposition can be done (see equation 2.3.3). It is shown that for a given set of n factors, is needed 2^n simulations to compute the decomposition. Following this procedure, the individual and synergies of the factors are obtained.

$$\begin{aligned} f_0 &= f(0, 0, ..., 0) = \hat{f}_0 \\ f_i &= \hat{f}_i + \hat{f}_0 \\ f_{ij} &= \hat{f}_{ij} + \hat{f}_i + \hat{f}_j + \hat{f}_0 \\ f_{123...n} &= \hat{f}_{123...n} + ... + \sum_{i,j,k=1,2,3}^{n-2,n-1,n} \hat{f}_{ijk} + \sum_{i,j=1,2}^{n-1,n} \hat{f}_{ij} + \sum_{i=1}^{n} \hat{f}_i + \hat{f}_0 \end{aligned} \tag{2.3.3}$$

As an example is shown the effects ($\hat{f}_i \equiv e_i$) for a set of three factors 1,2 and 3 (equation 2.3.4). *Effect* is understood as the role that has had the factor during the forecasting

of the field. Synergetic effects are only the effect of the mutual interaction without the counting part of the individual effect. Is unusual provide synergies of three or four factors, due to the difficulty to give an appropriated physical meaning of a triple or four factor synergy.

$$\begin{aligned} e_0 &\equiv \hat{f}_0 = f_0 \\ e_i &\equiv \hat{f}_i = f_i - f_0 \\ e_{ij} &\equiv \hat{f}_{ij} = f_{ij} - (f_i + f_j) + f_0 \\ e_{123} &\equiv \hat{f}_{123} = f_{123} - (f_{12} + f_{13} + f_{23}) + (f_1 + f_2 + f_3) - f_0 \end{aligned} \tag{2.3.4}$$

2.3.1 Differential application

FS results present a great dependency on the number of factors. All those effects due to factors that have not been selected remain as hidden or unknown synergies in the factor separation results or the basic simulation s_0. That ambiguity in the results can be treated in two different ways: applying the fractional approach of the FS technique (Krichak and Alpert, 2002), and/or studying the response of the pure effects to a change in the number of factors that are used in the FS (Alpert et al., 1995).

- **Fractional approach:** it tries to deal with the hidden factors summarised in the interaction of a specific factor with the environment (hidden factors). Considering interactions with the environment, FS equations are rewritten as:

$$\begin{aligned} f_0 &= \hat{f}_0 \\ f_{a0} &= \hat{f}_0 + \hat{f}_a + \hat{f}_{a0} \\ f_{b0} &= \hat{f}_0 + \hat{f}_b + \hat{f}_{b0} \\ f_{ab0} &= \hat{f}_0 + \hat{f}_b + \hat{f}_b + \hat{f}_{a0} + \hat{f}_{b0} + \hat{f}_{ab0} \end{aligned} \tag{2.3.5}$$

  where $\hat{f}_{\chi 0}$, contribution of interaction of the factor χ with the background or hidden factors; $\hat{f}_\chi$, pure contributions of factor χ. The solution of the system keeps as:

$$\begin{aligned} \hat{f}_0 &= f_0 \\ \hat{f}_a &= f_{a0} - f_0 - \hat{f}_{a0} \\ \hat{f}_b &= f_{b0} - f_0 - \hat{f}_{b0} \\ \hat{f}_{ab} &= f_{ab0} - (f_{a0} + f_{b0}) + f_0 - \hat{f}_{ab0} \end{aligned} \tag{2.3.6}$$

  where usually $\hat{f}_{a0}, \hat{f}_{b0}, \hat{f}_{ab0}$ are neglected. In order to study hidden synergies an intercomparison of the considered effects (factors a, b) to gradual strengths of modification of each factor ($\hat{f}_{-k\chi},\ k = [0, 1]$) can be done. If the importance of the factor

or synergy is not linear with the strength of modification ($\hat{f}_\chi(k)$ *not* $\propto k\hat{f}_\chi$) implies that this factor must have a strong nonlinear interaction with a non-considered factor ($\hat{f}_{\chi 0}$). Fractional approximation of the FS technique multiplies the number of simulations by a minimum value of 3 (that means three-degree strengths of modification of the factor). This growths considerably the computational cost of the studies and limits its application.

- **Collection of factors:** The modification of the group and number of selected factors does not need additional simulations. In this method a pure effect (an effect related only to one factor, f_a) is selected. The effectivity of this factor is recalculated for each possible group of factors of the study (a, b, c) as follows:

$$\begin{array}{rcll} \hat{f}_a & = & f_a - f_0^a & \\ \hat{f}_a & = & f_a - f_0^{a,b} & \rightarrow \hat{f}_a \notin f_{ab} \\ \hat{f}_a & = & f_a - f_0^{a,c} & \rightarrow \hat{f}_a \notin f_{ac} \\ \hat{f}_a & = & f_a - f_0^{a,b,c} & \rightarrow \hat{f}_a \notin f_{ab}, f_{ac}, f_{abc} \end{array} \tag{2.3.7}$$

where, f_0^a, simulation without factor a (corresponding to a FS of one factor a); $f_0^{a,\chi}$, simulation without factors χ, k (corresponding to a FS of two factors a, χ); $f_0^{a,b,c}$, simulation without factors a, b, c (corresponding to a FS of three factors a, b, c).

Due to the aforementioned increasing consequence of the hidden synergies, the same factor will have less effect in a three factor study, than in a two factor study (see F_a surface diminishing as the number of factors increase in figure 2.3.1). However, the differences between effects should be linearly proportional to the number of factors included if the selected factor is an important factor for the evolution of the studied system. A difference on the behaviour of the effect as function of the collection of factors, could be a reflection of the synergy of this effect with another factor not included in the study, however this synergy would remain hidden and unknown in the result.

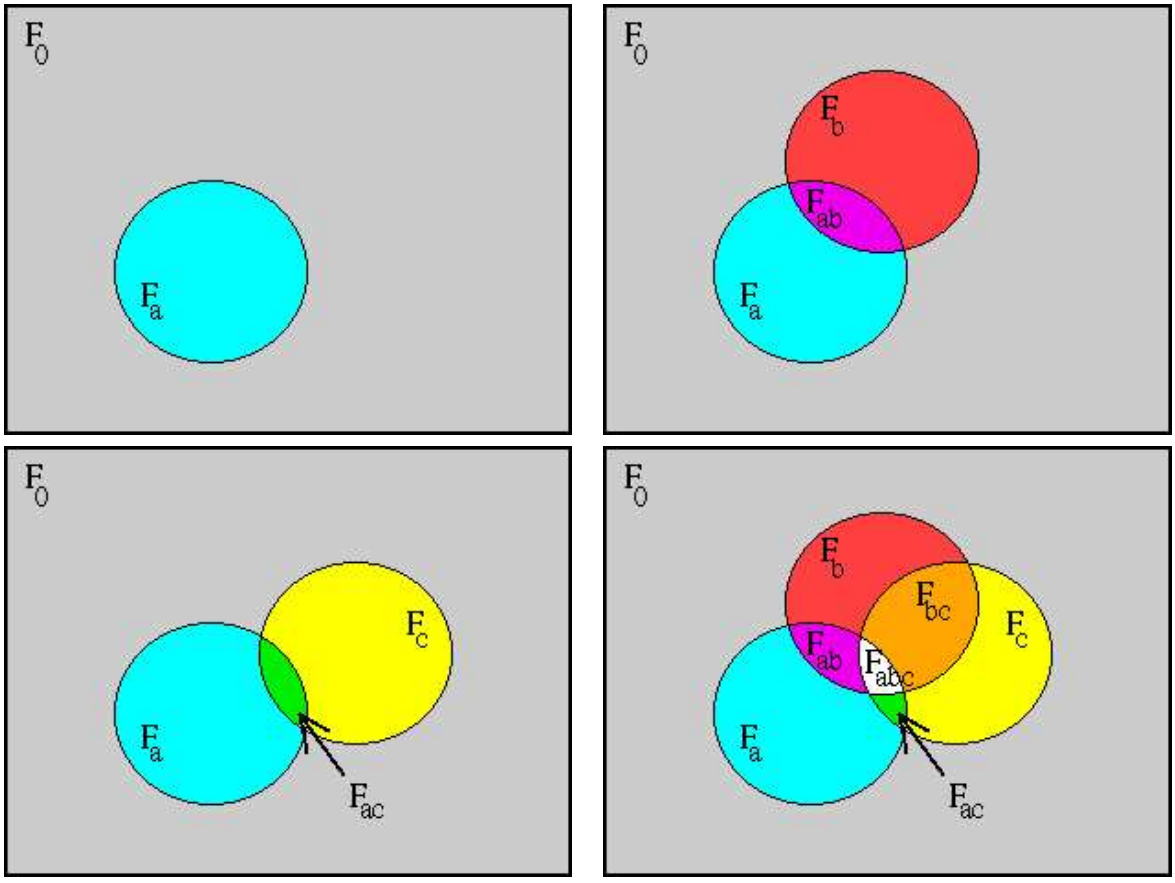

Figure 2.3.1: Representation of the factor separation for a factor F. Top left panel: FS for one factor a. Top right panel: FS for two factors a, b. Bottom left panel: FS for two factors a, c. Bottom right panel: FS for three factors a, b, c. Surface of F_a, diminishes as function of the selected factors

Chapter 3

Dynamical aspects of the cyclogenesis

Articles on which this chapter is based:

Ll. Fita, R. Romero and C. Ramis, 2006: *Intercomparison of intense cyclogenesis events over the Mediterranean basin based on baroclinic and diabatic influences*, Adv. in Geosci. (Proceedings PLINIUS 2006), **7**, 333-342

L. Fita, R. Romero and C. Ramis, 2007: *Objective quantification of perturbations produced with a piecewise PV Inversion technique*,Ann. Geophys., **25**, 2335-2349

Dynamical aspects of cyclogenesis is studied in two different manners. First study is focused on the role and influence of atmospheric features present at the beginning of a particular deep cyclogenetic case. Second study is a climatology of different cyclogenetic dynamical features of 11 cases that occurred allover the Mediterranean basin.

3.1 Baroclinicity

It is a way of development, growing and enhancing of cyclones. Basically it consists in the mutual interaction between upper and low level disturbances. One of the singularities of the mechanism is that coupling between disturbances reinforce each one and it can last a large period of time.

A favourable environment in which cyclones can be developed in the Northern hemisphere is based in the presence of a meridional low level horizontal thermal gradient and an upper level trough. Mediterranean basin often presents strong horizontal thermal gradients due to the coexistence of dry and warm air masses from the North African arid plateau and the north continental cold air masses. By this way, baroclinicity (see figures 3.1.1 and 3.1.2 for a schematic description) is one of the most common ways from which the cyclones develop in the Mediterranean basin. A deep and accurate study of the developing mechanism might help to improve forecasting of high impact hazardous weather as much as mitigate potential high destructive impact of cyclones on the densely habitated Mediterranean coastal lines and abrupt mountain ranges. Baroclinic development is a very frequent way of cyclone growing in the Mediterranean basin.

Baroclinic mechanism will interact with other phenomena that can enhance or mitigate the cyclogenic role. These other influences could be: sea surface, orography, coastal lines, surface fluxes, cloud formation. Meanwhile cloud formation is going on, large amount of water vapour is condensating in drops. As a result of it, large quantities of heat at middle levels are released due to latent heat of condensation. The warming of middle levels will influence in the development of the cyclone (see explanation in methodology section 2.2). Due tot the complexity of the Mediterranean basin all these influences (or even others) could have a role and they should be taken into account. Non linearities that are derived from these features will add complexity into the atmospheric phenomena. Thus baroclinicicty studies and other kind of meteorological studies in the Mediterranean basin become complicated due to the large amount of features, mechanism and relations that develop at the same time.

3.1.1 November 2001 case

In order to study the baroclinic mechanism in a Mediterranean case, November 2001 strong cyclone has been selected (Fita et al., 2007b). The 9th-12th November 2001 cy-

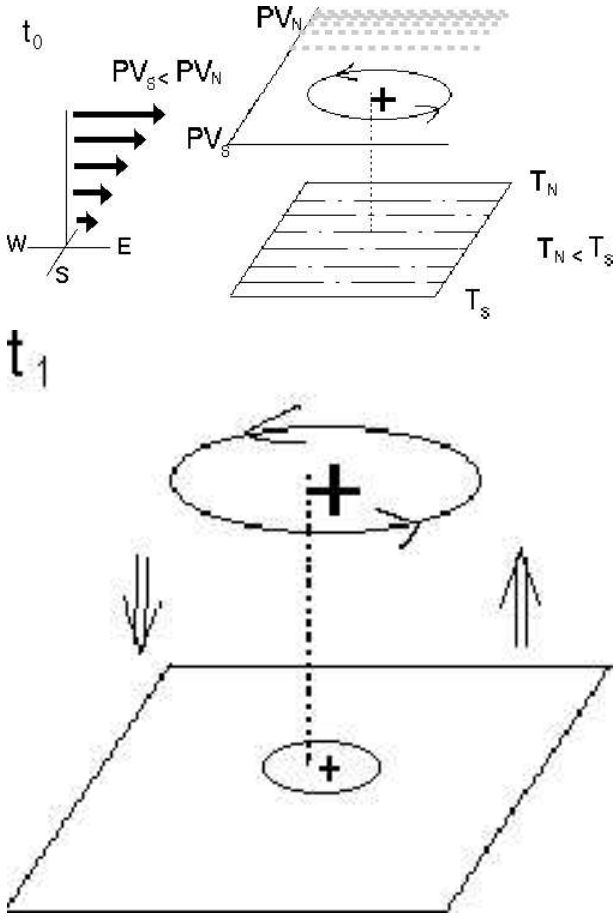

Figure 3.1.1: **Baroclinic Mechanism:** At initial time t_0, low levels present a pole-ward thermal gradient (dot-dash line), meanwhile at upper levels there is a positive PV anomaly (circle with arrows) and an westerly flow with a vertical shear (thick arrows). According to North hemisphere characteristics, temperature of the air is higher in south latitudes ($T_S > T_N$), and PV is higher in northern latitudes ($PV_S < PV_N$, reservoir in the polar zone shown as dashed thick gray lines). Upper level PV anomaly induces (t_1) cyclonic vorticity everywhere in the space that also influenced the surface (surface + circle). At the same time, in the front(back) zone of the PV anomaly upward(downward) motions of the air are developed (according to the ω equation (eq. 2.2.21), double arrows)

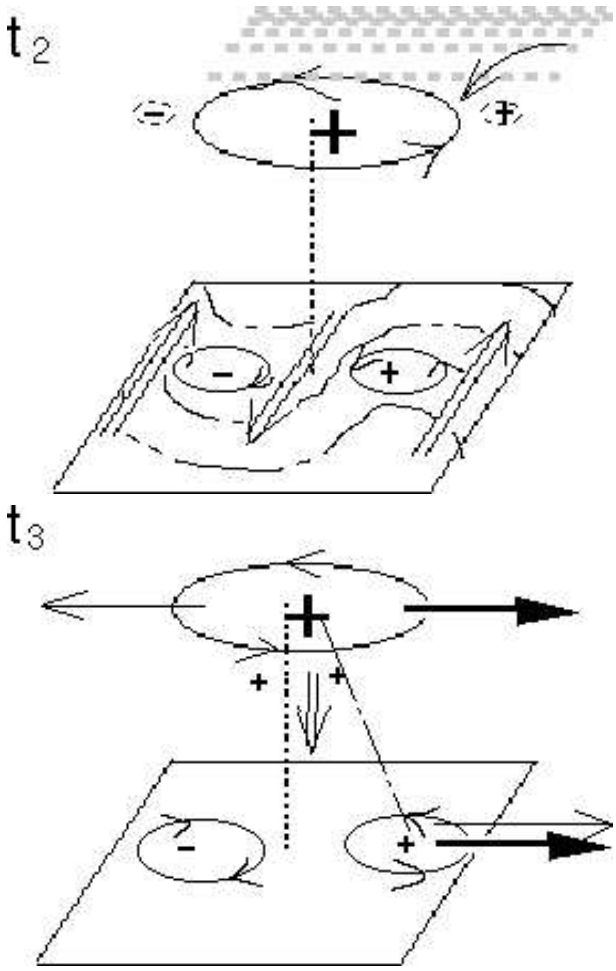

Figure 3.1.2: **Baroclinic Mechanism continuation:** As a result of the surface cyclonic induced circulation (t_2), surface thermal gradient curves its morphology and two rotational flows are generated: cyclonic (below of the frontal region of the PV anomaly) and anticyclonic (below the back region). The curvature of the horizontal thermal gradient increases thermal gradient, from which the surface rotational induced flows are enhanced. As a result of it, more warm south air is advected to the cold north region and vice-versa (double arrows). Surface pair of cyclonic/anticyclonic vortexes also influenced upper levels (small +/-, circles) and the frontal region of the PV is affected by positive PV advections from the polar reservoir. This PV advection will contribute to growth the PV upper level anomaly. Individual movements (in t_3 thin arrows) will separate upper and surface disturbances, but the background flow (thick arrows) and the influences provoke a coupling between disturbances. This coupling creates a reinforce of each anomaly. This phase-coupling between disturbances can last for large periods of time creating strong and deep cyclones.

clone has been described by the author as one of the most intense events in the Western Mediterranean basin during the last 25 years. The cyclone has been classified as a deep episode in the three-dimensional climatology done by Campins et al. (2006). It has been also widely studied (Davolio and Buzzi, 2004; Tripoli et al., 2005; Argence et al., 2006). In 24 hours a strong and deep vortex was formed. As a result, heavy precipitation and strong winds were recorded in Algiers and in the Balearic Islands. Seven hundred people died as a result of severe floods in Algiers, and 4 people died in Balearic Islands, where sustained winds of 30 ms^{-1} and precipitation above 200 mm/24 h were recorded and about two million trees felt down in the Mallorca Island.

The case is a clear and strong example of Pettersen-Smeybe class B cyclone evolution (Pettersen and Smebye, 1971), in which a cyclone is formed in a pre-existing upper level trough environment. The genesis and evolution of the case presents similar characteristics to the case occurred in December 1979 in the Western Mediterranean basin (Homar et al., 2002a). On 10th November 2001, a disturbance was formed at surface to the south of the Atlas mountains range (see figure 3.1.3, with the ECMWF analyses maps). A significant upper level disturbance was located over central Europe, extending from the Iberian peninsula to the Baltic Sea. This upper level disturbance shows a structure of two high PV positive anomalies (C0, C1, see labels in figure 3.1.3). Over the Mediterranean Sea there was a post storm situation with residual convective activity (not shown). As a result of the surface African low and the upper level disturbance, strong thermal gradients developed over the western Mediterranean basin. The low level cyclone moved northwards meanwhile the upper level disturbance translated southwards. While the low level low crossed the Atlas mountains, the upper level PV positive centres described a singular relative rotational movement, attributed to their interactions through PV advection. Mutual interaction between different positive PV vortices has been shown as an important factor that contributes to the cyclogenesis (Hakim et al., 1996). Although in this case, there was not a merge of the PV centres.

On 10th November at 18 UTC a strong interaction between upper level and low level disturbances was established. This is identified in figure 3.1.4 as the closeness between upper level disturbance (see the tropopause fold, or free cloud area), and a strong cyclonic cloud structure (cyclone, indicated by curved arrows). These configurations of proximity between strong surface thermal gradients and upper level trough disturbances become the ideal environmental conditions, under an appropriate vertical wind shear, to produce the baroclinic growth of disturbances. It has been described as one of the most important baroclinic processes from which deep cyclones can be formed (Hoskins et al., 1985; Bleck, 1990). From that time the cyclone crossed the Algerian coast and reached its mature state (Nov. 11th at 00 UTC), while strong cloud formation was present in the area. Strong winds were produced at surface (33 ms^{-1} sustained wind records were registered on Balearic Islands between 11th November 00 UTC and 06 UTC). Some time later the

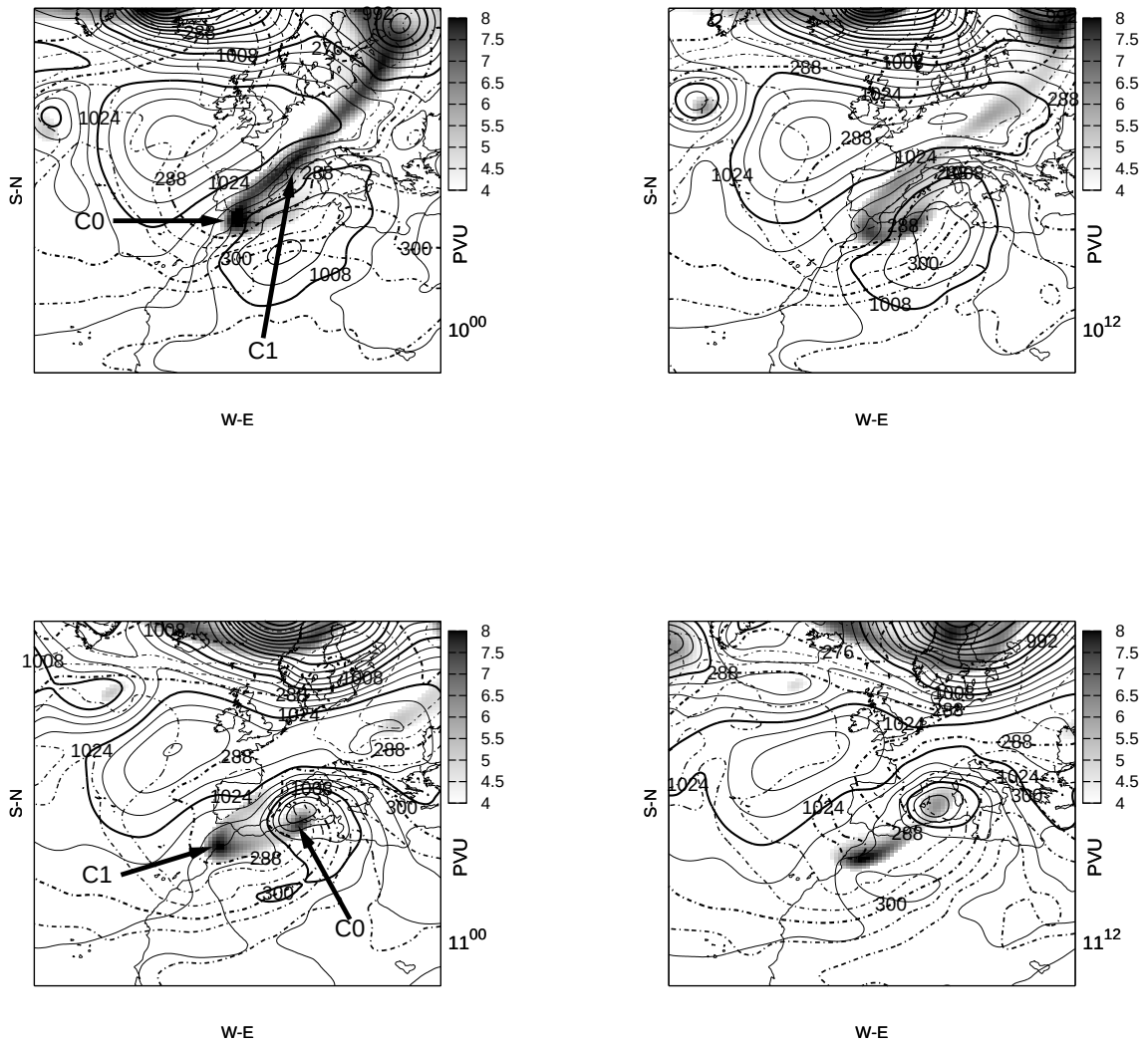

Figure 3.1.3: Sea level pressure (every 4 hPa, solid line), Potential temperature at 850 hPa (every 4 K, dashed line) and Isentropic Ertel PV at 330 K (1 PVU=$10^{-6} m^2 K s^{-1} kg^{-1}$, coloured field) from ECMWF analyses on Nov. 10th 2001 at 00 UTC (top left), Nov. 10th at 12 UTC (top right), Nov. 11th at 00 UTC (bottom left) and Nov. 11th at 12 UTC (bottom right)

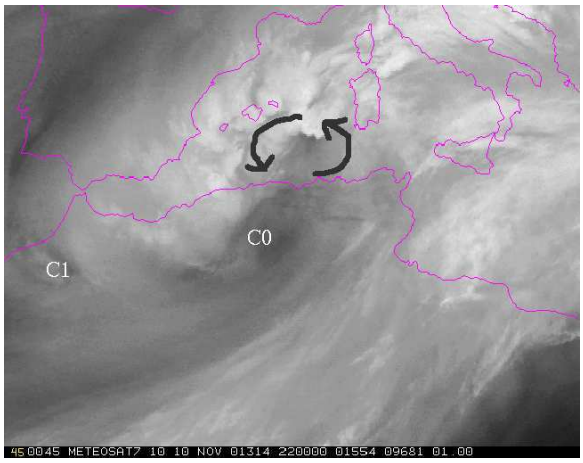

Figure 3.1.4: Normalised Water Vapour METEOSAT7 image on Nov. 10th 2001 at 22:00 UTC. EUMETSAT source

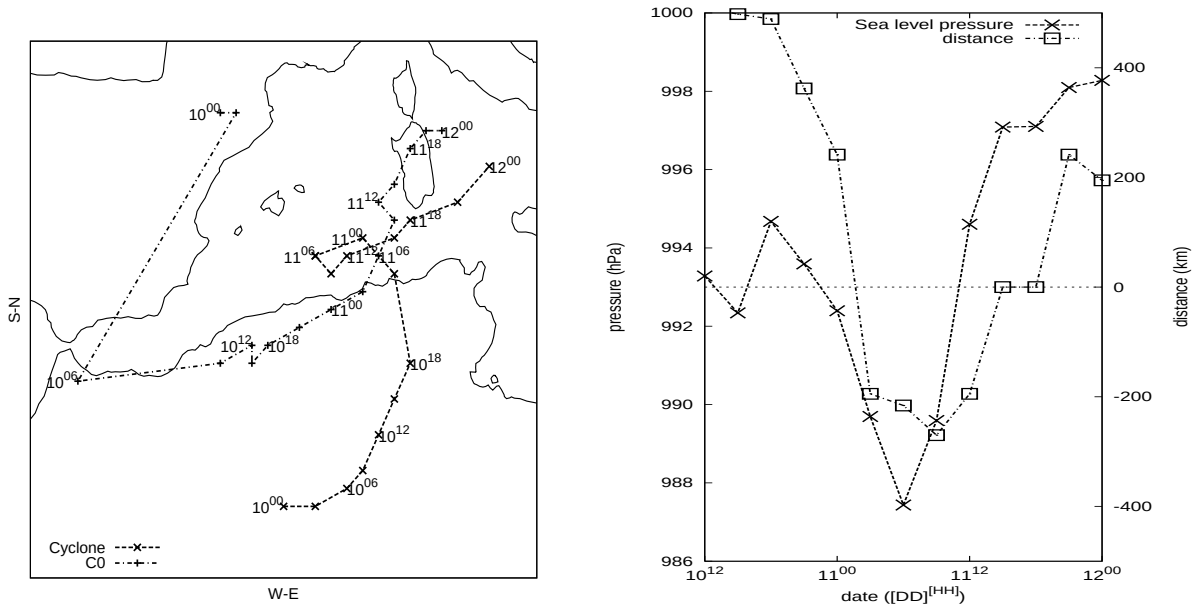

Figure 3.1.5: Control simulation results. Left panel: Evolution of the position of the cyclone (dashed line) and the C0 (slash-dot line), date of position is included ($[DD]^{[HH]}$). Right panel: Evolution of the central pressure of the cyclone (hPa, y-axis left) and its relative horizontal distance with C0 (km, y-axis right) since Nov 10th at 12 UTC. Relative horizontal distance is the distance between the positions of the centre of C0 and the cyclone. Positive(Negative) values of the relative distance occur when the cyclone is located eastward(westward) from C0

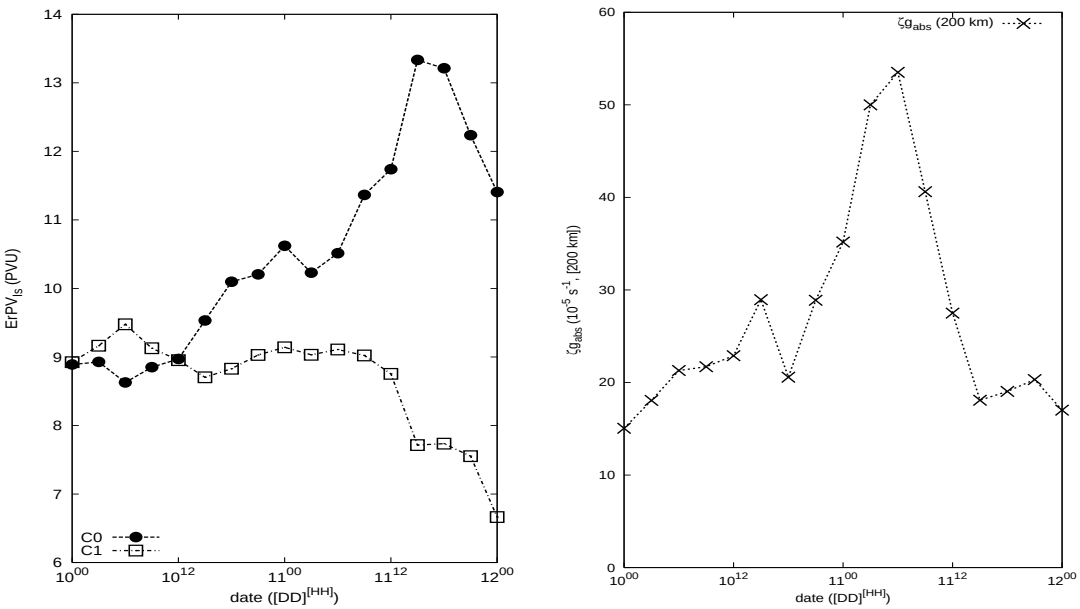

Figure 3.1.6: Left panel: Simulated central value (PVU) of the two upper level vortices C0 and C1, that are embedded within the upper level trough. Right panel: Evolution of the geostrophic vorticity calculated at 200 km (defined like in (Campins et al., 2000)) using a constant Coriolis value of $C_0 = 8.25 \times 10^{-6}\ s^{-1}$, and density $\rho = 1.225 kgm^{-3}$

upper-low levels interaction weakened because of the southward movement of the upper level disturbance and northward motion of the cyclone. At this point the cyclone weakened and described an eastward movement while it approached to the Sardinia Island.

The case will be studied using the MM5 nonhydrostatic primitive equation mesoscale model (Grell et al., 1994). A control simulation is run with one domain with a horizontal resolution of 54 km and 23 vertical levels. The simulated period comprises the interval between Nov. 10th 2001 at 00 UTC and Nov. 12th 2001 at 00 UTC. Control simulation will prescribe the main characteristics of the cyclone that will be compared to the simulated cyclones obtained from the PV-based sensitivity tests. All MM5 simulations will be run in the same configuration based on a graupel(reisner2) scheme for the explicit moisture processes, Kain-Fritsch scheme for the cumulus convection, mrf parametrisation for the planetary boundary layer and the 'rrtm' scheme (long wave) for the atmospheric radiation.

In order to track the baroclinic mechanism, the trajectories of 'C0' (the southwestern upper level PV vortex inside the upper level trough on Nov. 10th at 00 UTC, figure 3.1.3 of ECMWF analyses) and the surface cyclone are analysed. During the initial phase of the evolution, control simulation results show that meanwhile the upper level positive

vortex C0 moved southward, the cyclone moved northward. By this way the low-level disturbance and C0 got closer (Nov. 10th at 12 UTC in figure 3.1.5). While the relative horizontal distance between upper and low level disturbances decreased, the cyclone and C0 increased their intensity as a reflection of the baroclinic theory of phase coupling between upper and low level disturbances (Hoskins et al., 1985). However, the cyclone reached its mature state on a negative baroclinic-phase (C0 is located east relative to the cyclone, figure 3.1.5 on Nov. 11th at 00 UTC).

In this phase of the cyclone evolution, the cyclone reached the Mediterranean coast. Latent Heat Flux from the Sea surface and the vigorous release of latent heat due to a strong cloud formation at mid levels (see Water Vapour satellite image in figure 3.1.4) could contribute to the intensification of the cyclone. Intensification of cyclones due to the diabatic effects induced by the sea has been detected in other cases like in the North Atlantic 'bombs' (Sanders and Gyakum, 1980; Kuo et al., 1991a,b), or other Mediterranean cases (Homar et al., 2002a; Romero, 2001). Moreover, the block-phase mutual interaction of the baroclinic process is also shown by the increasing central value of the C0 (figure 3.1.6). A significantly different behaviour between the two upper level vortices is observed in the same figure. Whereas C0 became deeper, the other centre (C1) remained constant during the mutual interaction period (Nov. 10th 15 UTC to Nov. 11th 00 UTC, see figure 3.1.6). It is shown how C0 preserves its PV during the African phase of the cyclone. However, when the cyclone reached the Sea, strong diabatic processes are developed and C0 suffered an important increasing of its PV value (not shown). Meanwhile C1 conserves its PV during almost all the period of simulation.

During the African phase of the cyclone evolution (from Nov. 10th 00 UTC to Nov. 10th 18 UTC), the cyclone shows low vorticity (see figure 3.1.6). When the cyclone reached the sea it attained the mature state (Nov. 11th 00 UTC), depicted as: lowest surface central pressure value (988 hPa) and strong geostrophic vorticity (more than $30 \times 10^{-5} s^{-1}$ at the centre of the cyclone, computed using 200 km resolution geopotential data as in Campins et al. (2000)).

This episode is studied with the piecewise PV inversion technique following a new methodology of quantification of the initial modification.

3.1.2 Quantification of the initial modification

Piecewise PV Inversion technique combined with perturbed numerical simulations have been used as a tool to dynamically study different various of atmospherics systems (Hakim et al., 1996; Huo et al., 1999; Romero, 2001; Homar et al., 2002b; Argence et al., 2006). This technique can offer useful information about mechanisms and roles of wide range of features involved in the life cycle of the event. Although numerical solutions are well-

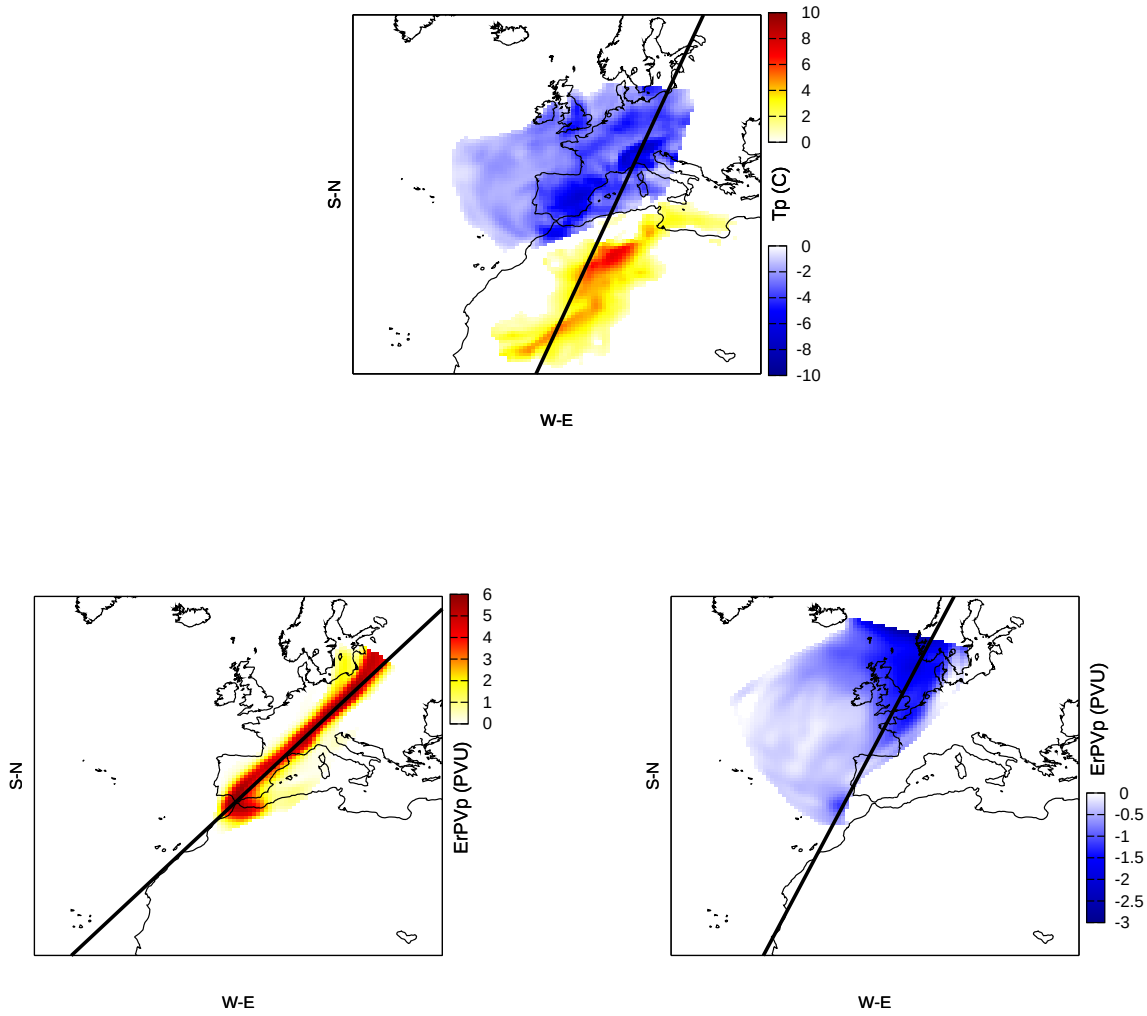

Figure 3.1.7: Surface thermal anomaly defined as ErPVpTerm (top; yellow-red, positive values; white-blue, negative values), Upper level PV perturbation (300 hPa) related to upper level trough defined as ErPVp01 (bottom left), Upper level PV perturbation (300 hPa) related to North Atlantic High defined as ErPVpHigh (bottom right), different scales are used. Solid lines show different vertical cross sections

defined throughout the set of equations, some uncertainties and subjectivities arise in its application, that can deeply influence the results. Some of these case dependent aspects are: set of balance equations used in the inversion, boundary conditions for the inversion, computation of reference state from which will be defined the PV anomalies (zonal mean, temporal mean, number of members to establish an average, etc), morphology and magnitude of the anomalies and degree of modification of the initial conditions.

In order to diminish subjectivity in the procedure, an objective way to quantify the initial modification introduced in the perturbed simulations is proposed as a method to quantify the latter aspect of the technique. The quantification of the perturbation is expressed as the mean absolute variation of the total energy between the initial and the modified fields, considering the whole horizontal domain of simulation and all vertical levels. The capability to compute the "total amount" of the introduced modification makes possible an objective control of one important aspect of the PV inversion technique, favouring meaningful intercomparisons of perturbed scenarios.

Selected anomalies might be morphologically and spatially different. The modification of the model initial conditions derived from these might be significantly different. In order to compare the roles of the PV anomalies, a 'normalisation' of the perturbation should be done. Then, one could be sure that the total amount of change introduced by means of the inverted fields remains initially constant among the simulations, independently of the size and strength of the anomaly. Thus the results can be adequately intercompared; meanwhile, the nonlinear evolution of the atmosphere will show the sensitivity of the event to changes in the initial conditions as differences between the derived simulations.

PV Inversion technique applied at each PV anomaly produces three-dimensional balanced fields (geopotential, temperature, stream function/horizontal wind). Since inverted fields are obtained for all the space, the normalisation or quantification of the perturbation requires a three-dimensional variable, and since PV inverted fields represent all atmospheric variables (except humidity), the index used for the normalisation should be a combination of these variables. The *total energy* (Bluestein, 1992) has been chosen as a plausible function. Using the energy, an energy-derived dynamical study of each anomaly can be accomplished. It can be an useful information from which a deeper understanding of the role of the collection of features can be obtained. This is possible since total energy can be split in three components: kinetic ($\delta\mathcal{ENG}_{kin}$), potential ($\delta\mathcal{ENG}_{pot}$) and internal energy ($\delta\mathcal{ENG}_{int}$). The grid point energy ($\mathcal{ENG}$) is obtained from the integration of the volumetric density of energy ($\delta\mathcal{ENG}$) across the volume of the grid point ($\delta\mathcal{V}$, see equations 3.1.1).

$$\mathcal{ENG} = \delta\mathcal{ENG}_{kin}\delta\mathcal{V} + \delta\mathcal{ENG}_{pot}\delta\mathcal{V} + \delta\mathcal{ENG}_{int}\delta\mathcal{V}$$

$$\begin{aligned}
\delta\mathcal{ENG}_{kin} &= \frac{1}{2}\|\vec{v}\|^2\rho = \frac{1}{2}(u^2+v^2)\rho \\
\delta\mathcal{ENG}_{pot} &= gH\rho \\
\delta\mathcal{ENG}_{int} &= C_vT\rho \\
\delta\mathcal{V} &= \frac{ds\Delta p}{\rho g}
\end{aligned} \tag{3.1.1}$$

where $\|\vec{v}\|$, wind speed; ρ, density; g, gravity; H, geopotential height; C_v, heat capacity at constant volume; T, temperature; ds, areal size of the grid point; Δp, pressure variation between bottom and top of the grid cell.

PV inverted fields used to modify the initial conditions generate a change of the total amount of energy in the atmospheric domain of the simulation. It is proposed to compute the energetic modification as the mean absolute variation of the total energy ($\mathcal{MAV}$, equation 3.1.2). Root Mean Square Variation ($\mathcal{RMSV}$) could have been proposed, but contributions of big and small energetic variation values are differently weighted in the $\mathcal{RMSV}$, since the differences are squared in the calculation.

$$\mathcal{MAV}_\chi = \frac{\sum_{i,j,k}^{Ni,Nj,Nk} |\chi_{mod}(i,j,k) - \chi_{ref}(i,j,k)|}{Ni \times Nj \times Nk} \tag{3.1.2}$$

where $\chi_{mod}(i,j,k)$ is the modified energy at each grid point; $\chi_{ref}(i,j,k)$ the unperturbed field and N_i, N_j, N_k, the number of grid points in each direction.

The proposed normalisation of the perturbations is realised by imposing the same energy variation in the initial conditions for each anomaly. Although each PV anomaly will modify with a different pattern the environment, the total amount of introduced/removed energy is forced to be the same. This condition will be condensed on a given percentage of the inverted balance fields to be used to modify the initial conditions.

However, one can not infer directly that an increase or decrease of the available energy to the environment will produce deeper or weaker systems. Any information about changes in morphology and position of the features in the fields, from which genesis and maintenance of the atmospheric systems are explained, must be also considered. Since zonal, meridional or vertical relations between features can dominate significantly the dynamics of a phenomena. That is the case of baroclinic instability as it was shown by Robinson (1989). The study of the impact and related dynamics of the energetic changes introduced by modifications of the initial conditions are out of the objectives of this study. They can be considered as a step further procedure once the certainty in the objective quantification can be verified.

The proposed quantification method of the piecewise PV inversion derived perturbations can be applied as a general methodology in dynamic meteorology. The application to various events would allow an objective intercomparison between cases independently of the morphology, characteristics and origin of the selected anomalies. This method of quantification could contribute to the PV study and analysis based on the most important features involved in the evolution of the cyclones or other atmospheric phenomena.

Energetic quantification of the modification introduced in the initial conditions will be used as a way to study the sensitivity to three different aspects of the case: upper level trough, low level thermal disturbances and environment (see equation 3.1.1). Quantification methodology fixes the total amount of modification introduced for each PV anomaly to be the same (from an energetic point of view). In the November 2001 case, the Upper level disturbances (ErPVp01 and ErPvpHigh) are clearly stronger than the surface thermal one (ErPVpTerm in figure 3.1.7). In order to avoid extremely high modification of the initial conditions or high percentages of modification with the inverted fields for one PV anomaly, the surface thermal anomaly will be used as reference. Thus a 70% of modification made with the PV inverted fields from the surface thermal anomaly is fixed as the reference. This reference of percentage of modification with the inverted fields of ErPVpTerm anomaly fixes an energy perturbation ($\mathcal{MAV}$, equation 3.1.2) of about 0.145 PJ (PJ = 10^{15} J) on the initial conditions. This energy value is used to fix the total amount of variation of the inverted fields of the upper level anomalies. In order to obtain the percentage of modification in the initial fields with the inverted fields for the other two PV anomalies, a Newtonian or bisection iterative numerical method (Arfken, 1985) is used. This method is used to obtain the percentage of the inverted fields from ErPVp01 and ErPVpHigh that preserves the same amount of energy variation as the ErPVpTerm modification. Basically in the bisection method, next numerical value introduced in the iterative process is obtained as an average from the last to pair of values that are higher or lower than the desired result. The results of this numerical computation are summarised in table 3.1.a.

Different perturbation energy profiles are derived from the anomalies as it is shown in figure 3.1.8. ErPVpTerm influences much more the low levels, whereas ErPVp01 and ErPVpHigh influence strongly the upper levels. ErPVp01 is more evenly distributed in the vertical than ErPVpHigh, depicting the structural differences between troughs or cut-off lows and anticyclones acting as upper level blocking features (Hoskins et al., 1985; Thorpe, 1986).

Figure 3.1.9 gives spatial information on the impact of each anomaly over the initial conditions. It shows the three-dimensional effect on the total energy. ErPVpTerm extracts and adds energy to the environment. Since ErPVpTerm anomaly is aimed to capture the surface baroclinicity of the initial environment, it has been constructed with

Table 3.1.a: Percentage of modifications of the inverted fields of each anomaly (%) used to modify the initial conditions following the bisection method. Mean absolute variation of the total energy ($\mathcal{MAV}$ in PJ, $10^{15}J$) introduced on the initial conditions (+, increasing case; -, decreasing case)

Final values		**ErPVpTerm**		**ErPVp01**		**ErPVpHigh**	
		%	δ_{ENG}	%	δ_{ENG}	%	δ_{ENG}
+	$\mathcal{MAV}$	70	0.14504	8.8780	0.14504	7.6002	0.14505
-	$\mathcal{MAV}$	70	0.14508	8.8002	0.14509	7.6401	0.14508

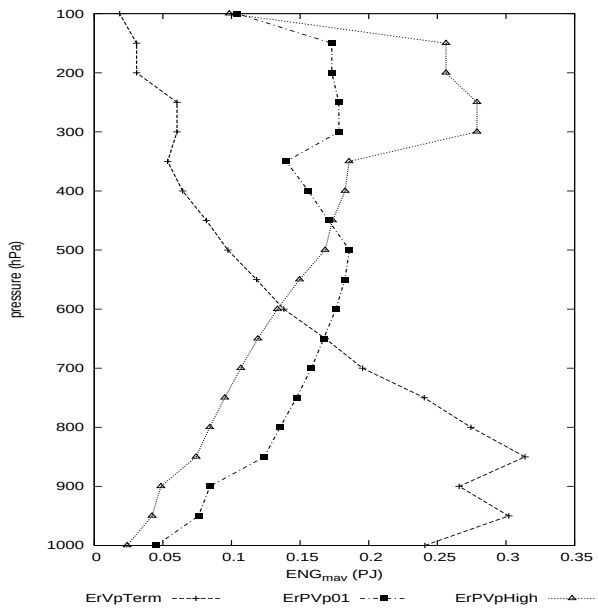

Figure 3.1.8: Vertical profile of the mean absolute energy variation ($\mathcal{MAV}$) of the initial conditions according to the positive percentage found for each anomaly. ErPVpTerm (cross), ErPVp01 (filled square), ErPVpHigh (triangles). Note that the same area is enclosed by each curve (same total energy)

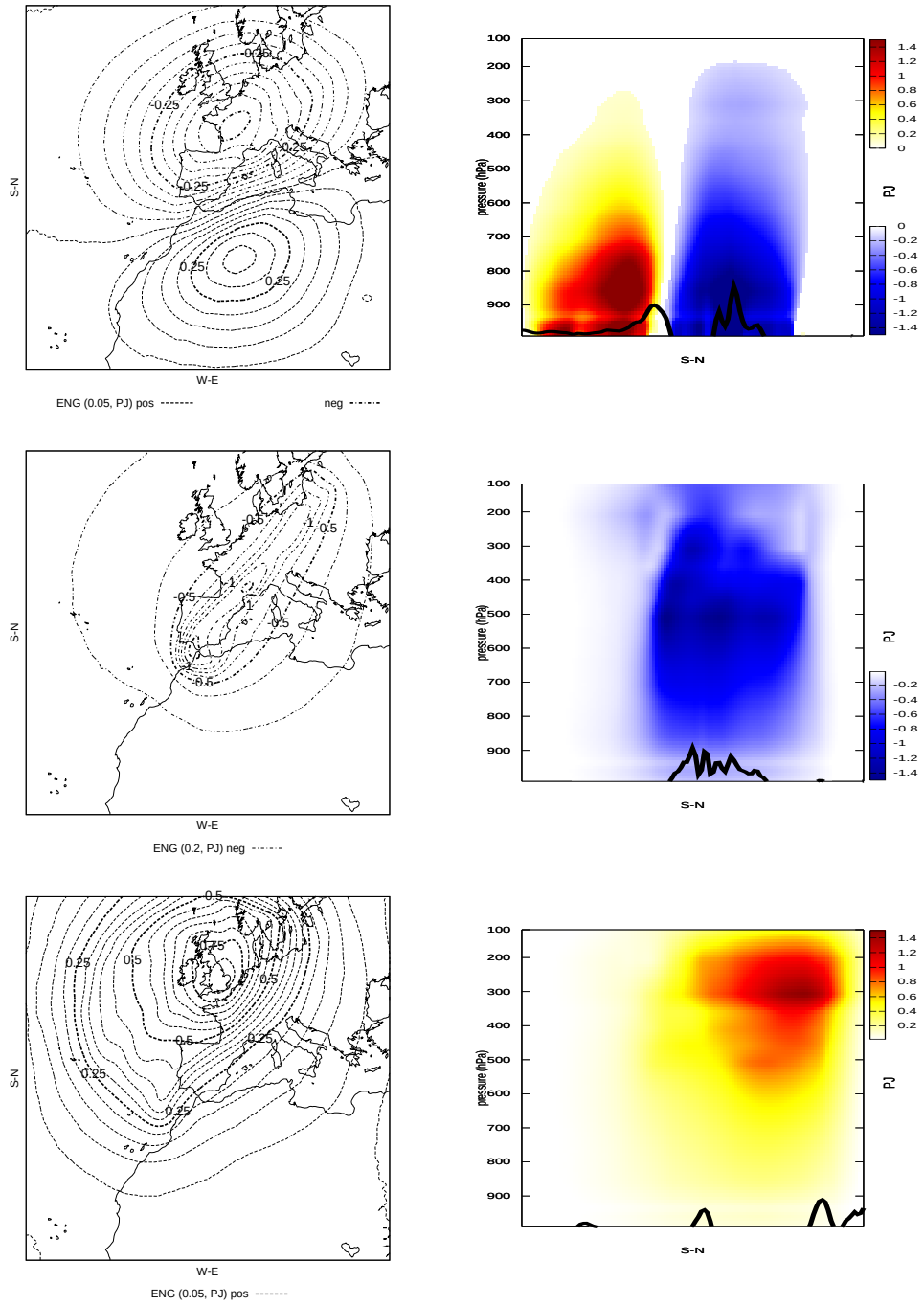

Figure 3.1.9: Energy variations (PJ, $10^{15}J$) introduced after the modification of the initial conditions (Nov. 10th 2001 at 00 UTC), according to each positive percentage of modification of the PV Inverted fields of each anomaly; ErPVpTerm (top), ErPVp01 (middle), ErPVpHigh (bottom). At 500 hPa (left) and following vertical cross sections defined at figures 3.1.7 (right)

both the positive and negative surface thermal anomaly. Perturbations carried out with positive(negative) thermal anomaly is related to a decrease(increase) of the total energy. Upper level positive(negative) potential vorticity perturbations are related to a decrease(increase) of the total energy (see figure 3.1.13). Results of ErPVpTerm anomaly (top panel in figure 3.1.13) does not show and upward decrease profile as the $\mathcal{MAV}$ value (dash and cross line in figure 3.1.8). This is because ErPVpTerm is based on both positive and negative thermal anomalies (top figure 3.1.7). As a result the inverted fields increase/decrease the energy of the environment. Figure 3.1.13 gives the averaged total variations of this energy (thus allowing compensation between terms), meanwhile in $\mathcal{MAV}$ computation this is not allowed since absolute values are used.

The perturbation energy partition among kinetic, potential and internal for each anomaly is shown in figures from 3.1.10 to 3.1.12 and 3.1.13. ErPVpTerm is related to a variation of the internal and potential energies. The effect is almost constant at all vertical levels. ErPVp01 and ErPVpHigh energy contributions are broadly similar. These anomalies have an important effect on the potential and internal energy, with the maximum energy variation found at upper levels. Significant perturbations of the kinetic energy are also found at upper levels, where the anomalies are defined. ErPVp01 has the highest impact on the potential energy, while ErPVpHigh on the internal energy.

However, one can not infer directly that an increase or decrease of the available energy to the environment will produce deeper or weaker systems. As it has been shown, increasing the upper level positive PV anomaly induces a significant decrease of potential and internal energy in spite that a strong upper level positive PV anomaly is usually related to strong cyclogenesis (Pettersen and Smebye, 1971; Hoskins et al., 1985). Energy impacts are shown as horizontally averaged values. Any information about changes in morphology and position of the features in the fields, from which genesis and maintenance of the atmospheric systems are explained, is not provided. Energetic implications for the baroclinic instability (Robinson, 1989) is out of the objectives of this study.

The sensitivity to changes in the initial conditions will be derived from the differences between the collection of simulated cyclones. The impacts on the simulated trajectories, central pressure value and central vorticity of the cyclones will be examined. Besides, a short description of the upper level vortex (C0) properties and evolutions will be given. The computation of the vorticity characteristics of the cyclones follow the criteria of Campins et al. (2000), where a 200 km grid length mesh is used.

Generally, in terms of central pressure values of simulated cyclones, is shown a symmetric response between positive and negative modifications of the initial fields (see figure 3.1.16). That is, the simulated two cyclones as a result of modification of the initial conditions adding or removing a percentage of the inverted fields of one perturbation, show

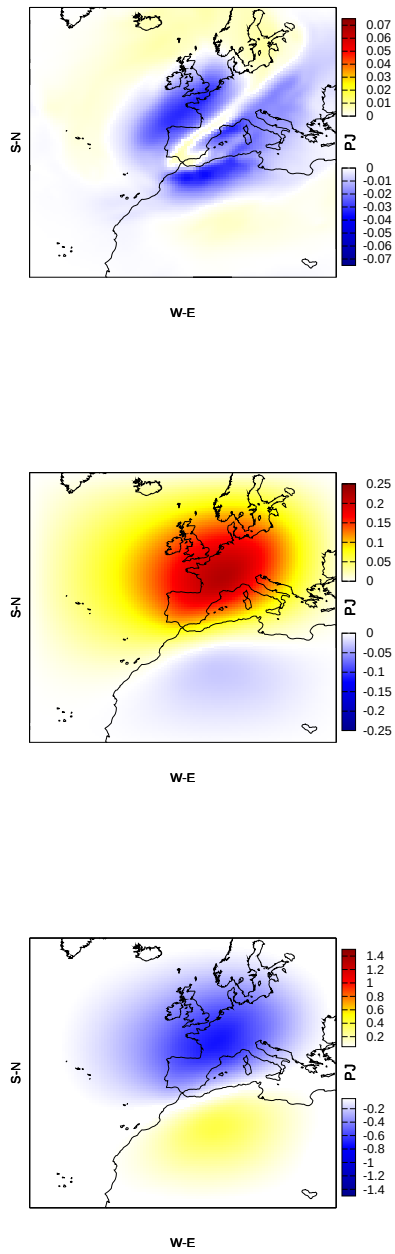

Figure 3.1.10: Energy variations (PJ, $10^{15}J$) introduced after the modification of the initial conditions (Nov. 10th 2001 at 00 UTC), according to the positive percentage of modification of the PV Inverted fields for anomaly ErPVpTerm. At 500 hPa for the kinetic term (top), internal (middle) and potential (bottom)

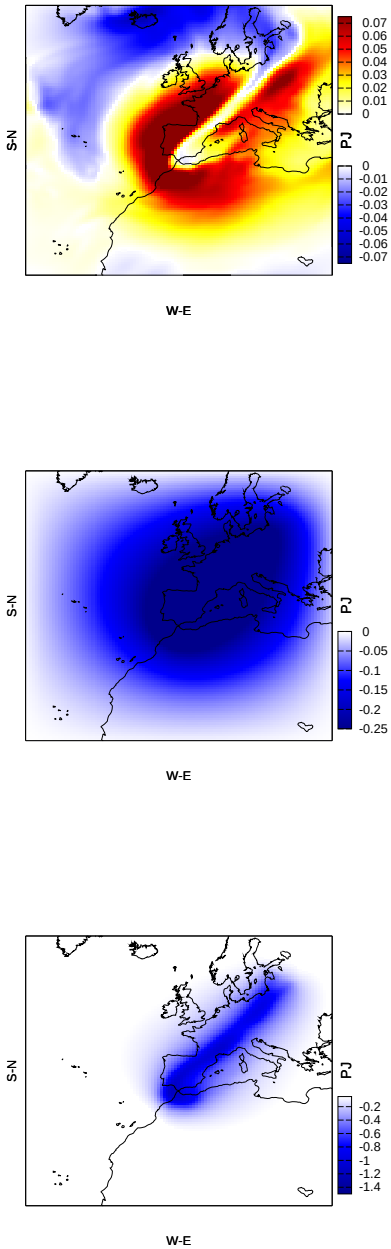

Figure 3.1.11: As in figure 3.1.10, but for the ErPVp01 anomaly

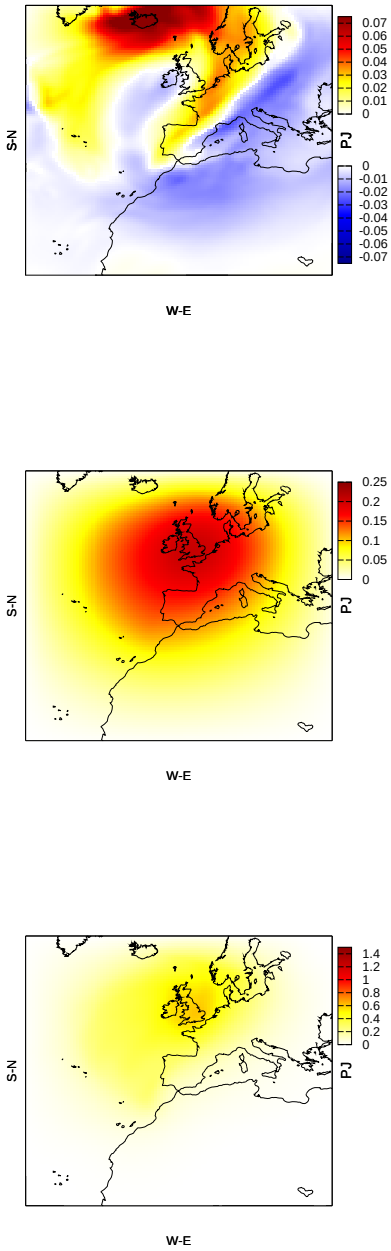

Figure 3.1.12: As in figure 3.1.10, but for the ErPVpHigh anomaly

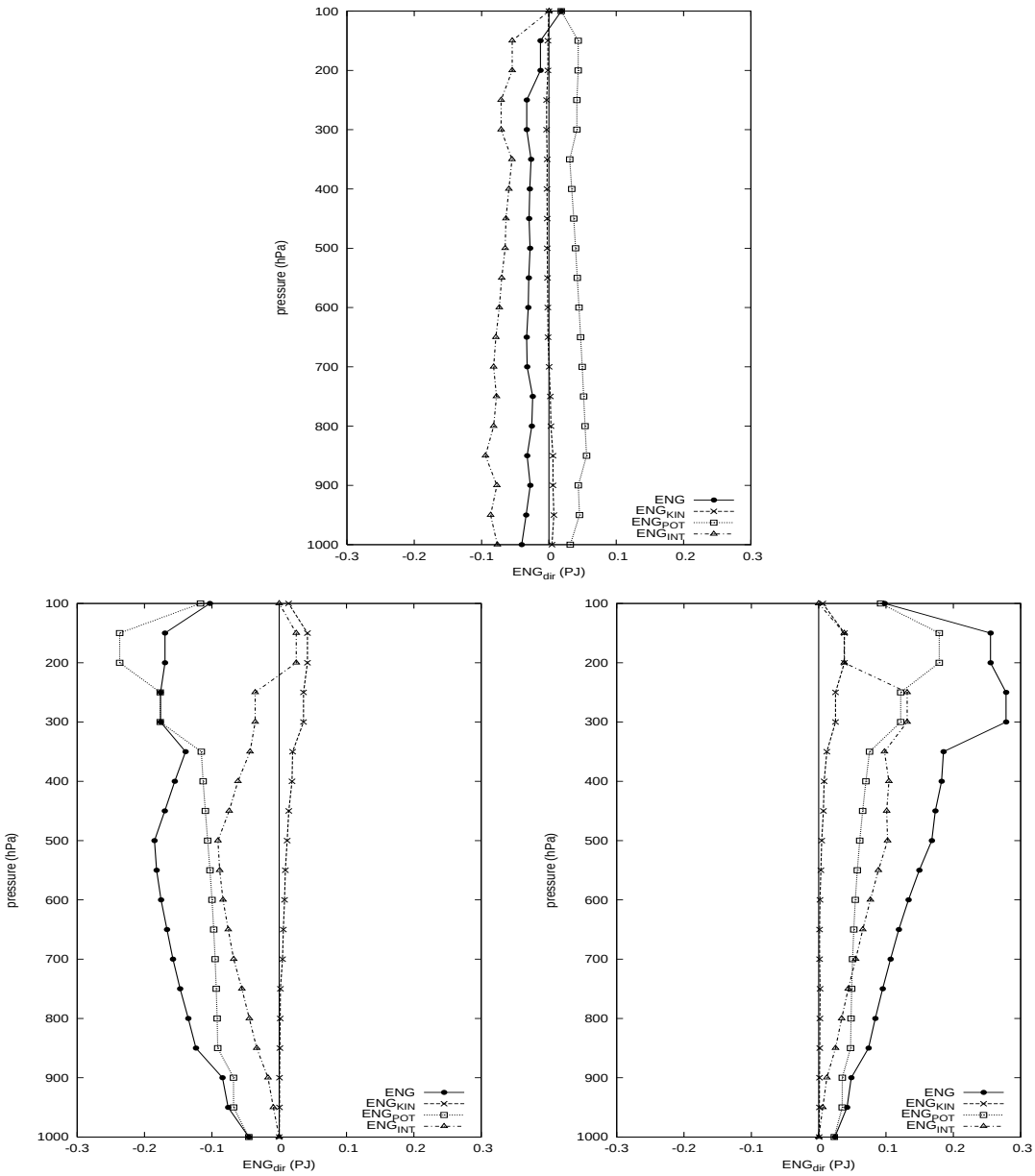

Figure 3.1.13: Vertical profiles of the horizontally averaged total variations of energy (in PJ, $10^{15}J$) according to the positive percentage of modification for each anomaly. Total energy variation (solid line, filled circles), Potential energy ($\mathcal{ENG}_{pot}$, dotted line with squares), Kinetic energy ($\mathcal{ENG}_{in}$, dashed line with crosses), Internal energy ($\mathcal{ENG}_{int}$, dot-dash line with triangles). ErPVpTerm (top), ErPVp01 (bottom left), ErPVpHigh (bottom right)

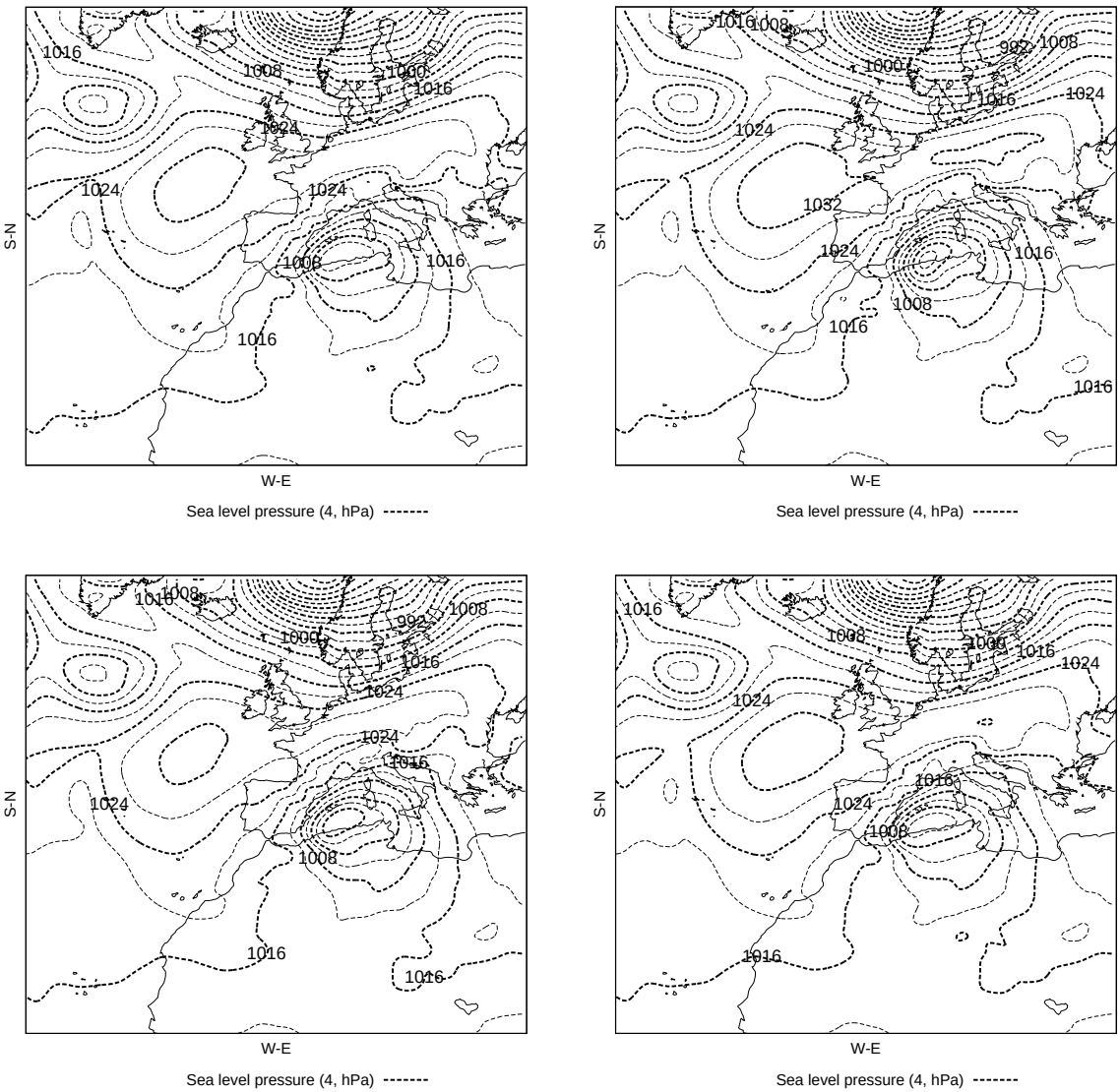

Figure 3.1.14: Sea level pressure at the mature state of the cyclone (Nov. 11th 00 UTC). Lines every 4 hPa. For the control simulation (top left), +ErPVpTerm (top right), +ErPVp01 (bottom left) and +ErPVpHigh (bottom right)

the same variations, with opposite sign, from the control one. These differences are not very strong owing to the small degree of modification introduced.

3.1.3 Sensitivity to upper level trough

The cyclone simulated through the ±ErPVp01 perturbations reveals significant impacts of the upper-level trough. The effects are most notable during the mature state of the cyclone on Nov. 11th at 00 UTC. The simulated cyclones and the C0 centres describe similar trajectories as the control ones (see lines with squares in figure 3.1.15). However, the evolution of the central surface pressure values and the C0 magnitudes have been changed (see lines with squares in figures 3.1.16, 3.1.17). Low differences are observed between the final PV values of C0 between the +ErPVp01 and -ErPVp01 cases (figure 3.1.17), probably due to diabatic influences.

Initially the perturbation of ErPVp01 is localised at upper levels, where the trough is altered (central pressure of the cyclones for ±ErPVp01 cases are initially only $\pm 1hPa$ different than the control one). During initial phase the cyclones preserve similar vorticities (see figure 3.1.18), but they change significantly their dimensions (not shown). Stronger or weaker upper level PV vortex do not produce any strong effect on the trajectory of the disturbances (similar trajectories as the control one are obtained, see figure 3.1.17). However, a weaker upper level disturbance (-ErPVp01 case) decreases the upper-low level interaction and this is depicted as a shallower mature cyclone. With a stronger upper level trough (+ErPVp01 perturbation) cyclone moves faster than the control one (figure 3.1.15). Significant geostrophic vorticity differences are obtained at the mature stage of the cyclone (Nov. 11th at 00 UTC, figure 3.1.18), as a reflection of the changes in the vorticity advections due to a stronger(weaker) upper level trough. In the last phase of the evolution of the cyclone, C0 value is similar to the control one, but central pressure values of the cyclone are clearly different (about $\pm 2hPa$), possibly related to changes in the relative phase between C0 and the cyclone at this ending phase. Like for the ErPVpTerm anomaly simulations, small differences between positive/negative cases in the maximum growth rate of the cyclone is also observed for this anomaly.

3.1.4 Sensitivity to low level thermal disturbances

The modification of the low level environmental baroclinicity (± ErPVpTerm) reveals significant variations with respect to the control simulation during the initial and last phases of the cyclone evolution. These differences are the largest ones among all the set of perturbations at the initial phase of the simulations. According to the results, the differences in the initial position of the cyclone are about 480 km (see figure 3.1.15), and for the initial central pressure value of the cyclone approx. $\pm 4hPa$ (see figure 3.1.16).

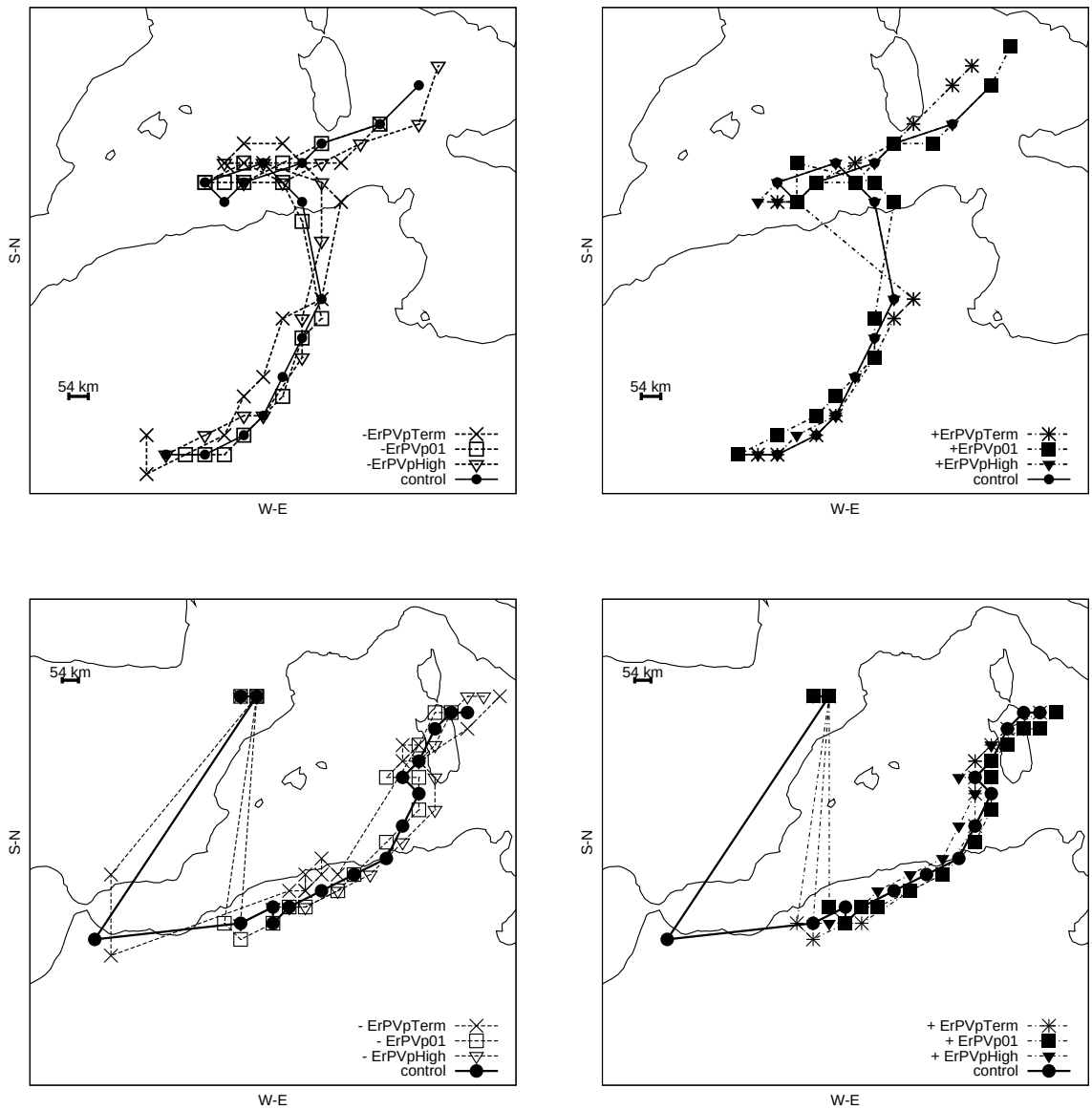

Figure 3.1.15: Top panels: Trajectories of the cyclone obtained from the initially perturbed simulations. Bottom panels: Trajectory of C0 for the different simulations. For the negative modifications (left), for the positive modifications (right). According to values on table 3.1.a. -ErPVpTerm (simple cross), +ErPVpTerm (full cross), -ErPVp01 (empty square), +ErPVp01 (filled square), -ErPVpHigh (empty triangle), +ErPVpHigh (filled triangle)

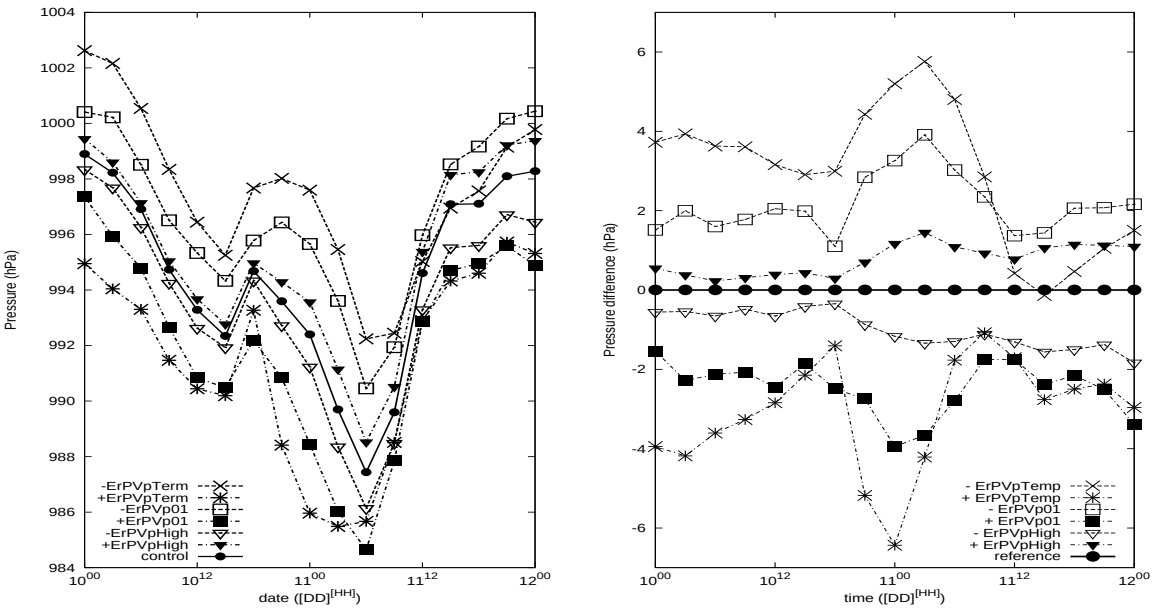

Figure 3.1.16: Labels as in figure 3.1.15, but Left panel: evolution of the central pressure of the cyclone. Right panel: evolution of the central pressure of the cyclone rescaled to control simulation results

At the same time, the simulated cyclones show strong variations in their vorticity (about $\pm 5\ s^{-1}$ at 200 km gridmesh point, in figure 3.1.18). As a result of the change in the initial position of the cyclone, the interaction between the upper and low level disturbances has also changed (the relative phase between the disturbances is significantly changed in comparison to the other simulations, figure 3.1.17).

In the -ErPVpTerm(+ErPVpTerm) case (perturbation of the initial conditions by subtracting(increasing) the fields related to the horizontal thermal anomaly) the initial trajectory of the cyclone is clearly different from the control one (see the two dashed lines with crosses in figure 3.1.15). The mature cyclones at Nov 11th 00 UTC show the largest variations with the control one: on the lowest central pressure value ($\pm 6\ hPa$, figure 3.1.16), relative distance with C0 (between 100-200 km in figure 3.1.17) and central value of the upper level trough C0 about 1 PVU less than in the control one, (figure 3.1.17). ErPVpTerm perturbations have a deep impact when the cyclone crosses the Atlas mountains, modifying the relation between the cyclone and the upper level trough. It is shown in the phase-relative-distance (figure 3.1.17). As result of it, the perturbed cyclone from -ErPVpTerm changes to a negative relative phase (C0 is located in an eastern position relative to the cyclone) 9 hours later than the +ErPVpTerm cyclone.

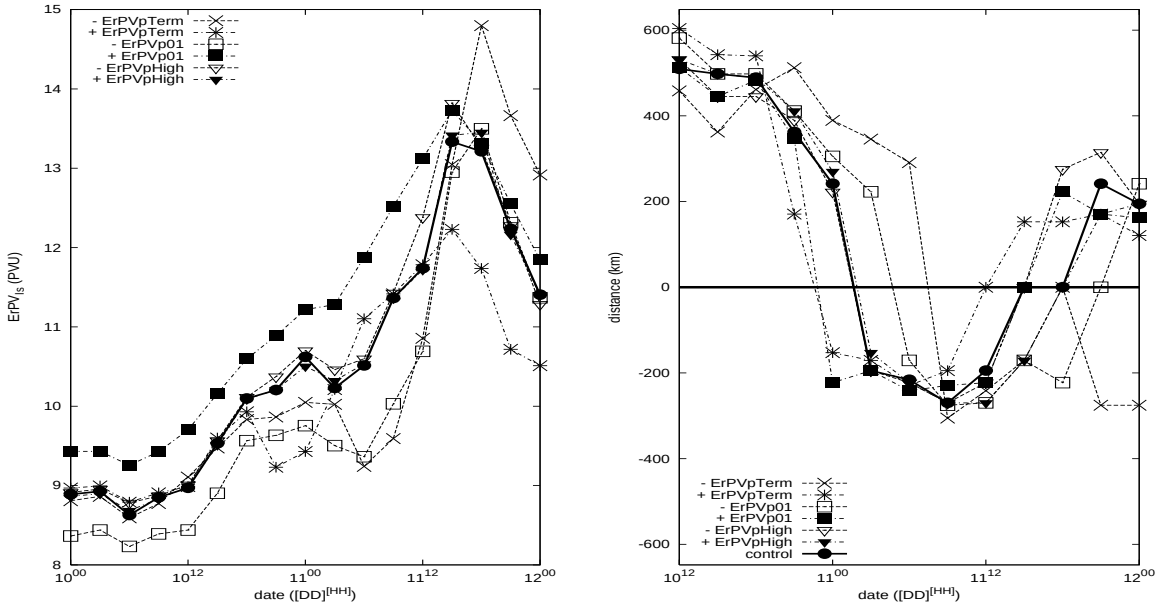

Figure 3.1.17: Labels as in figure 3.1.15, but Left panel: evolution of the C0 central value (PVU). Right panel: Evolution of the relative distance (km) between C0 and cyclone, positive(negative) sign denotes eastward(westward) relative position of the cyclone (starting date on Nov. 10th at 12 UTC)

Initially the C0 simulated from the ± ErPVpTerm perturbations are similar respect to the control one. However, at the mature state of the cyclone, C0 values are about 1 PVU lower (see figure 3.1.17). The strong differences may be related to the change of phase of the mutual interaction with the surface cyclone attributed to the baroclinic deepening processes. This aspect is also reflected in the +ErPVpTerm cyclone simulation. The cyclone exhibits a stronger vorticity than the control one (see figure 3.1.18) associated to a deeper cyclone and stronger North Atlantic high, which results in much stronger surface pressure gradients (see figure 3.1.14). During the dissipative phase of the cyclone (from 11th Nov. at 12 UTC to 12th Nov. at 00 UTC), the differences with the control cyclone become strong. The final position is clearly shifted about 54 km from control one on both cases (figure 3.1.15), the central pressure value is changed about $\pm 2hPa$ (figure 3.1.16), and final values of C0 are stronger (about $\pm 1.5PVU$, figure 3.1.17). At the end of the simulated period lower vorticity of the -ErPVpTerm cyclone is obtained because of the smaller dimensions of the cyclone in comparison to the +ErPVpTerm one (not shown). The strongest deepening of the cyclone occurred between Nov. 10th at 18 UTC and Nov. 11th at 06 UTC (see figure 3.1.16). In contrast with the strong sensitivity to the ErPVpTerm anomaly, the growth rate of the cyclone does not vary significantly (about -8 hPa/12 hours in positive case and -6 hPa/12 hours in the negative).

3.1.5 Sensitivity to to the Atlantic high pressure zone

The cyclones obtained in the simulations with the ErPVpHigh anomaly present the lowest sensitivities. The differences with respect to the control simulation are rather low until the last phase of the cyclone. The largest variations are obtained in -ErPVpHigh case. A weaker North Atlantic anticyclone (as a result of the -ErPvpHigh initial perturbation) can help to a faster movement of the Mediterranean disturbance, owing to a weaker blocking of the anticyclone. That is, a weaker North Atlantic high pressure zone might allow a faster movement of the cyclone and changes in the advections from higher latitudes. Final values of the C0 centre and relative distances between low and upper level disturbances do not differ from the control one (see figure 3.1.17), but final phase trajectories are significantly shifted from the control one (see lines with triangles in figure 3.1.15).

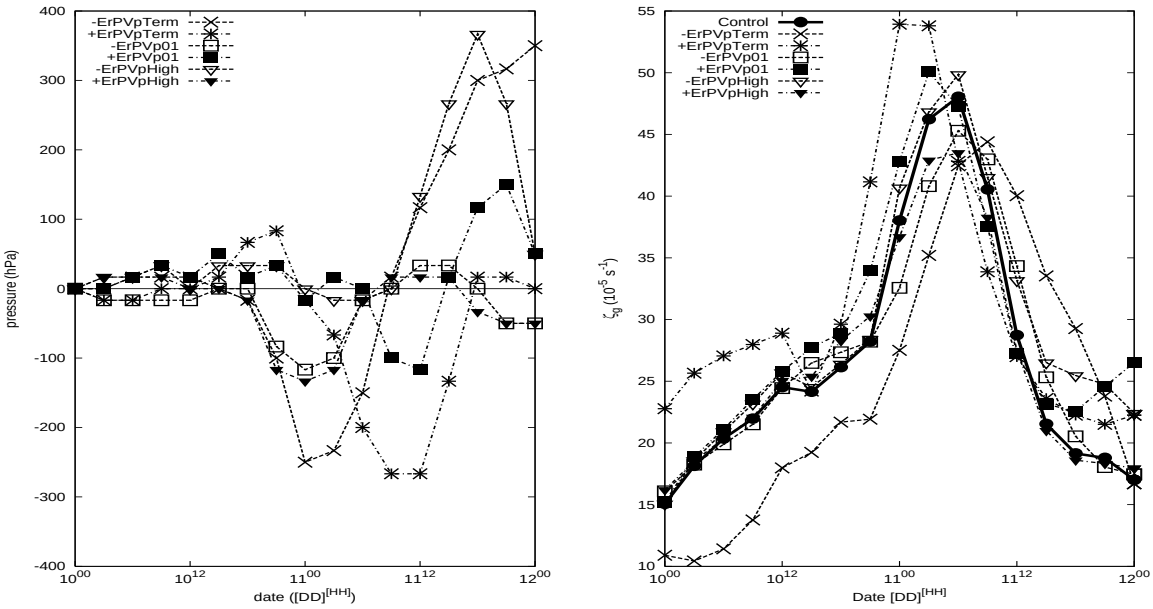

Figure 3.1.18: Labels as in figure 3.1.15, but Left panel: evolution of the depth of the cyclone rescaled to control simulation results (defined as the first minimal vorticity value above the centre of the cyclone, left). Right panel: evolution of the vorticity of the cyclone at distance of 200 km (defined like in (Campins et al., 2000)). Each figure has been temporally filtered through a mobile-average filter of 3 time-points

3.2 Intercomparison throughout Mediterranean basin

Mediterranean basin presents unique geographical and morphological characteristics that might derive to a cyclgonesis in the all basin with particularities and specific processes. The existence of a characteristic Mediterranean cyclogenesis could be shown with a climatology of roles and influences of some features involved in the cyclogenesis in the area.

In order to evaluate the cyclogenesis allover the basin a climatology of 'dynamical' aspects is made (Fita et al., 2006). It is investigated the possible similarities and differences among the selected cases of the relative weight of cyclogenesis. The study is done through the analysis of the role of cyclogenetic factors on the cyclone evolutions as function of cyclone type and geographical area.

The climatology is obtained from the study of eleven Mediterranean cyclones. As dynamical aspects, some evolving features of the atmosphere that are involved and related to the cyclone's evolution are considered: The upper level PV anomaly associated to the undulating tropopause (PVp above 700 hPa, with a relative humidity (RH) less than 70 %), the low level PV anomaly (PVp under 700 hPa, drier than 70 % together with surface thermal anomalies (Bretherton, 1966)) and the diabatically induced PVp (PVp below 500 hPa, with humidity higher than 70 %). The inclusion in the study of diabatically induced PVp aims to isolate the effects associated with latent heat release in the cyclone cloudy structure. The thermal anomaly induced by massive water vapour condensation at mid-upper tropospheric levels enhances the static stability above and this is reflected as a distinct PV positive anomaly (Hoskins et al., 1985; Davis and Emanuel, 1991)

The eleven selected cyclones have been chosen from the MEDEX[1] data base. This data base has been constructed from contributions of different National Weather Services, research institutes and universities of the entire Mediterranean basin. The cyclones have been classified in terms of their social impact. These 11 cases (see table 3.2.a) have been chosen from the most severe MEDEX group, usually involving deep cyclogenesis. These cases have been selected trying to encompass all the Mediterranean basin. Cyclones have been classified according to a geographical area of evolution and to a typology of formation. Geographical classification is chosen from three main areas of the Mediterranean basin: Western (from Eastern coast of Iberian peninsula until Sardegna-Corsica Islands), Central (from Sardegna-Corsica Islands until Peloponnese) Eastern (from Peloponnese until Middle-East). Has been determined three typologies of formation of the cyclone: Alpine lee (cyclogenesis at the lee of the Alps mountains), African (cyclone originated in the north African region) and Marine (cyclogenesis above the sea).

The dynamical study is based on solving the geopotential height tendency due to

[1] `http://medex.inm.uib.es`

Table 3.2.a: Table of the 11 selected cases. 1st col. indicates the name of the case ([DD]/[MM]/[YY]), 2on col. indicates the date of cyclone's mature state ([DD]/[MM]/[YY]) and P_{min} indicates minimum central pressure value (hPa) and corresponding time according to ECMWF analysis. 3rd col. indicates the Mediterranean region where the cyclone evolved. 4th col. indicates cyclogenesis area

Case	**maximum depth** (P_{min})	**Med. region**	**cyclone type**
6-9/10/96	7/10 06 (1003.6)	Central	Alpine lee
16-18/03/98	16/03 00 (984.1)	Eastern	African
6-9/11/99	7/11 06 (997.5)	Central	Alpine lee
13-16/10/00	15/10 06 (1001.9)	Western	African
9-13/11/01	11/11 00 (993.0)	Western	African
23-24/11/01	25/11 12 (989.3)	Eastern	Alpine lee
3-4/12/01	2/12 12 (997.7)	Eastern	Maritime
14-15/12/01	14/12 00 (1005.5)	Western	Maritime
6-8/05/02	7/05 00 (993.0)	Western	African
13-14/07/02	14/07 00 (1002.8)	Central	African
8-10/10/02	12/10 06 (997.8)	Western-Central	Maritime

the different factors using the prognostic system of equations proposed by Davis and Emanuel (1991) see section 2.2.2. Via this PV-based set of prognostic equations, the impact of each PV anomaly could be studied by switching on and off those anomalies in the atmospheric state and combining the results for the height tendency using the Factor Separation technique (Stein and Albert, 1993). Both, the individual effects as well as their mutual interactions could be properly isolated with such methodology. The methodology is solved on ECMWF global analyses fields (every 6 hours) that comprise all the period of evolution of each cyclone.

This methodology contributes widen the perspective of the dynamical aspects of the cyclones. A large variety of Mediterranean cyclonic climatologies have been done (Campins et al., 2000; Picornell et al., 2001; Campins et al., 2006). All of these climatologies have been focused in morphological aspects of the cyclones such as central pressure value, vorticity and trajectories. The methodology based on the geopotential height tendency gives information about the dynamical processes involved in the cyclone evolution. Dynamical aspects are shown as their direct or interaction effect on the evolution of the cyclone. These effects or synergies are objectively quantified trying also to give some information about the couplings between features that are involved in the cyclogenesis. By this way a new main view of the dynamics of the cyclogenesis in the Mediterranean basin can be obtained. Detailed information of the principal features of the cyclogenesis

is given once one have selected and detected the most important ones. That allows to made intercomparisons of the roles of the same features involved in different cases. At the same time can be found the existence of specific characteristics of the cyclone evolution in the Mediterranean basin.

3.2.1 Description of cases

Each case represents a different cyclone evolution over the Mediterranean basin. Their major characteristics are briefly described (see MEDEX database for more details at `http://medex.inm.uib.es`) as well as depicted trajectories in figures 3.2.1 to 3.2.11:

1. *6-9/10/96*: An upper level cut-off evolved into the Mediterranean basin, from which the cyclone was created off the coastal line of Algiers. The eastward progression of the cut-off produced an evolution of the cyclone over the sea toward the east.

2. *16-18/03/98*: A north African thermal low was developed to the south of the Atlas mountains. Through the interaction with an upper level trough, the cyclone moved over the Sahara desert and entered into the Mediterranean Sea across the Egyptian coast when it reached the mature state.

3. *6-9/11/99*: This cyclone can be considered as an Alpine-lee cyclogenesis (Buzzi and Tibaldi, 1978). The mature cyclone moved Southeastward over the Mediterranean Sea.

4. *13-16/10/00*: A thermal low over African plateau interacted with an upper level trough. The cyclone moved toward the Mediterranean Sea over Algiers following a northward trajectory. When the cyclone reached the sea, the low reached the mature state.

5. *9-13/11/01*: This case is very similar to the previous one (*13-16/10/00*). In this case the cyclone is deeper and stronger.

6. *23-24/11/01*: The cyclone presented two phases. An Alpine-lee cyclone moved from the Golf of Genoa following the Adriatic Sea forced by an upper level trough. Meanwhile the upper level trough became a cut-off, the cyclone moved then northeastward and reached the Black Sea where it attained its mature state.

7. *3-4/12/01*: A low latitude upper level disturbance induced a cyclone over the Cyprus island region. The cyclone stayed on the region during all its life cycle.

8. *14-15/12/01*: An upper level cut-off moved southwestward from the Central Europe region. As a result, a cyclone was developed on the lee of the Alps mountains.

9. *6-8/05/02*: Another case similar to *16-18/03/98* where the interaction between an African thermal low and an upper level trough induced a cyclone which reached the mature state when it entered in the Mediterranean basin in front of the coast of Algeria.

10. *13-14/07/02*: A thermal North African cyclone interacted with an upper level trough. In this case the cyclone moved into the Mediterranean basin across the coastal region of Tunis, and moved northward to Balkan countries.

11. *8-10/10/02*: An Atlantic cyclone moved southeastward owing to the southeastward movement of an upper level trough. The cyclone crossed the north of Spain and moved eastward along the Mediterranean Sea reaching Greece.

In this case the following effects are isolated and labelled as (See section 2.3 for the meaning of the effects):

- E_0: Effect of the Background flow
- E_1: Effect of the Upper level PVp (P <700 hPa, RH<70 %)
- E_2: Effect of the Low level PVp (P >700 hPa, RH<70 %)
- E_3: Effect of the Diabatic PVp (P >500 hPa,RH>70 %)
- E_{ij}: Effect of the synergy E_i & E_j
- E_{123}: Effect of the synergy of the three anomalies

The study is focused on the effects of each factor on the most relevant total geopotential height tendency signal (at 925 hPa) that governs the cyclone evolution from its genesis to its decay. The most relevant geopotential height tendency zone responsible for the cyclone evolution is detected at each time-step. Geopotential height tendency and sea level pressure fields are visually intercompared in order to detect the most related geopotential height tendency to the cyclone evolution. Most related geopotential height tendency zone has been selected in two ways: as the closest enclosed tendency zone or the enclosed tendency zone where the cyclone moves the next step. This geopotential zones are defined as an enclosed tendency threshold and/or geometrical line defined sections of the tendency. A spatial-average of the effects of each factor/interaction on the selected height tendency is depicted for each time-step. By this way effects should reflect the evolution of the characteristics of the cyclone and/or its movement. Negative values indicate deepening and/or movement of the cyclone, whereas positive values would act to fill or slow the disturbance.

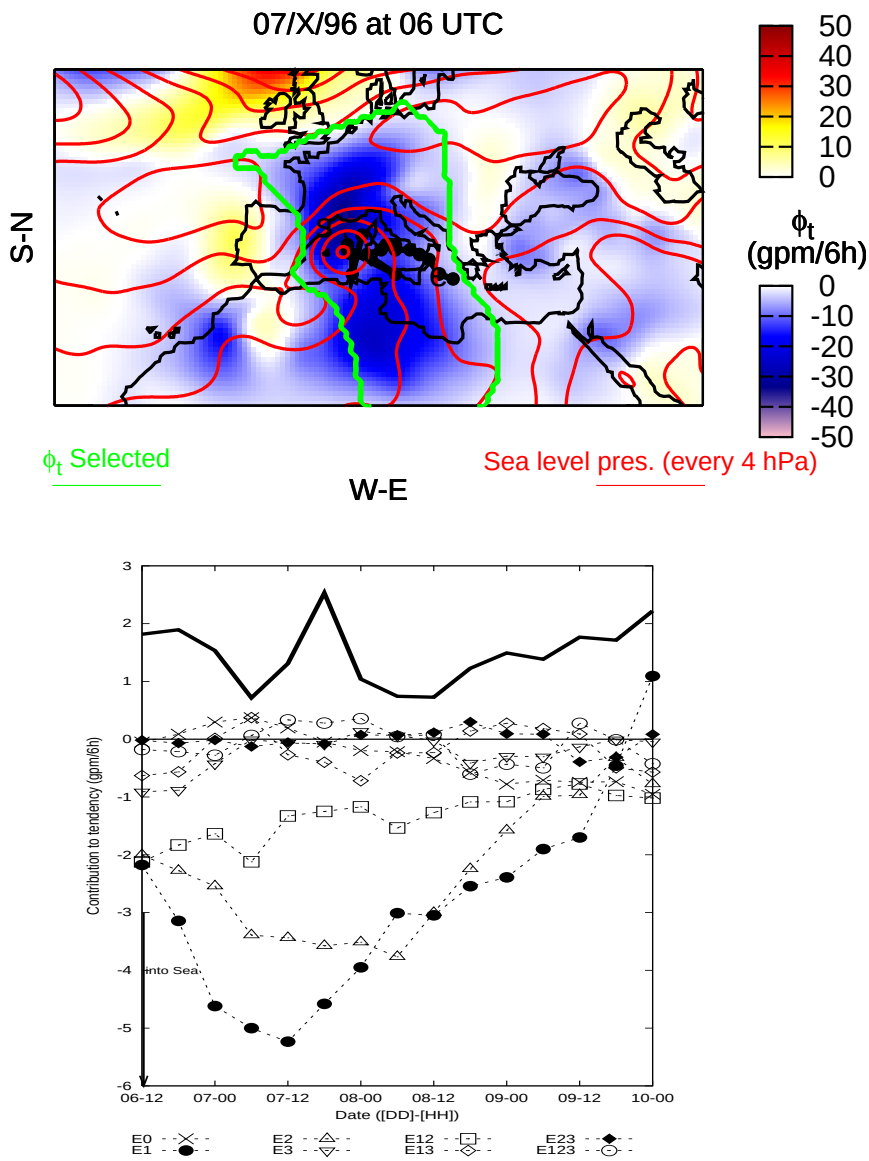

Figure 3.2.1: 'Alpine lee' & Central Mediterranean case 6-9/10/96. On left panel: Cyclone trajectory (solid thick line with circles), ϕ^t at 925 hPa (white to red positive, white to blue negative, every 10 gpm/6h), Sea level pressure (dot line, every 4 hPa) and geopotential height tendency signal used to compute the effects (thick dash-dot line) at mature cyclone time. Labels indicate starting (s) and ending (e) central cyclone position. Right panel: Evolution of the space-average tendency by each factor/interaction filtered with a three-step moving filter (dashed lines, and corresponding symbols as defined in bottom figure). Black arrows show when the cyclone reached/left the Sea. The cyclone central pressure evolution is shown as the solid thick upper line (no scale).

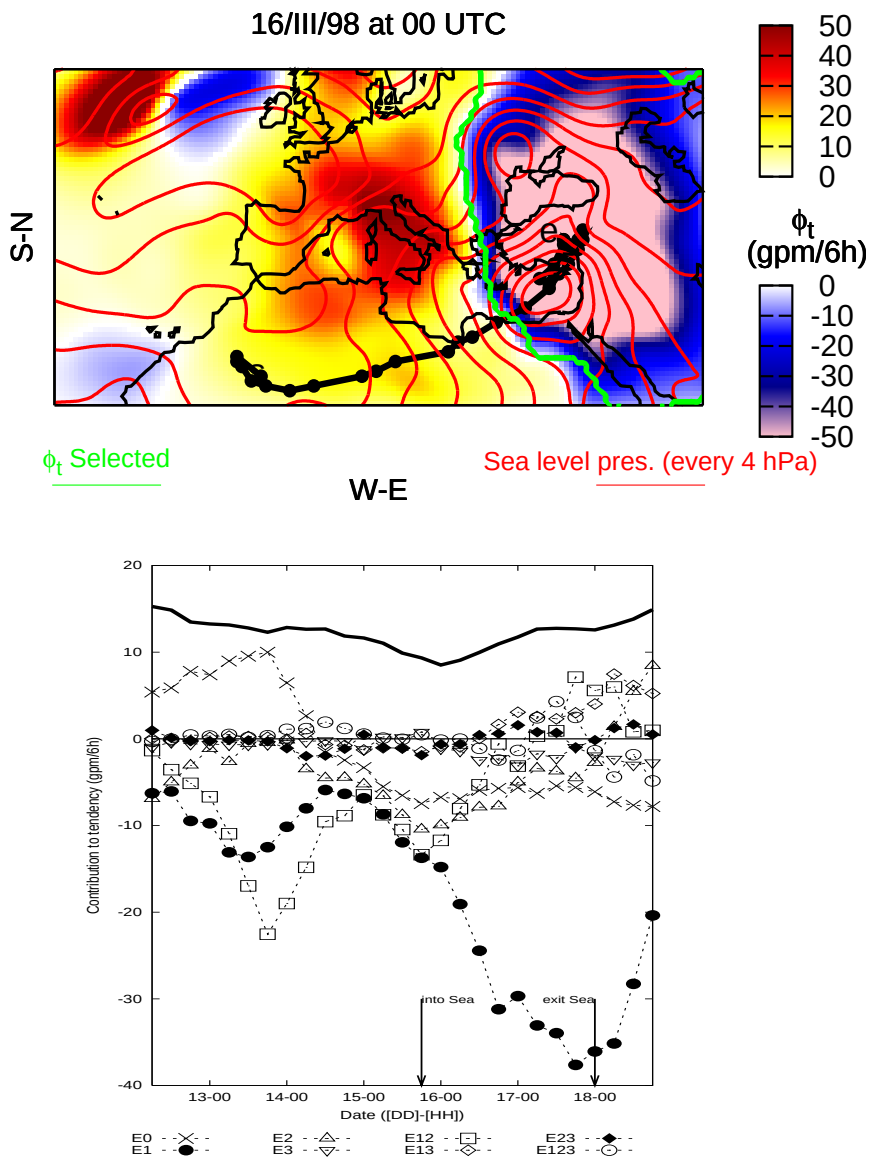

Figure 3.2.2: As in figure 3.2.1 for 'African' & Eastern Med. case 16-18/03/98

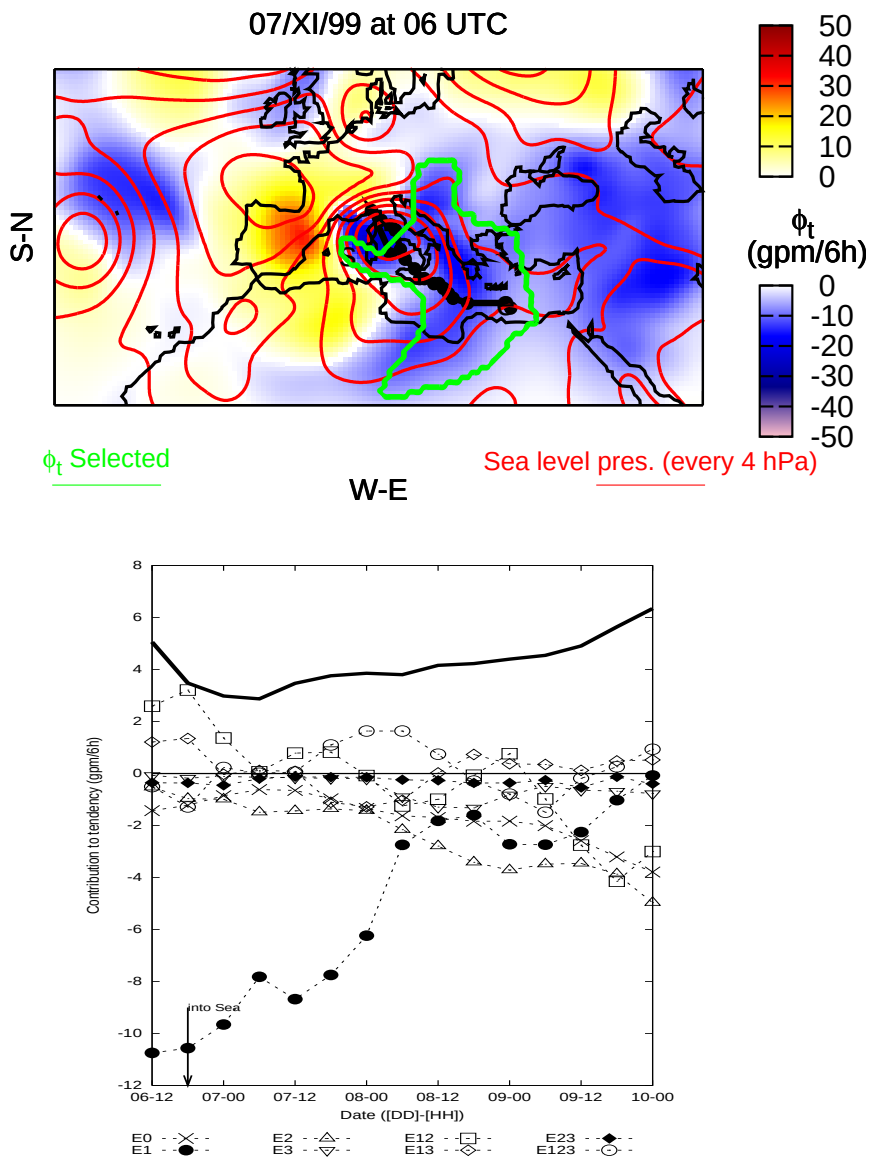

Figure 3.2.3: As in figure 3.2.1 for 'Alpine lee' & Central Med. case 6-9/11/99

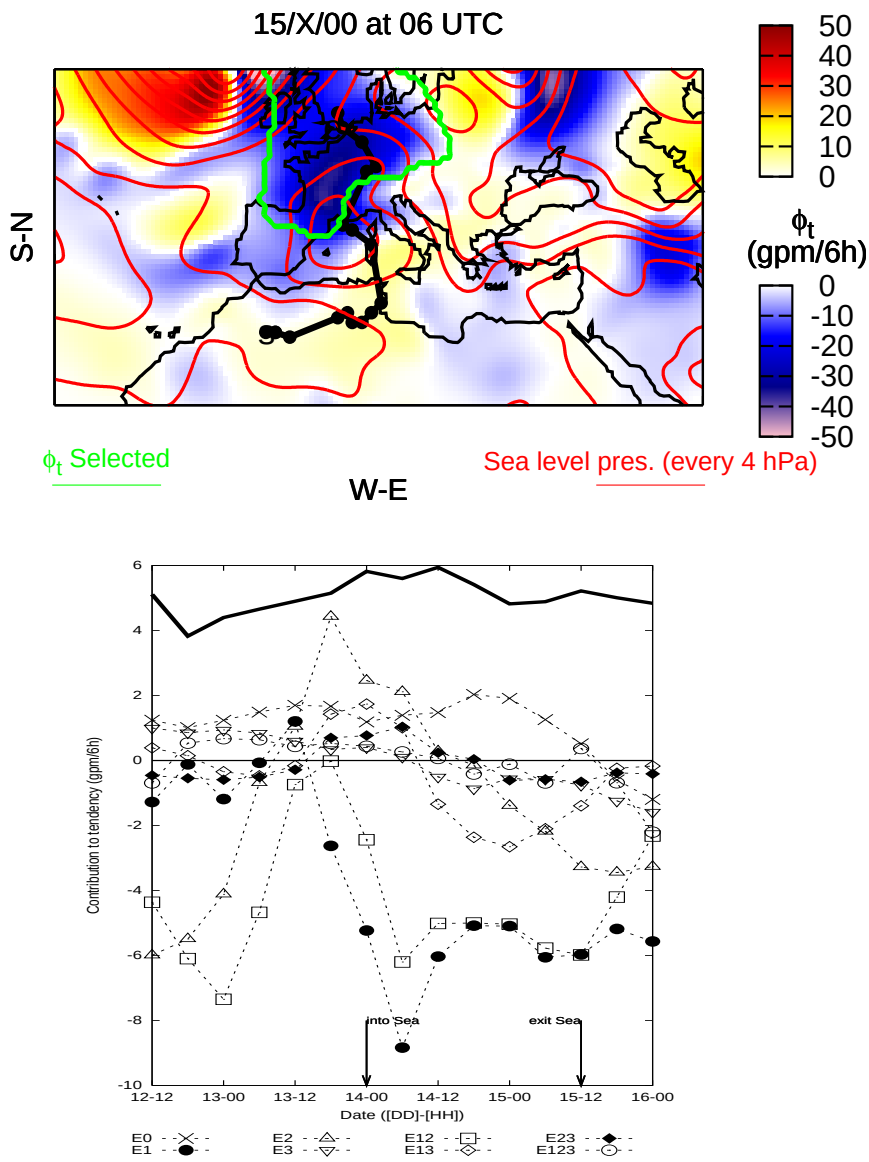

Figure 3.2.4: As in figure 3.2.1 for 'African' & Western Med. case 13-16/10/00

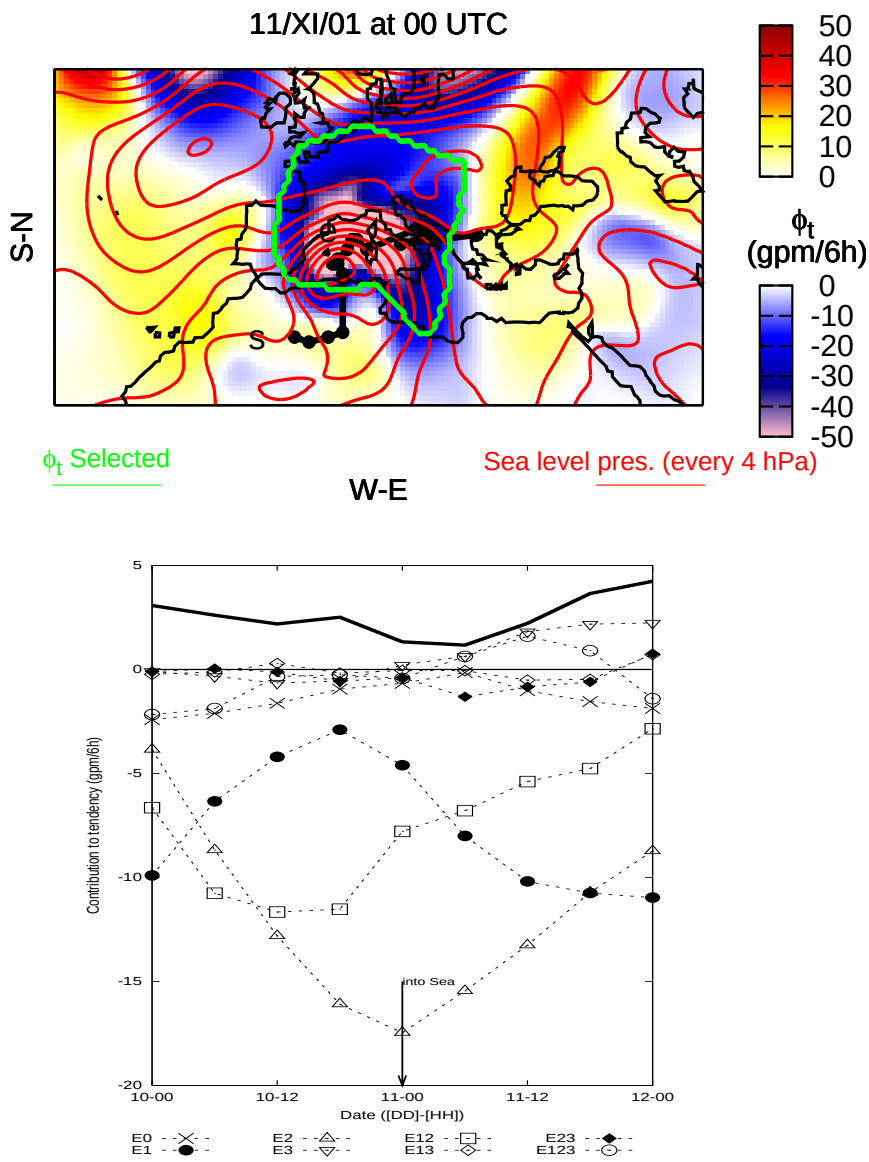

Figure 3.2.5: As in figure 3.2.1 for 'African' & Western Med. case 9-13/11/01

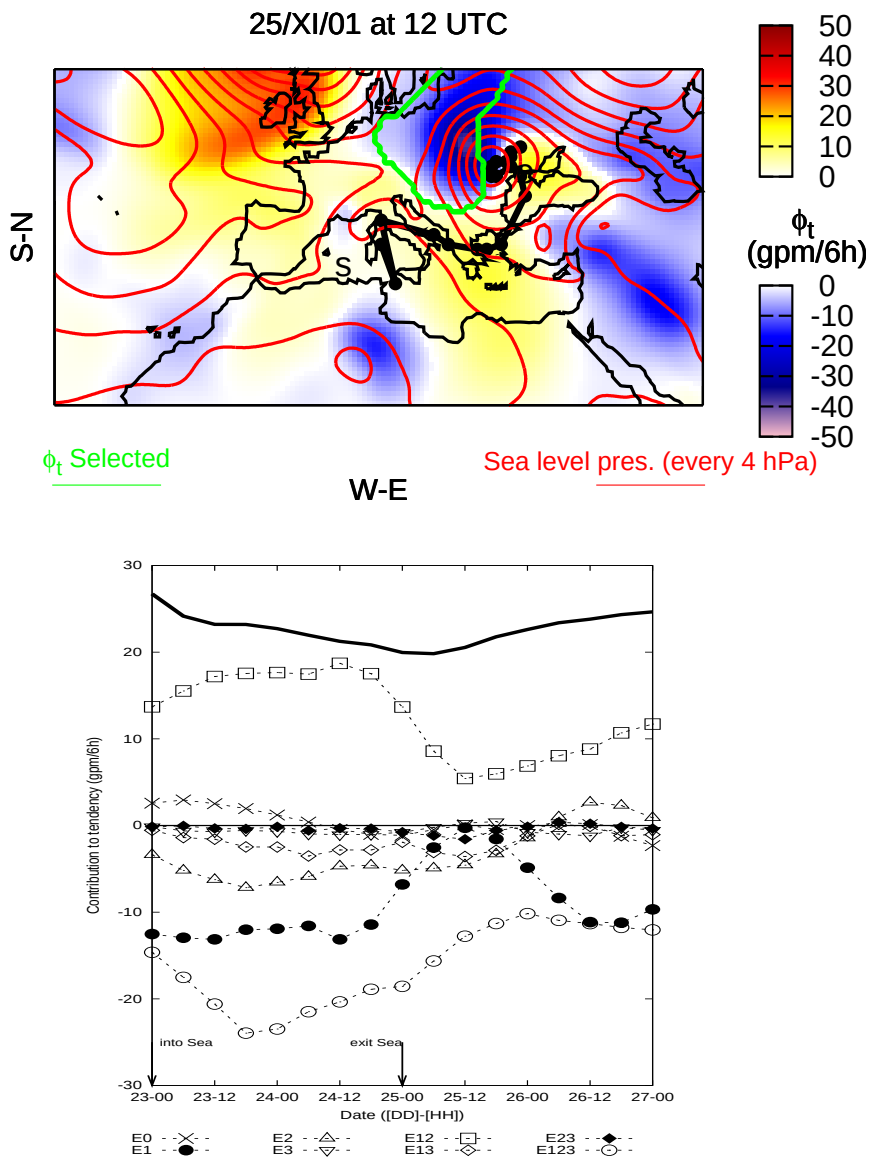

Figure 3.2.6: As in figure 3.2.1 for 'Alpine lee' & Eastern Med. case 23-24/11/01

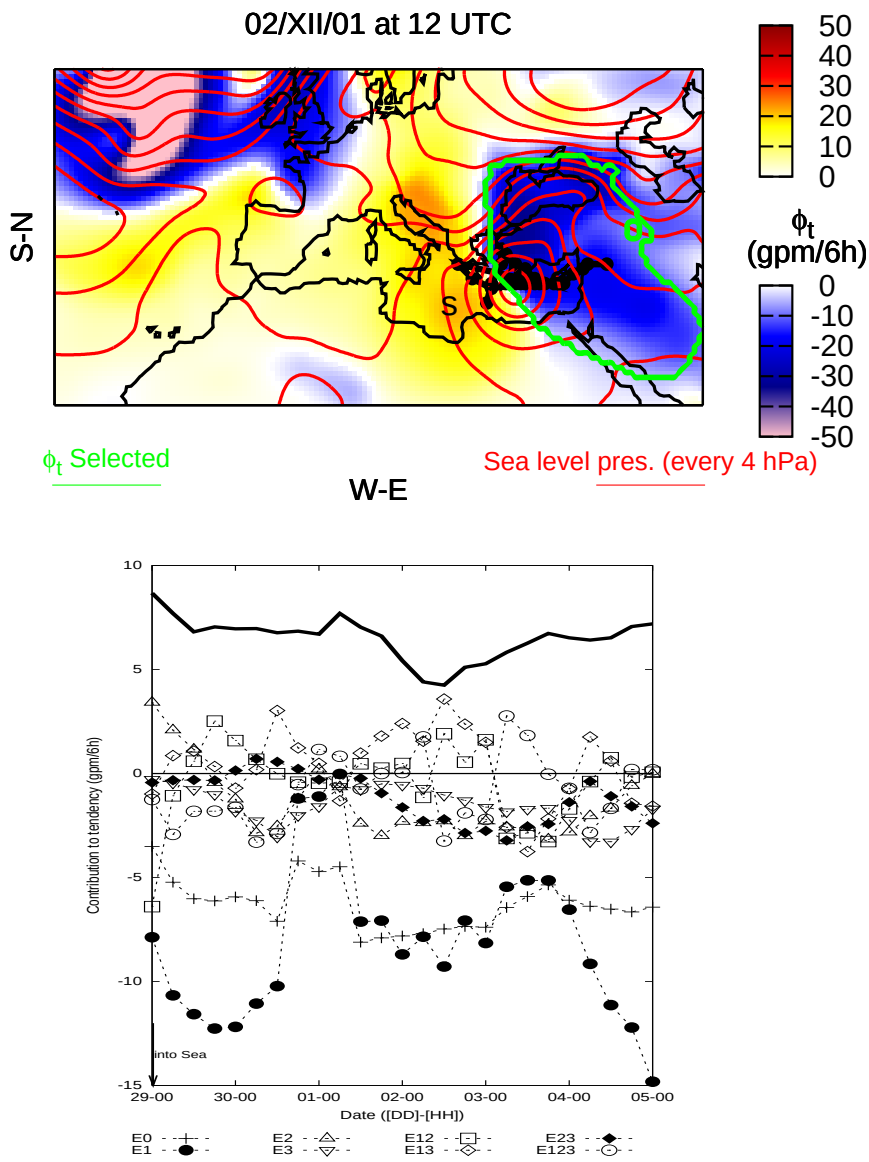

Figure 3.2.7: As in figure 3.2.1 for 'Maritime' & Eastern Med. case 3-4/12/01

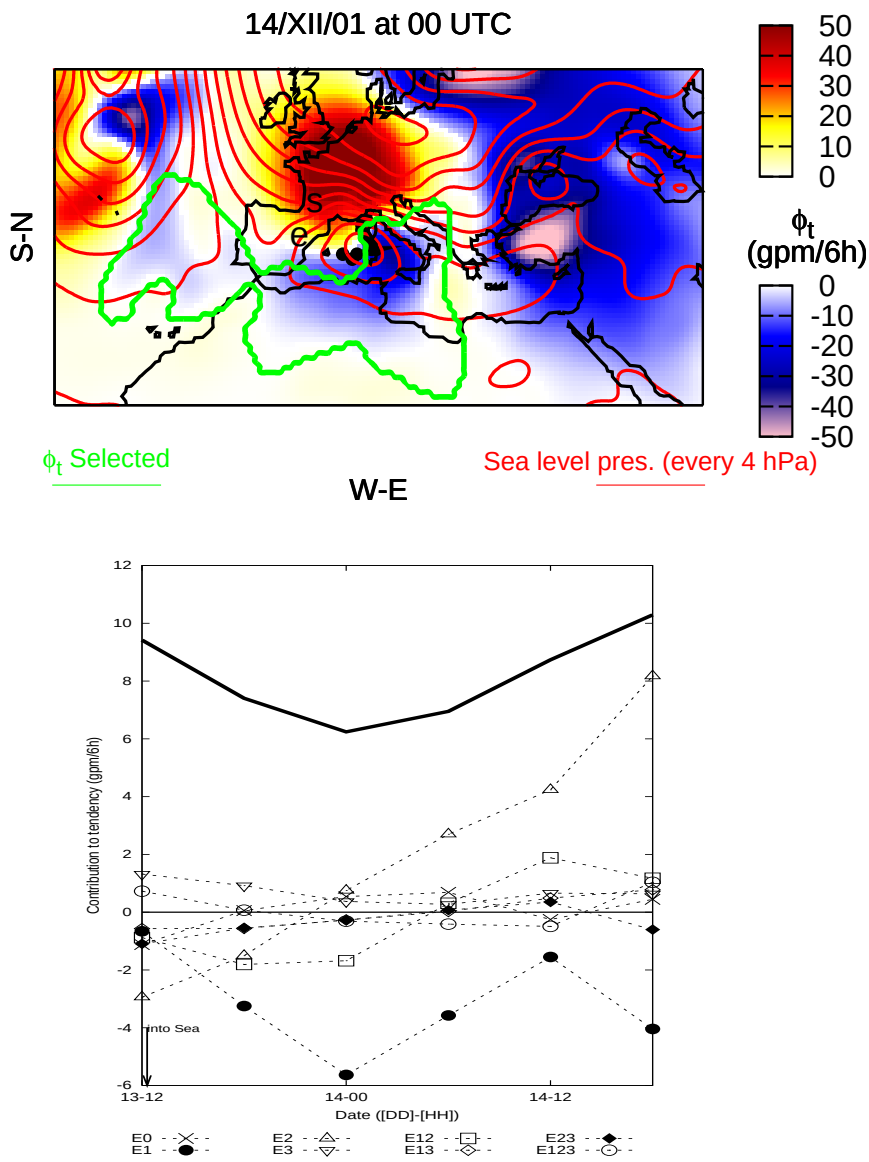

Figure 3.2.8: As in figure 3.2.1 for 'Maritime' & Western Med. case 14-15/12/01

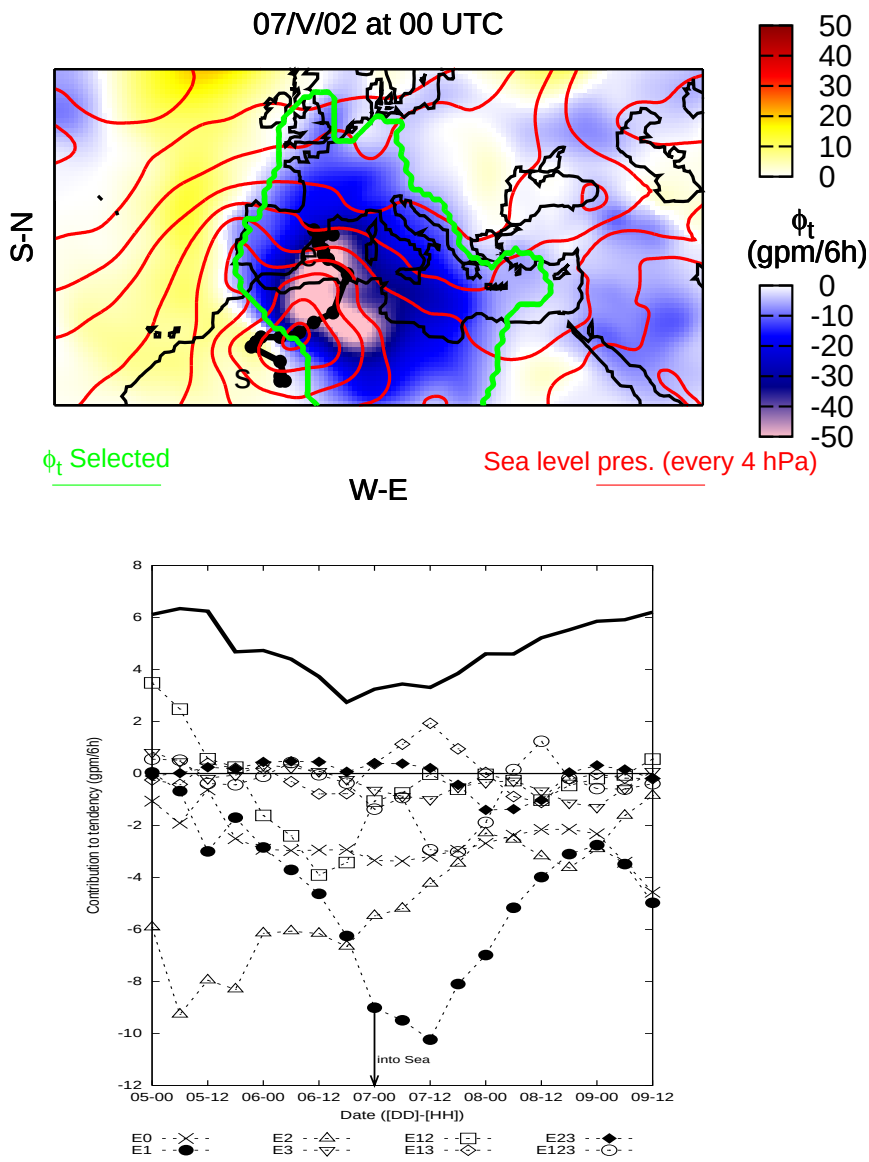

Figure 3.2.9: As in figure 3.2.1 for 'African' & Western Med. case 6-8/05/02

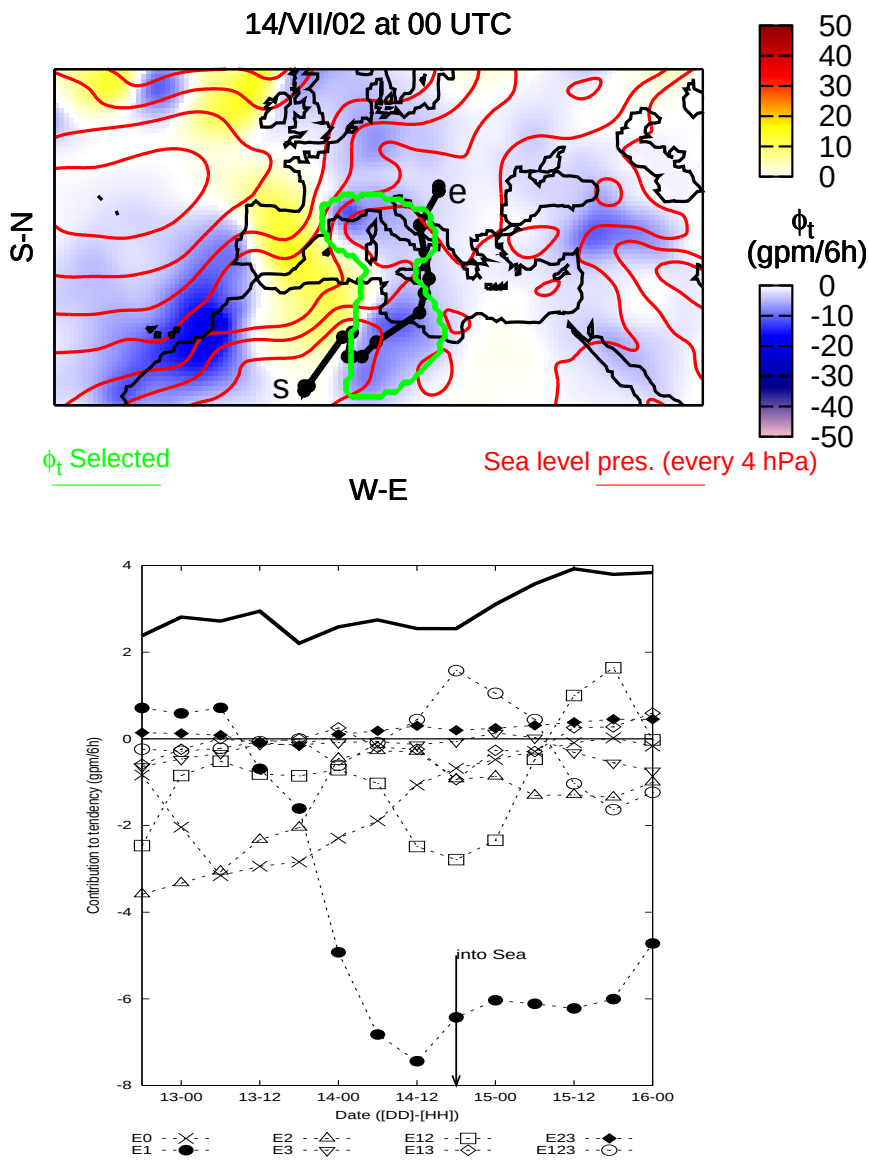

Figure 3.2.10: As in figure 3.2.1 for 'African' & Central Med. case 13-14/07/02

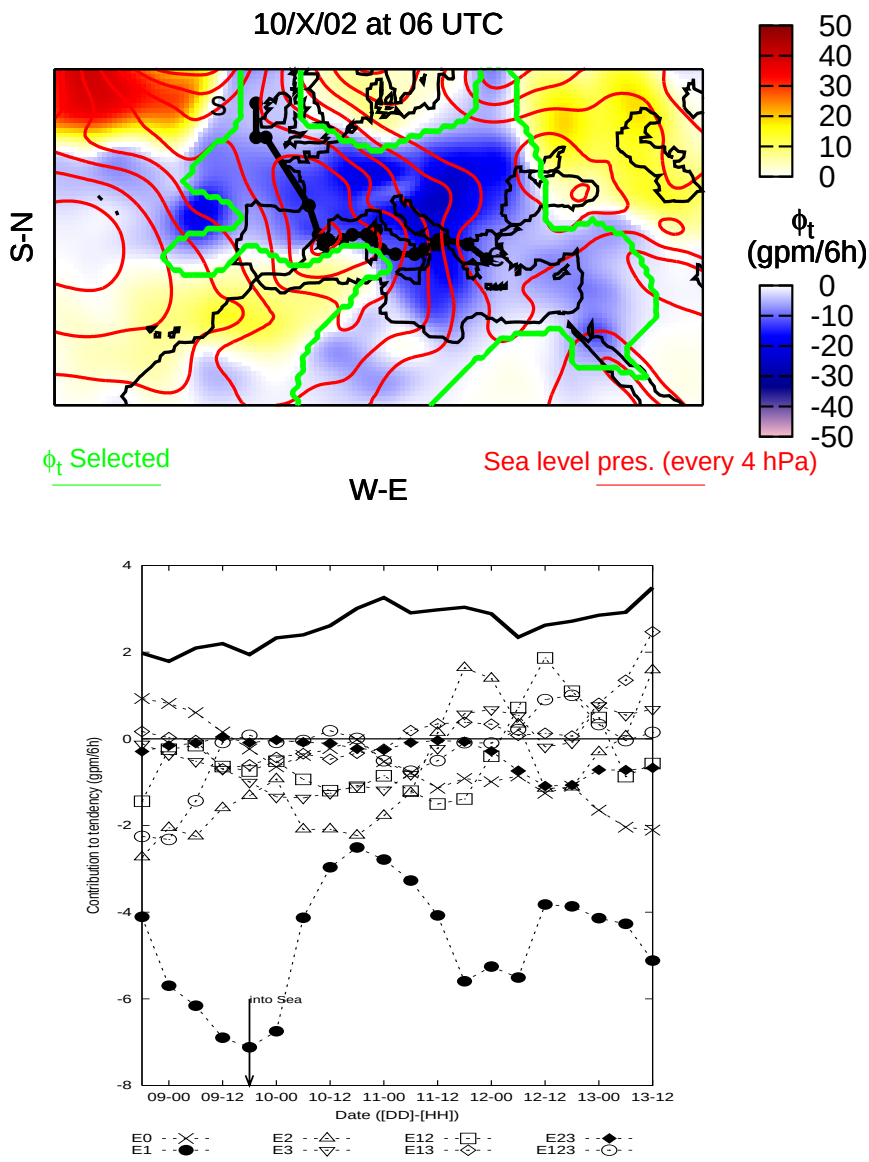

Figure 3.2.11: As in figure 3.2.1 for 'Maritime' & W-Central Med. case 8-10/10/02

3.2.2 Results

From figure 3.2.1 to 3.2.11 the results for each cyclone are shown. The results are generally case dependent with respect to the importance of the selected effects and the role of each one. However some conclusions can be emphasised: Generally the upper level PVp (effect E_1) is the most relevant (showing the important role of the baroclinicity over the Mediterranean basin, like in 13-14/7/02 and 14-15/12/01 cases). It is noticeable that in almost all of the selected cases a significant upper level trough or cut-off was present during the cyclone evolution (not shown).

Low level PVp (E_2) & synergy E_{12} mainly play secondary roles (like in cases shown in figures 3.2.4, 3.2.5 and 3.2.11). This result depicts the importance of the role of the dry low level PV. Positive surface layer PV can be related to a surface layer thermal anomaly (Bretherton, 1966). Many times a surface thermal anomaly is evolves into the baroclinic development of disturbances. Low level PV might be also related to a surface thermal anomaly and at the same time to the thermal anomaly associated to the cyclone (in some Mediterranean cases related to the North African warm and dry plateau).

The background flow (E_0) is mainly responsible for the displacement of the disturbance (e.g. in figure 3.2.10 of case 13-14/07/02; where this weak cyclone moved northward due to general circulation reflected by this factor). In this case, cyclone does not follow an usual eastward movement due to influence of an upper level trough elongated meridionally (see figure 3.2.12).

The effects related with the diabatically induced PVp (E_3, E_{13} and E_{23}) present the lowest contribution, even for the cyclones presenting high deepening process when reaching the sea (leading to mature state) like in figures 3.2.2 and 3.2.5. Note that the above effects are related with the role of diabatically-generated PV, not with the diabatic forcing itself as it is included in the right hand sides of equations 2.2.19 and 2.2.21. Thus PV at low levels might reflect a part of the diabatical aspects of the latent heat release due to strong cloud formation. Moreover ECMWF analyses (with a grid mesh of about 0.3 degrees) could be not fine enough to capture this effect as positive PV at low level with high moist values. Explicit consideration of the diabatic terms of the equations as new factors should be developed in order to confirm these hypothesis.

Factors are often cyclogenetic and cyclolitic probably owing to different phases of evolution of the cyclone or to the complex topographical configuration of the basin and other evolving interactions involved in baroclinic developments. One of these influences is the upper-level-low level interaction (Hoskins et al., 1985). For example E_2 and E_{12} change sign in 8-10/10/02 case owing to the change of vertical tilt of the upper and low level disturbances (see figure 3.2.13). Another kind of influence is the cyclone position

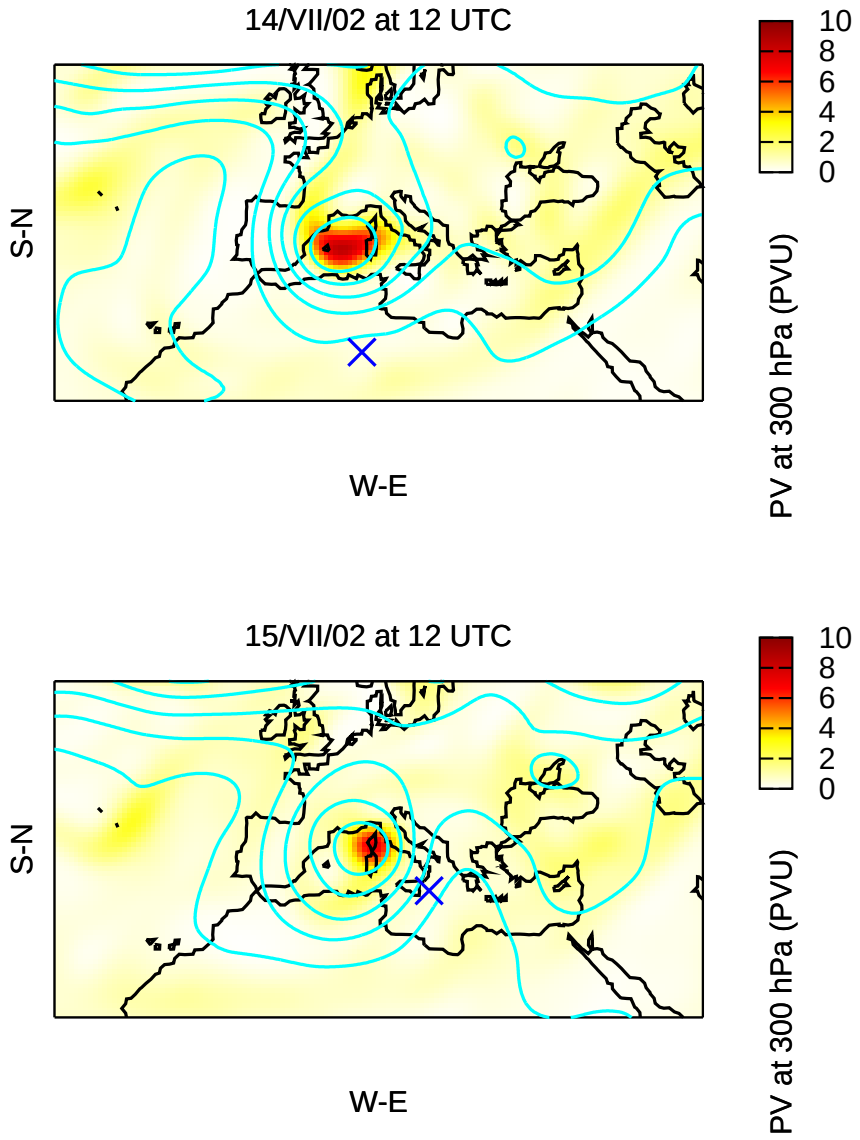

Figure 3.2.12: Potential Vorticity at 300 hPa (dashed), geopotential height (every 50 gpm, solid light blue line) and position of the centre of cyclone (blue cross) for the 13-14/07/02 case on 14th at 12 UTC (left) and on 15th at 12 UTC (right)

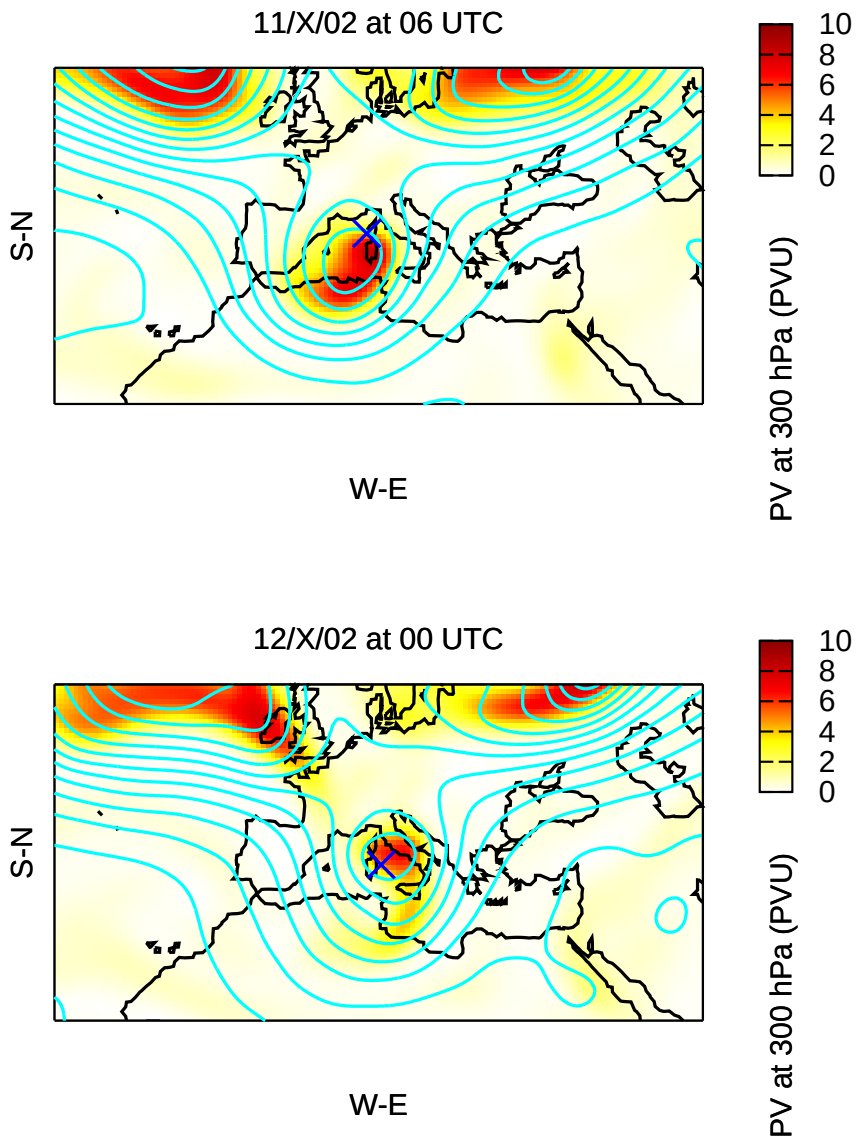

Figure 3.2.13: As in figure 3.2.12, but for the 8-10/10/02 case on 11th at 06 UTC (left) and on 12th at 00 UTC (right)

relative to the orography and background flow. For example, E_0 became cyclogenetic until the cyclone moved over the Tunis planes on case 16-18/03/98. At this time-step (about 14th 12 UTC), background flow loses its cyclolitic role in the cyclone evolution. It is notorious to see that background flow is in leeward geographical disposition with Atlas range. However, cyclone is a little bit further of the lee cyclogenetic ideal position (see figure 3.2.14).

Cyclogenesis events in the Mediterranean have often been classified attending to affected geographical zone, social impact, NWP performance and/or deepening rate (e.g. MEDEX database, see `http://medex.inm.uib.es`). In this work the emphasis is made on the role of evolving and interacting dynamical aspects of the synoptic-scale circulation as represented by PV anomalies, and it is hoped that the approach can be extended and refined to perform a dynamical climatology of deep cyclogenesis events in the Mediterranean basin. The results presented do not close the question, but seem to indicate that some dynamical differences in Mediterranean cyclogenesis can be related to the nature and track location of the disturbance.

3.2.3 Geographical sensitivity

Western & Central Mediterranean cyclones seem to be mainly dominated by PV anomalies E_1, E_2 and their synergy E_{12} (as is shown by 3.2.5). In contrast eastern Mediterranean cyclones show a non unique principal factor dependence. They are dominated by a variety of effects of distinct nature like E_{12}, E_1, E_{123} or E_0 as it is shown in figures 3.2.2 and 3.2.6. This apparent regional characteristic of the Mediterranean cyclones could be attributed to the different kinds of cyclone owing to the origin of formation that present different influences with large variety of characteristics. Western and central cases are mainly North African plateau and Alps lee cyclones. However, the Eastern cyclones present different genesis zones and trajectories. Eastern geographical area presents the most extent maritime area without any large orographical or island influence. Moreover, South-Eastern part of the Mediterranean basin is basically constituted by desertic plains and Crete and Cyprus islands are the major islands.

3.2.4 Dynamical sensitivity

'African' cyclones (like in figures 3.2.2 and 3.2.10) are mainly dominated by Upper level disturbances (factor E_1) or the synergy E_{12}. 'Maritime' cyclones (shown in figures 3.2.7 or 3.2.11) seem to be dominated mainly by E_1 and in lower degree by the background flow (E_0 effect). This should reflect the inexistence of orographic features that might influence in the synoptic driven trajectory of the cyclone. The selected 'Alpine Lee' cyclones (like in figures 3.2.1 and 3.2.3) seem to present three phases: an initial dominated by the role of the upper level tropopause disturbance (factor E_1), a second one dominated by E_2 prob-

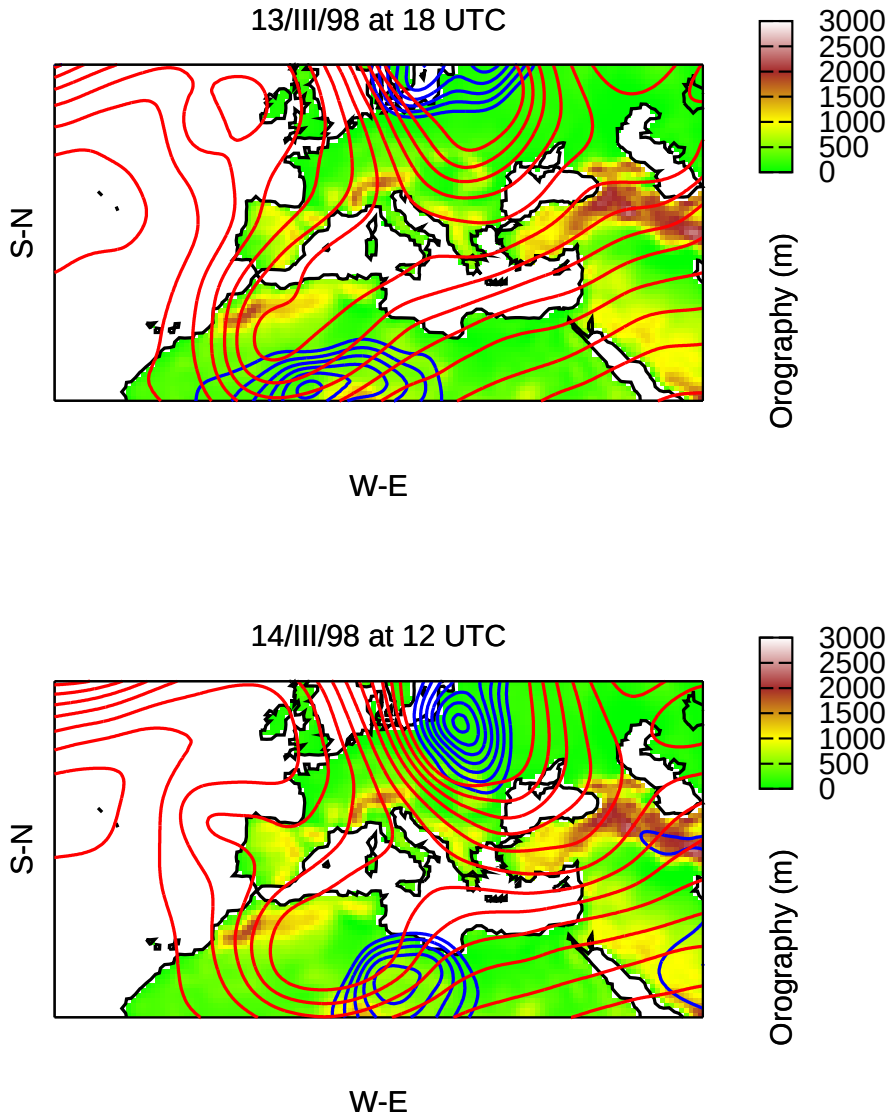

Figure 3.2.14: Orography (dashed) geopotential height at 500 hPa (every 50 gpm, solid red line) and sea level pressure (every 2 hPa lower than 1010 hPa, solid blue line) for the 16-18/03/98 case on 13th at 18 UTC (left) and on 14th at 12 UTC (right)

ably related to the induced PV banners of a lee cyclogenesis, and later maritime phase dominated by E_2 probably due to the role of the moist processes. Finally it is sometimes obtained a compensation between large cyclogenetic and cyclolitic effects (e.g. E_{123} and E_1 cyclogenetic effects are compensated by E_{12} and E_0 on 23-24/11/01 case during the initial steps of the evolution of the cyclone).

A larger and deeper study should be done with more cases in order to obtain more general results and better representation of the population of cyclones over the Mediterranean Sea. However, the presented approach, carried out with 11 cases, attempts to correct the lack of number of cases with the election of an appropriated set of cases that incorporate cyclones of different geographical areas and different dynamical evolution. At the same time wider number of factors should be used to ensure a correct capture of the most important features involved in the Mediterranean cyclogenesis.

Chapter 4

Thermal and topographic lee influences

Articles on which this chapter is based:

E. García-Ortega, L. Fita, R. Romero, L. López, C. Ramis and J.L. Sánchez, 2007: *Numerical simulation and sensitivity study of a severe hail-storm in northeast Spain*, Atmos. Res., **83**, 225-241

K. Horvath, Ll. Fita, R. Romero and Branka Ivancan-Picek, 2006: *A numerical study on the first phase of a deep Mediterranean cyclone: Cyclogenesis in the lee of the Atlas Mountains*, Meteorologische Z. 1, **15**, 133-146

4.1 Thermal influences

In specific regions, where a strong isolation is reproduced, lows can be generated. As a result of strong and continuous radiation, land surface can be strongly heated. Air above the surface is also heated and reach high temperatures. Increase of the buoyancy produce an upward motion of the air, decreasing the surface pressure. This cyclogenetic mechanism is known as the thermal-low (Alonso et al., 1994), due to the thermal origin of the cyclone. This could be the case of the initial surface disturbance of two studied cases: November 9-12th 2001 case and November 11-14 2004 case. In both cases, a weak surface disturbance was present above the hot and dry North African plateau south of the Atlas mountains.

The increasing of buoyancy due to solar radiation might have an effect as precursor of strong convection. At the end of a diurnal period with strong isolation, air above the surface may be very unstable and in the afternoon deep convection, heavy rain or even extreme weather can be developed. This peculiarities are very common for example in the Iberian peninsula during summer (Font, 1983). As an other consequence of the increase of buoyancy, in strong isolated regions weak and shallow lows are frequently generated (Campins et al., 2006). Convective phenomena usually have local characteristics and their effects usually affect small areas. In some locations this solar triggered convection might have local influences. One of this zones is the central part of the Ebro river basin (see figure 4.1.1).

The Ebro river basin run allover the Northwestern part of the Iberian peninsula and it is orientated NWSE. The Ebro is valley is bordered by the mountainous range of the Pyrenees to the north, the Iberian mountainous System to the southwest, and the Mediterranean Sea to the east (see figure 4.1.1). Due to its topographical characteristics, the Ebro basin is a corridor for the entrance of two types of air masses: one cold downward the basin of Atlantic origin, and another one of warm and moistened air flowing upward the Ebro basin incoming from the Mediterranean Sea.

Usually these two air of masses merge in an area of the basin known as the Central Ebro valley. The convergence of these two types of air masses is reproduced in an area in which high temperatures are registered during the summer months. By this way triggering effects of the solar radiation at the end of the day can be enhanced due to the convergence of these two air masses. This peculiar configuration makes hailstorms a frequent phenomena during these months. In fact, the Ebro Valley is one of the areas in Europe with the highest number of cases of severe convective phenomena. There are 20 thunderstorms per year in the southern part of the Valley (Font, 1983). These storms are usually of the warm-based cloud type (Sánchez et al., 1999) and most of them can be classified as multicellular, whereas supercells only represent 3% of all cases (Sánchez and Fraile, 1992).